NATIONAL ADVISORY COMMITTEE FOR AERONAUTICS

TECHNICAL NOTE 3346

PREDICTION OF DOWNWASH BEHIND SWEPT-WING AIRPLANES AT SUBSONIC SPEED

By John DeYoung and Walter H. Barling, Jr.

Ames Aeronautical Laboratory
Moffett Field, Calif.

Washington
January 1955

NATIONAL ADVISORY COMMITTEE FOR AERONAUTI(

TECHNICAL NOTE 3346

PREDICTION OF DOWNWASH BEHIND SWEPT-WING AIRPLANES AT SUBSONIC SPEED

By John DeYoung and Walter H. Barling, Jr.

SUMMARY

A rapid method for estimating the downwash behind swept-wing airplanes is presented. The basic assumption is that of a flat horizontal sheet of vortices trailing behind the wing. The integrations for the downwash are handled in a manner similar to both Multhopp's and Weissinger's approximate integrations in their span-loading calculations. The principal effects of rolling-up of the wake are treated as corrections to the flat-sheet wake. A simple approximate correction for the effect of the fuselage is applied. The agreement with available experimental data taken behind airplane models is good. Computing forms are included together with charts of pertinent functions, so as to enable simple direct application.

INTRODUCTION

The downwash induced by a lifting wing has, in the past, been predicted by considering the wing as a lifting line with a vortex sheet trailing aft of the wing in a horizontal plane. It was assumed that spanwise distribution of vorticity did not change with downstream position and that the sheet did not roll up behind the wing. With these assumptions, a procedure for determining downwash is given in references 1 and 2. In references 1 and 2, the wing span loading is approximated by several horseshoe vortices. The total downwash is the sum of the downwashes of the horseshoe vortices. It is apparent that such a procedure can be extended to swept wings by using swept horseshoe vortices. The arithmetic of this procedure is, however, rather tedious and laborious. In reference 3, a more rapid method in the form of an influence-coefficient approach is presented for the downwash at the center of the wake. References 1 and 2 also investigated the limitations of representing the lifting surface by a lifting line, and of the effects of the rolling-up of the trailing sheet. It was concluded that both effects were negligible for the then conventional airplane configurations.

At the present time, the use of low-aspect-ratio plan forms and occasionally of further rearward positions of the tail has made necessary a re-examination of the assumption that the trailing vortex sheet

can be considered nonrolling-up. An analysis of the rolling-up process is given in reference 4 which reveals that the trailing sheet becomes rolled-up at shorter distances behind the wing as (1) aspect ratio decreases, (2) lift coefficient increases, and (3) span loading increases outboard and decreases inboard. It is apparent that the downwash fields determined on the assumption of the flat trailing vortex sheet or a completely rolled-up sheet (the simplified cases) omit wings of aspect ratio of about two to four at moderate or high C_L's.

The purposes of this report are, (1) to make available an influence-coefficient type of method of computing the downwash behind swept wings having arbitrary spanwise loading, a procedure that will be quicker and simpler to use than methods summing up the downwash due to elemental horseshoe vortices, (2) to estimate the principal changes in the downwash field due to the rolling-up process, and (3) to suggest a simple first approximation to the downwash at the tail due to a fuselage. The effect upon the downwash field due to substituting a lifting line for surface loading will also be investigated and an approximate method for taking this effect into account will be presented for wings of low aspect ratio.

PRINCIPAL NOTATION

A aspect ratio, $\frac{b^2}{S}$

a_{sn} influence coefficients for a swept load line plus a swept trailing vortex sheet
(These coefficients act as integration factors of the wing loading at station n to obtain downwash at position (τ,η,Ω).)

a_{Tn} influence coefficients, similar to a_{sn}, but for only an unswept trailing vortex sheet (no bound vortex)

b wing span measured perpendicular to the plane of symmetry, ft

c local wing chord measured parallel to the plane of symmetry, ft

c_{av} average wing chord, $\frac{S}{b}$, ft

$\bar{c}$ mean aerodynamic chord, $\frac{\int_{-1}^{1} c^2 d\eta}{\int_{-1}^{1} c\, d\eta}$

c_l local lift coefficient, $\frac{\text{local lift}}{qc}$

C_L wing lift coefficient, $\frac{\text{lift}}{qS}$

C_{L_α} lift-curve slope, per radian or per deg

D_n integration factor for interpolating downwash in the vertical direction

f empirical relation giving the effect of sweep upon the rolling-up, $f = 1 - 0.0075\ (\Lambda^{\circ}_{TE} + 7^{\circ})$

F_c strength factor of the tip vortices, $\frac{\Gamma_c}{\Gamma(\eta = 0)}$

F_{sn} strength factor denoting loss of vorticity of the trailing sheet at span station n

$G(\eta)$ spanwise loading coefficient or dimensionless circulation along wing quarter-chord line, $c_l \frac{c}{2b}$ or $\frac{\Gamma}{bV}$

G_n $G(\eta)$ at span station $\eta = \cos \frac{n\pi}{8}$

K_n spanwise loading coefficient for unit lift, $\left(\frac{c_l c}{C_L\ c_{av}}\right)_n$ or $\frac{2A}{C_L} G_n$ where n refers to the span station $\eta = \cos \frac{n\pi}{8}$

M_o free-stream Mach number

q free-stream dynamic pressure, lb/sq ft

R_f radius of fuselage, ft

S wing area, sq ft

V free-stream velocity, ft/sec

w downwash, positive downward, ft/sec

x,y,z right-hand Cartesian coordinate system with x positive downstream and y positive to the starboard with the origin at the apex of the wing quarter-chord line (See fig. 1.)

Z vertical distance in wing semispans measured from extended chord plane, positive upward

α inclination of wing from zero-lift attitude, deg

α_{TE} slope of camber line at trailing edge relative to free stream, deg

β $\sqrt{1 - M_o^2}$

Γ circulation, ft^2/sec

ϵ angle of downwash, positive downward, radians or deg

Λ sweep angle of the wing quarter-chord line, positive for sweepback, deg

Λ_β $\tan^{-1}\left(\frac{\tan \Lambda}{\beta}\right)$, deg

λ taper ratio, $\frac{\text{tip chord}}{\text{root chord}}$

ξ,η,ζ dimensionless Cartesian coordinates, $\frac{x}{b/2}$, $\frac{y}{b/2}$, $\frac{z}{b/2}$

ξ_c longitudinal position at which sheet is essentially rolled-up into wing tip vortices

η_c lateral position of center of wing-tip vortex, $\frac{y_c}{b/c}$

τ dimensionless longitudinal coordinate, measured from the lifting line ($\xi - \eta \tan \Lambda$)

φ trigonometric spanwise coordinate ($\cos^{-1} \eta$), radians

Ω height above trailing sheet, $\zeta - \zeta_s$

Ω_c height above wing tip vortices, $\zeta - \zeta_c$

Subscripts

av average

c tip vortices

f fuselage

n,ν integers corresponding to span stations given by $\eta = \cos \frac{n\pi}{8}$, or $\eta = \cos \frac{\nu\pi}{8}$ (For n or ν = 1, 2, 3, or 4; η_ν or η_n = 0.9239, 0.7071, 0.3827, or 0.)

s pertaining to downwash at the sheet or displacement of the sheet

TE wing trailing edge

PHYSICAL PROBLEM AND BASIC ASSUMPTIONS

The physical picture is one of a lifting surface shedding a trailing sheet of vortices. As the trailing vortices are left farther behind the wing, the sheet of vortices is displaced downward in varying amounts depending upon the span station considered, that is, it assumes a curved shape. While this displacement is going on, the vorticity in the sheet is continually shifting from the sheet toward the tips or edges of the sheet. The lifting surface and the trailing vortex sheet are inclined with respect to the free-stream direction.

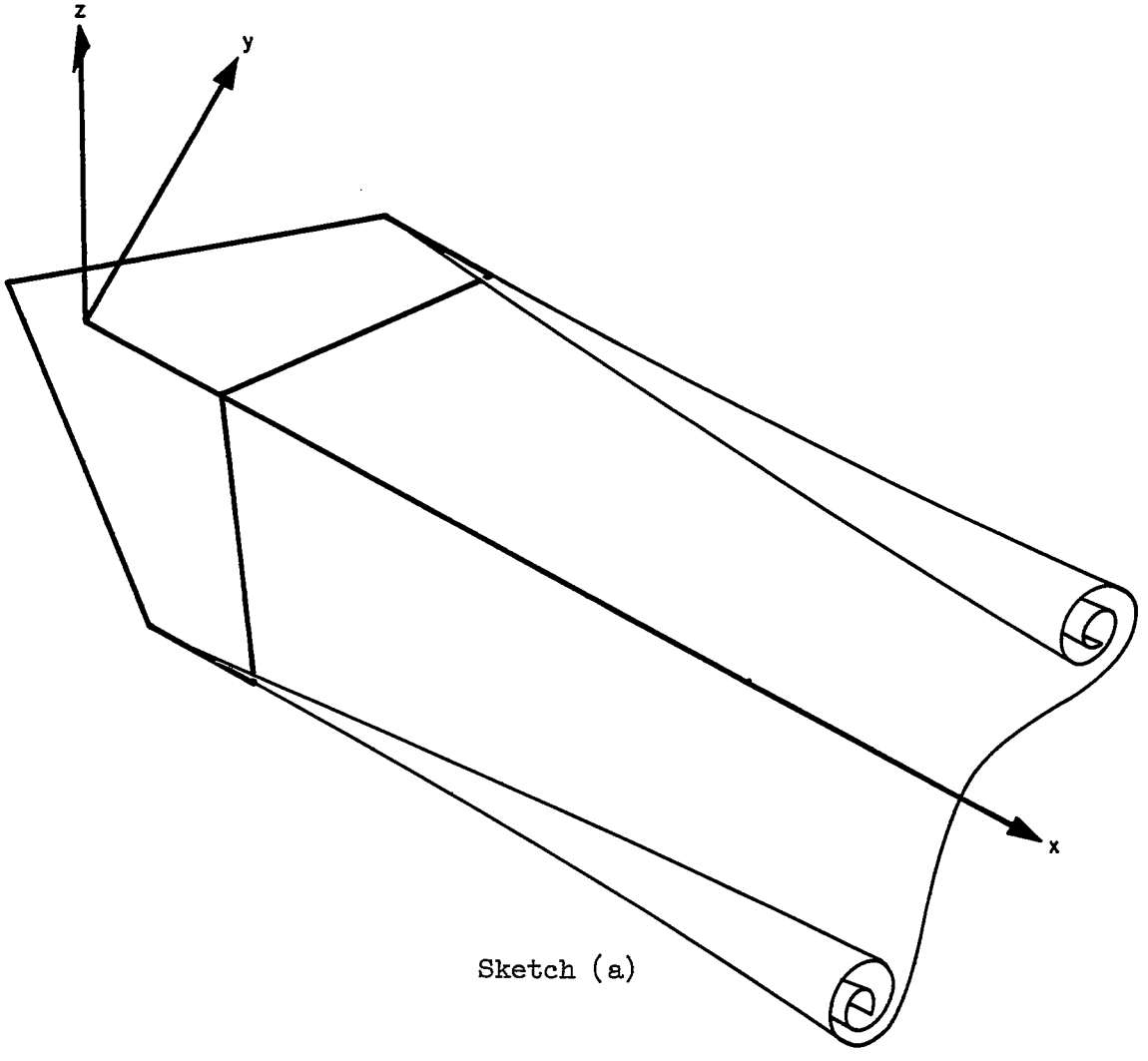

Sketch (a)

The first assumption for the analysis will be that all of the chordwise lift is concentrated at the chordwise center of pressure which will be taken as the wing quarter-chord line. Second, it will be assumed that the flow on the wing is not separated. Third, it will be assumed that the

downwash due to a symmetrical sheet can be approximated by a horizontal flat sheet passing through the symmetrical sheet at the lateral station where the downwash is to be computed. It should be noted that at

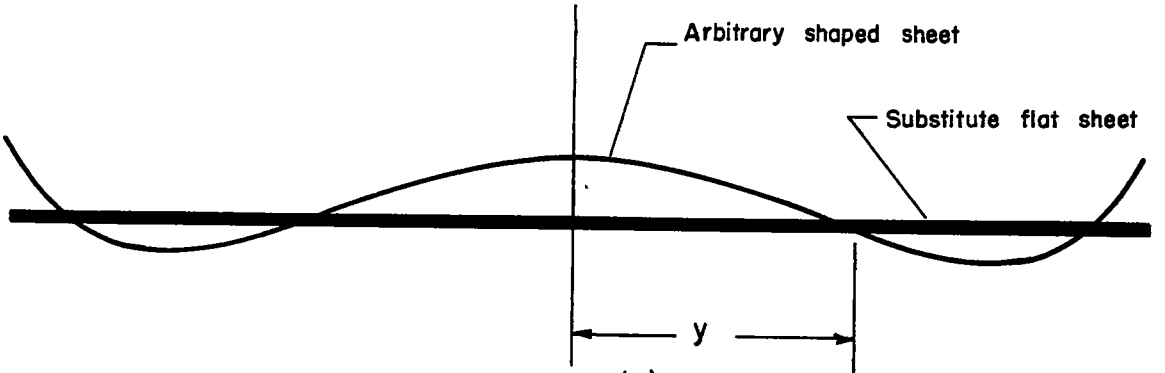

Sketch (b)

each η station, the horizontal flat sheet is given a different vertical location and thus some allowance is made for the shape of the sheet. Fourth, it will be assumed that the vertical-longitudinal inclination of the system has no effect upon the downwash. Hence, the real system will be approximated by a horizontal flat system passing through the real system at the downstream station, x, at which downwash is to be computed, as is shown below. The coordinates of the real and substitute systems

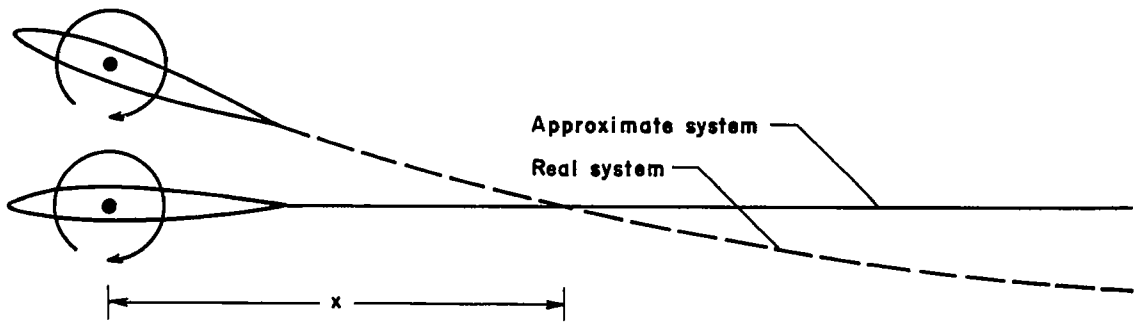

Sketch (c)

are shown in figure 1. It should be noted that these four assumptions are identical with those made by Silverstein and Katzoff in references 1 and 2. The first two assumptions are common in aerodynamics and the limitations are fairly well known for the higher aspect ratios. The first assumption will now be further investigated for wings of fairly low aspect ratio.

Two wings having taper ratios of 0 and 1.0, aspect ratio equal to 2.0, and sweep angle of 56° were investigated. Each wing was assigned both cotangent-type chord loading and uniform chord loading. The spanwise loadings were obtained from reference 5. For each wing and chordwise loading, the downwash in the wake, ϵ_s, was computed with each of three alternative approximations; namely, the chordwise loading was replaced, respectively, by a single lifting line, by three lifting lines,

and by five lifting lines. The strength and chordwise positions of the lifting lines were set by dividing the chord into equal segments and finding the lift and center of lift of each segment. Each lifting line was treated as a flat, horizontal vortex system in the $\Omega = 0$ plane. The downwash angles of the lifting-line systems were added and the sums are plotted in figure 2 for four spanwise stations.

Figure 2 indicates that the single lifting line does not give accurate downwash predictions just aft of the trailing edge of the wing. The downwash fields for the wings of equal λ are essentially the same one mean chord (one semispan) aft of the wing trailing edge. This concurrence at one mean wing chord aft agrees with the two-dimensional example of reference 1. For cotangent chord loading, the five-lifting-line method very nearly predicts ϵ/α equal to unity at the wing trailing edge. This can be considered as a check to the approximation since the flat-plate downwash must be equal to α at the trailing edge. Examination of figure 2 shows that the curve of downwash obtained by using one lifting line is translated forward a nearly constant longitudinal distance from the curve of downwash obtained by using five lifting lines. In figure 2(a), this distance is one eighth the mean wing chord.

In reference (1), contours of downwash angles due to a two-dimensional Clark Y airfoil section are compared to contours of downwash angles computed for a lifting line at the c/4 point. If the lifting line is shifted back to the (3/8)c point, the shifted field agrees well with that of the airfoil section even very near the trailing edge. From this, it would appear that the downwash field due to surface loading might be well approximated for all wings by using a single lifting line with all longitudinal distances reduced by $(1/8)c_{av}$, or replacing τ by $\tau - (1/4)(c/b)_{av}$. It should be noted that this correction is of significance only in vicinity of the trailing edge.

The third assumption has been considered by comparing the results obtained by using the assumption against results calculated for an elliptically shaped sheet whose ratio of minor to major axes was 0.4. At $\eta = 0$, 0.383, and 0.707, the difference of the results was less than the differences found in the examination of the first assumption. At $\eta = 0.924$, use of the above third assumption did not compare well with the results for the elliptically shaped sheet. However, at low angles of attack, since the distortion of the sheet is small the downwash can still be computed at $\eta = 0.924$. The fourth assumption has been checked by numerical computation for a 60° sweptback wing of aspect ratio equal to 3.5. It was found that provided that ϵ of the noninclined system is taken as w/V rather than $\tan^{-1}(w/V)$, the difference between the downwashes was less than the differences noted in examination of the first assumption. This appears to hold true up to about $\alpha = 20^\circ$. Thus, throughout this report, ϵ will be taken as w/V and the subject is thus treated as if only small angles were involved.

It should also be noted that these four assumptions are commonly used in the calculation of wing span loading. As a result, the "non-rolling-up"[1] system can be treated in a manner analogous to Multhopp's (ref. 5) or Weissinger's (given in ref. 6) approximate integrations in their calculations of span loading. However, a principal problem not encountered in span-loading work is the downwash at arbitrary vertical locations.

Generally, the amount of rolling-up present is so small that the foregoing assumptions are sufficient for good answers. However, as C_L/A increases, an increasing amount of rolling-up appears and a correction must be made for this effect. The principal features of a trailing-vortex system where the rolling-up is conspicuous are, (1) the vorticity becomes vertically displaced and shifts outboard from the plane of symmetry, and (2) the wing tip vortices trail back approximately in a horizontal plane which is parallel to the free stream. The center of the sheet, however, is still displaced downward. As the vortex sheet is left farther behind the wing, the tips of the sheet roll up and form concentrated tip vortices. An outward motion of the vorticity in the sheet between the tip vortices results in less vorticity in the mid-semispan regions. These two changes in vorticity configuration can (in the main) be taken into account by making a fifth assumption, (1) a vertically displaced trailing flat sheet having a reduced amount of vorticity, and (2) a pair of tip vortices which lie in a horizontal plane and whose strength is drawn from the sheet. With this arrangement, the sheet can be handled in much the same fashion as the flat sheet, that is, by using the first four assumptions. The tip vortices can then be handled as a separate computation.

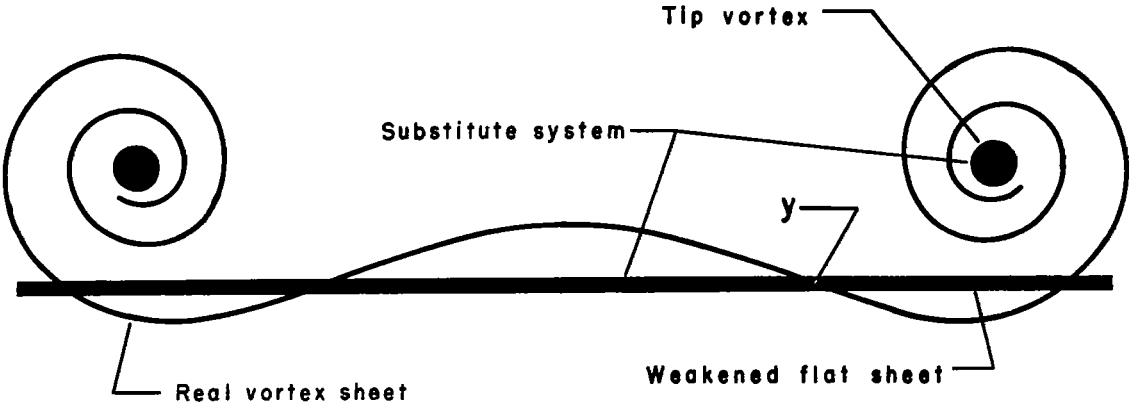

Sketch (d)

At various distances behind the wing, the rolling-up is in various stages of development. To obtain an accurate approximation, one should

[1]Nonrolling-up system assumes that the trailing vortex sheet has the same lateral distribution of vorticity at all distances behind the wing as at the wing trailing edge. However, it need not be flat although for determining downwash it is assumed flat.

consider the trailing system in longitudinal segments, each segment having a different amount of rolling-up. The downwash would then be the sum of the downwashes of all the segments. However, this involves an exorbitant amount of work and to obtain a practical solution, a sixth assumption will be made. It will be assumed that the entire trailing system behind the wing is of one form, namely, the form which the real system has at the selected downstream location ξ. The substitute rolling-up system is then pictured as shown in sketch (e).

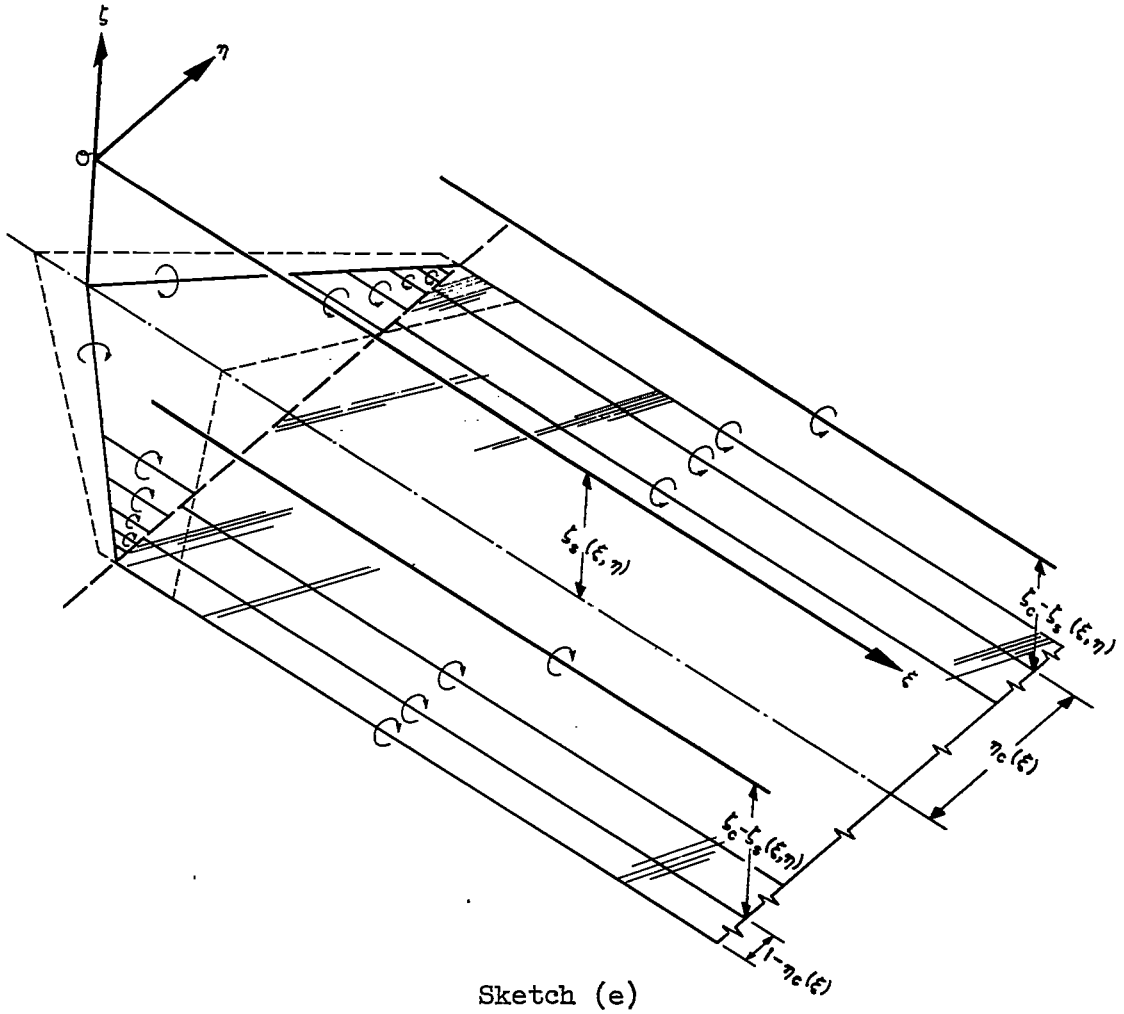

Sketch (e)

This sixth assumption was examined by numerical computations for a 60° sweptback wing of $A = 3.5$ using the segment approximation. It was found that the results of the use of this assumption were within the accuracy of the theory for this case.

While the foregoing assumptions aid in simplifying the physical picture, additional information is necessary in order to calculate the effect of the rolling-up process. The relative strengths of the vortex

sheet as well as the tip vortex and also the position of the tip vortex for various distances behind the wing must be obtained. From an analysis of the downwash behind a series of swept-wing plan forms obtained from large-scale wind-tunnel data, an empirical relationship was developed giving the approximate lateral position of the tip vortex. From this, a method is developed for obtaining the relative strengths of the tip vortex and flat sheet.

As will be shown in the text, the use of such a simplified substitute system enables one to express the downwash due to a rolling-up system as being the flat-sheet results plus an additive correction (generally, fairly small) which, for the case checked, predicted the downwash well and goes to the right limit as the rolling-up becomes complete.

ANALYSIS AND DEVELOPMENT OF METHOD

The first part of the analysis is concerned with the flat-sheet procedure, that is, evaluating the downwash using the first four assumptions. The location of the wake relative to the tail will be considered and some assessment of the effects of the fuselage upon the downwash is to be made. In the second part of the analysis, the rolling-up of the trailing vortex sheet is considered.

Flat-Sheet Procedure

General calculation of downwash.- The downwash at a point (x,y,z) due to a swept-vortex system (assumed for the present at $z_s = 0$) is equal to the sum of that due to the swept-load vortex (or bound vortex) and that due to the trailing vortex sheet.

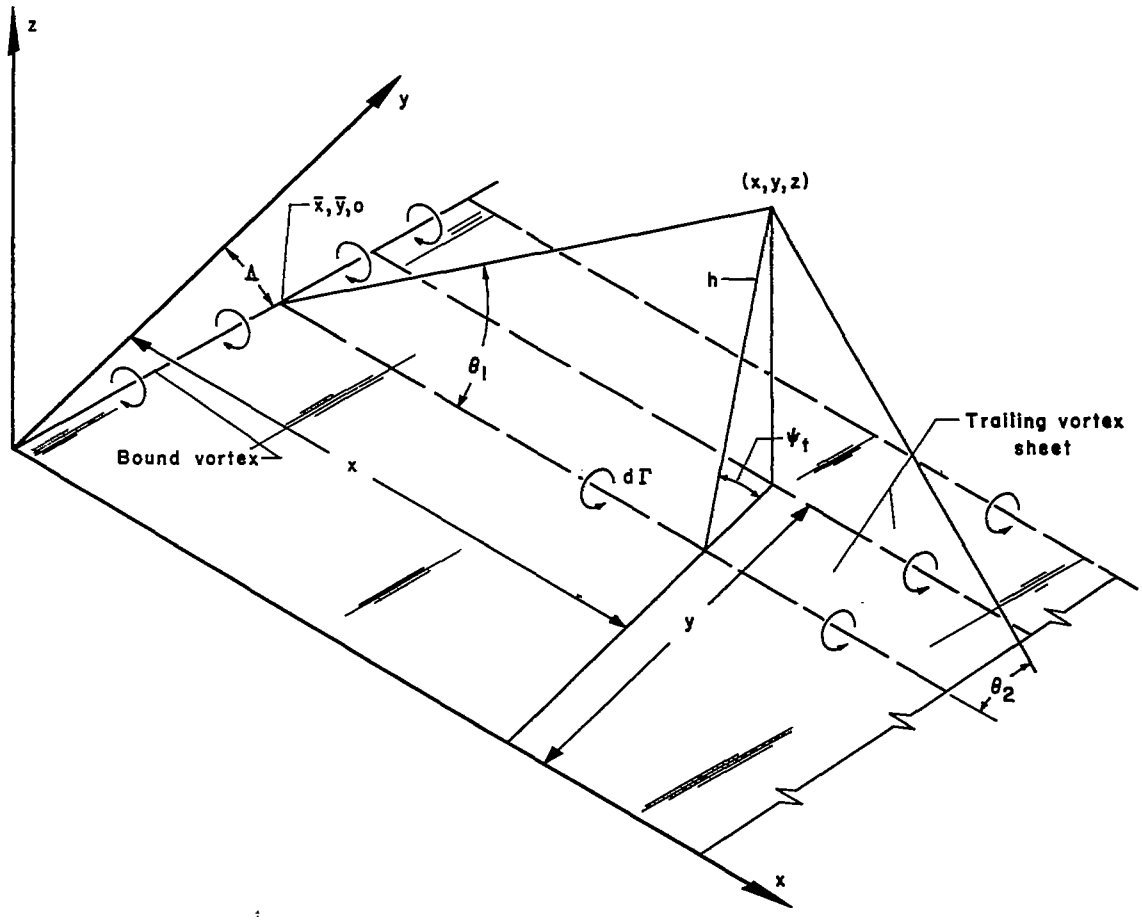

Sketch (f)

The induced velocity due to an arbitrary elemental trailing vortex extending to infinity downstream (see sketch (f)) is given by Glauert (ref. 7).

$$dw = \frac{d\Gamma}{4\pi h} (\cos \theta_1 + \cos \theta_2) \cos \psi_t \tag{1}$$

where $\theta_2 \longrightarrow 0$. The vertical induced velocity at (x,y,z) due to the small element ds of the load vortex (see sketch (g)) is given by

$$dw = \frac{\Gamma h \, ds \cos \psi_b}{4\pi r^3} \tag{2}$$

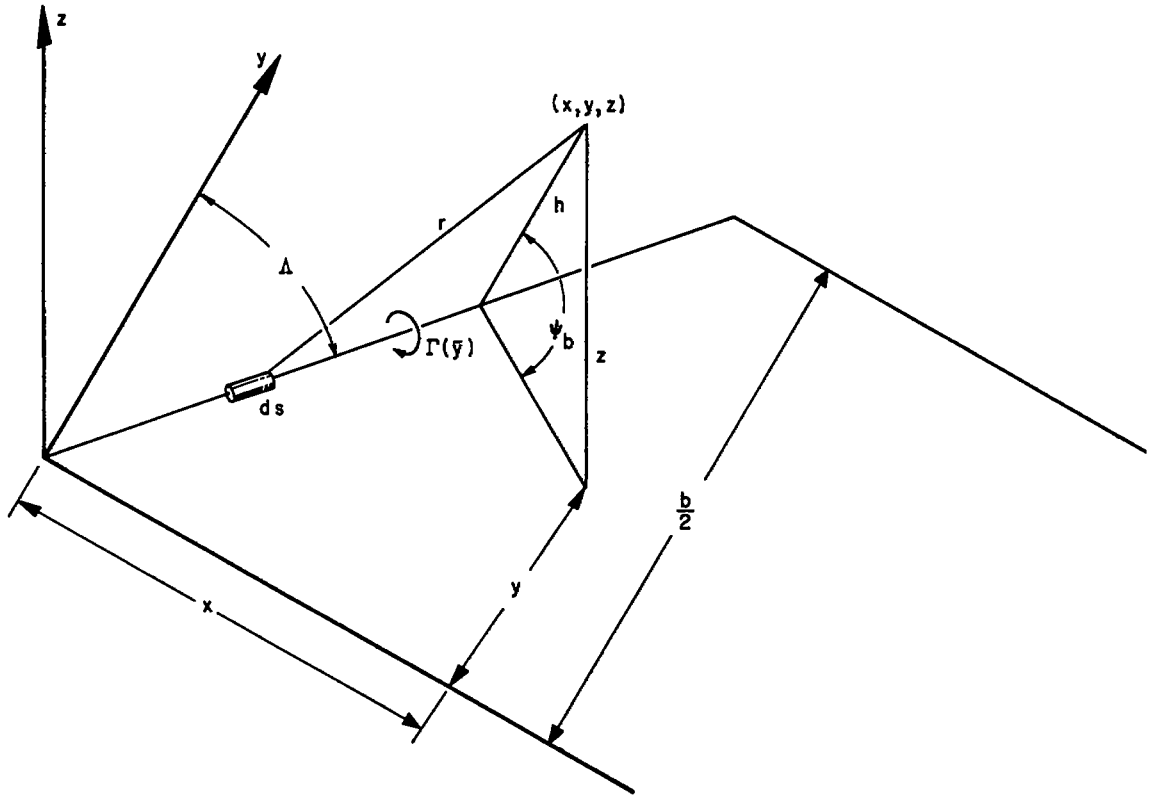

Sketch (g)

The total downwash due to the entire vortex system is equal to the integration over the wing span of the sum of equations (1) and (2) (which are converted to rectangular coordinates by the relations indicated in the respective sketches). Further, the integral of equation (2) is integrated by parts such that the new integrand contains the factor $d\Gamma/d\bar{\eta}$. Then in terms of dimensionless relations, the total downwash can be written as:

$$\frac{w}{V} = \frac{1}{\pi}\int_{-1}^{1} \frac{(\eta-\bar{\eta})G'(\bar{\eta})d\bar{\eta}}{\Omega^2 + (\eta-\bar{\eta})^2} + \frac{1}{2\pi}\int_{-1}^{1} L_{s\mu}\, G'(\eta)\, d\bar{\eta} \qquad (3)$$

where for $\bar{\eta} \geq 0$,

$$L_{s\mu} = \frac{\dfrac{(\eta-\bar{\eta})\,[\tau + (|\eta|-|\bar{\eta}|)\tan\Lambda]}{\Omega^2 + (\eta-\bar{\eta})^2} - \dfrac{[\tau + (|\eta|-\eta)\tan\Lambda]\left(\dfrac{\bar{\eta}}{\cos^2\Lambda} - \eta - |\eta|\tan^2\Lambda - \tau\tan\Lambda\right)}{[\tau + (|\eta|-\eta)\tan\Lambda]^2 + \Omega^2/(\cos^2\Lambda)}}{\sqrt{[\tau + (|\eta|-|\bar{\eta}|)\tan\Lambda]^2 + (\eta-\bar{\eta})^2 + \Omega^2}} - \frac{\eta - \bar{\eta}}{\Omega^2 + (\eta-\bar{\eta})^2} \tag{4}$$

and for $\bar{\eta} \leq 0$,

$$L_{s\mu} = \frac{\dfrac{(\eta-\bar{\eta})\,[\tau + (|\eta|-|\bar{\eta}|)\tan\Lambda]}{\Omega^2 + (\eta-\bar{\eta})^2} - \dfrac{[\tau + (|\eta|+\eta)\tan\Lambda]\left(\dfrac{\bar{\eta}}{\cos^2\Lambda} - \eta + |\eta|\tan^2\Lambda + \tau\tan\Lambda\right)}{[\tau + (|\eta|+\eta)\tan\Lambda]^2 + \Omega^2/(\cos^2\Lambda)}}{\sqrt{[\tau + (|\eta|-|\bar{\eta}|)\tan\Lambda]^2 + (\eta-\bar{\eta})^2 + \Omega^2}} +$$

$$\frac{\dfrac{[\tau + (|\eta|-\eta)\tan\Lambda](\tau\tan\Lambda + |\eta|\tan^2\Lambda + \eta)}{[\tau + (|\eta|-\eta)\tan\Lambda]^2 + \Omega^2/(\cos^2\Lambda)} + \dfrac{[\tau + (|\eta|+\eta)\tan\Lambda](\tau\tan\Lambda + |\eta|\tan^2\Lambda - \eta)}{[\tau + (|\eta|+\eta)\tan\Lambda]^2 + \Omega^2/(\cos^2\Lambda)}}{\sqrt{(\tau + |\eta|\tan\Lambda)^2 + \eta^2 + \Omega^2}} -$$

$$\frac{\eta - \bar{\eta}}{\Omega^2 + (\eta - \bar{\eta})^2} \tag{5}$$

Both integrals of equation (3) are, in general, difficult to integrate by analytical means. The numerical integration method used herein is that employed by both Multhopp and Weissinger. In fact, equation (3) appears in reference 6 for the case of $\Omega = 0$. As was done in reference 6, the downwash integrals can be written as a summation of products of mathematical coefficients, a_{sn} (a_{vn} in refs. 3 and 6), and the spanwise loading, $K_n = (c_l c/C_L\, c_{av})_n$. As is shown in Appendix A, the numerical integration of equation (3) can be put into the form (using a four-term expression)

$$\epsilon = \frac{w}{V} = \frac{C_L}{2A} \sum_{n=1}^{4} a_{sn} K_n \tag{6}$$

where for $n = 1, 2, 3$, and 4, the K_n's correspond to values of $c_l c/C_L c_{av}$ at $\eta = 0.924$, 0.707, 0.383, and 0, respectively. The a_{sn}'s, like the $L_{s\mu}$ in equation (3), are solely dependent, for a given sweep angle, upon the location of a point (τ,η,Ω). Thus, after the a_{sn}'s have been evaluated, one may compute the downwash using any desired span loading. To facilitate computations, the a_{sn}'s (from general equations of Appendix A) have been computed for points at $\eta = 0$, 0.383, 0.707, and 0.924 lying behind the quarter-chord line and for two vertical locations relative to the vortex sheet, $\Omega = 0$ and $\Omega = \pm 0.5$, that is, at the sheet and one-half semispan above or below the sheet. The computed values have been plotted in figures 3 and 4. Thus, given a plan form, span loading, and the desired longitudinal position, one obtains values of a_{sn} from figures 3 and 4 and applies equation (6) to obtain the downwash.

It is obvious that the accuracy of a summation depends upon how many terms are considered. For the four-term summation used herein, acceptably accurate answers are obtained in most cases without an unreasonable expenditure of labor. However, for cases in which the spanwise loading differs from that expressible by a four-term sine series, the four-term summation may not be acceptably accurate as it would tend to gloss over such changes in span loading. The derivation of the a_{sn}'s in Appendix A has been left in a fairly general form so as to allow the reader to compute the a_{sn}'s for summations involving more points across the span.

Choice of vertical coordinates.- Three possible vertical coordinates are the parameters Ω, ζ, and Z. The vertical position of the downwash point for these three is measured respectively from (1) the trailing sheet, (2) a horizontal plane (parallel to free stream) through the apex of the load line, and (3) the extended chord plane. Each has some advantages. With Ω, the downwash field is symmetric about the value $\Omega = 0$ (for a flat sheet), or about the trailing sheet. Also, computations are simplified with this parameter and the downwash varies linearly with C_L. On the other hand, with ζ, the downwash field is referred to a fixed coordinate system, independent of angle of attack and sheet position. With Z, the downwash field is referred to the coordinate system (extended chord plane) of the airplane but is dependent on angle of attack. Thus, with Z, the downwash field is described relative to the tail plane.

The relations between Ω, ζ, and Z are:

$$\left.\begin{aligned} \Omega &= \zeta - \zeta_s(\eta) \\ Z &= \Omega + \zeta_s(\eta) + \xi \tan \alpha \\ &= \zeta + \xi \tan \alpha \\ &= \zeta + (\tau + \eta \tan \Lambda)\tan \alpha \end{aligned}\right\} \tag{7}$$

When the downwash has been computed for various Ω's and the displacements, $\zeta_s(\eta)$, have been evaluated, the field can be plotted against a choice of Ω, ζ, or Z.

Lateral interpolation of downwash.- The a_{sn} values of figures 3 and 4 allow a direct evaluation of downwash at four span stations. Sometimes it is of value to know the downwash at other span positions or to plot a more accurate lateral variation of downwash. For these purposes a lateral interpolation formula is convenient.

The product $\epsilon(\varphi) \sin \varphi$ can be expanded in a Fourier series, the coefficients of which can be numerically evaluated in terms of the four known values of ϵ_n. Then (for symmetric distribution of downwash)

$$\epsilon(\varphi)\sin \varphi = \sum_{\mu_1=1,\text{odd}}^{7} \sin \mu_1\varphi \sum_{n=1}^{7} \frac{\epsilon_n \sin \varphi_n}{4} \sin \mu_1\varphi_n \tag{8}$$

where $\varphi = \cos^{-1} \eta$. Then the downwash at a given η position can be expressed as the sum of products of tabulated numbers and values of the known downwash. Thus

$$\epsilon = H_1\epsilon_1 + H_2\epsilon_2 + H_3\epsilon_3 + H_4\epsilon_4 \tag{9}$$

where the H's are tabulated in table I for η = 0.098, 0.195, 0.290, 0.556, 0.831, and 0.981, and ϵ_n are the known values of downwash at η = 0.924, 0.707, 0.383, and 0.

Examination of table I shows that in the range of η from 0 through 0.556, H_1 is very small, less than 4.5 percent of the sum of H_2, H_3, and H_4. For this range of η, one can simplify the calculations by letting $\epsilon_1 = \epsilon_2$, then equation (9) reduces to, for $0 \leq \eta \leq 0.556$,

$$\epsilon = (H_1 + H_2)\epsilon_2 + H_3\epsilon_3 + H_4\epsilon_4 \tag{10}$$

This method of interpolation, in effect, puts a curve of the form

$$\epsilon(\eta) = e_0 + e_2\eta^2 + e_4\eta^4 + e_6\eta^6$$

(where the e's are constants) through the known values of ϵ at the four regular span stations. Of course, equation (10) goes through only three of the four known values.

The lateral interpolation formula applies for a given Ω along an arbitrary $\xi(\eta)$ curve (e.g., at constant ξ or at a constant τ).

Vertical interpolation of downwash.- The a_{sn} values of figures 3 and 4 allow a direct evaluation of downwash at $\Omega = 0$ and ± 0.5. To present a_{sn} charts for many Ω values is too cumbersome. However, with only two values of Ω available, an interpolation procedure is a prime necessity.

Reference 8 presents a simple method in which downwash, for small Ω, is expressed as a Taylor series of $|\Omega|$. Reference 7 contains a simple equation of downwash as a function of Ω for large Ω values. With these functions of Ω and the computed value of downwash at $\Omega = \pm 0.5$, a fitted function of Ω is developed in Appendix B that approaches the correct functions at low and high values of Ω and fairs through the computed value at $\Omega = \pm 0.5$.

The vertical interpolation function is given as

$$\epsilon = C_1\epsilon(\tau,\eta,o) + C_2\epsilon\left(\tau,\eta,\frac{1}{2}\right) + \frac{C_L}{2A}\sum_{n=1}^{4} D_nK_n \qquad (11)$$

where C_1, C_2, and D_n are tabulated in table II for several $\pm\Omega$ values; $\epsilon(\tau,\eta,o)$ and $\epsilon(\tau,\eta,\pm 1/2)$ are the values of downwash computed by equation (6) at $\Omega = 0$, and $\pm 1/2$, respectively.

Vertical displacement of the sheet.- The vertical displacement of the sheet is given by the integration in the longitudinal direction (for constant η) of the downwash in the sheet from the wing trailing edge to the τ and η position of the downwash point. Thus, for a given η,

$$\zeta_s(\tau) = \zeta_{TE} - \int_{\tau_{TE}}^{\tau} \epsilon_s[\tau_T,\zeta_s(\tau_T)]\, d\tau_T \qquad (12)$$

where ζ_s is the vertical displacement of the sheet, τ_T is a dummy variable of integration, and ζ_{TE} is the vertical displacement of the wing trailing edge. Now Ω is defined as $\zeta - \zeta_s$, then $\zeta_s(\tau_T)$ in the integrand corresponds to the value $\Omega = 0$. With the flat-sheet assumptions, ϵ_s (the downwash angle at the sheet, i.e., $\Omega = 0$) is independent of any vertical parameter and can be integrated to evaluate $\zeta_s(\tau)$.

The integration in equation (12) can be simplified considerably by approximating ϵ_s with an integrable function of τ_T. An analytical study of figure 2 indicates that the downwash behind the surface-loaded wing varies closely as $1/\tau^2$, also that the single-load-line method underestimates the downwash near the wing. The simplicity of the $1/\tau^2$ behavior suggests a very convenient curve-fitting function for downwash that can in addition be made to correspond with the downwash near the wing as predicted by surface-loading methods. Thus it will be assumed that the downwash is given by the following function ($\Omega = 0$, and using the dummy variable τ_T)

$$\epsilon_s(\tau_T) = E_1 + \frac{E_2}{(\tau_T - j)^2} \tag{13}$$

where E_1, E_2, and j are undetermined coefficients. For the determination of E_1 and E_2, two conditions are given by

$$\left.\begin{array}{lll} \text{at } \tau_T = \tau_{TE}, & \epsilon_s(\tau_T) = \alpha_{TE} & \\ \text{at } \tau_T = \tau\ , & \epsilon_s(\tau_T) = \epsilon_s, & \text{known downwash at the position at which displacement is to be computed} \end{array}\right\} \tag{14}$$

With E_1 and E_2 determined it remains to evaluate j. Comparison of the results of several values of j with the downwash fields given in figure 2 shows that for $j = c/2b$ very good agreement is obtained even with ϵ_s taken at a distance of two semispans aft of the wing trailing edge.

With the value $j = c/2b$ and the determined values of E_1 and E_2, equation (13) becomes

$$\epsilon_s(\tau_T) = \frac{1}{\left(\tau - \frac{c}{2b}\right)^2 - \left(\tau_{TE} - \frac{c}{2b}\right)^2}\left[\left(\tau - \frac{c}{2b}\right)^2 \epsilon_s - \left(\tau_{TE} - \frac{c}{2b}\right)^2 \alpha_{TE} + \frac{\left(\tau - \frac{c}{2b}\right)^2 \left(\tau_{TE} - \frac{c}{2b}\right)^2 \left(\alpha_{TE} - \epsilon_s\right)}{\left(\tau_T - \frac{c}{2b}\right)^2}\right] \tag{15}$$

Inserting equation (15) into equation (12) evaluates the vertical displacement.

$$\zeta_s = \zeta_{TE} - \frac{\tau - \tau_{TE}}{\left(\tau - \frac{c}{2b}\right) + \left(\tau_{TE} - \frac{c}{2b}\right)} \left[\left(\tau - \frac{c}{2b}\right) \epsilon_s + \left(\tau_{TE} - \frac{c}{2b}\right) \alpha_{TE} \right] \tag{16}$$

where ϵ_s is computed at any τ, η position but with $\Omega = 0$.

For a wing having an airfoil section such that the load line is at the one-quarter chord and with $\alpha_{TE} = \alpha$, equation (16) simplifies to

$$\zeta_s = -\left[(\tau + \eta \tan \Lambda)\alpha - \frac{\left(\tau - \frac{3c}{2b}\right)\left(\tau - \frac{c}{2b}\right)}{\left(\tau + \frac{c}{2b}\right)} (\alpha - \epsilon_s) + \left(\frac{3c}{2b} + \eta \tan \Lambda\right)\left(\tan \alpha - \alpha\right) \right] \tag{17}$$

It should be noted that the last term of equation (17) is negligibly small for many practical cases.

Equation (16) expressed as vertical displacement of the trailing sheet or wake from the extended-chord plane is given by (see eq. (7))

$$Z_s = \frac{\tau - \tau_{TE}}{\left(\tau - \frac{c}{2b}\right) + \left(\tau_{TE} - \frac{c}{2b}\right)} \left[\left(\tau - \frac{c}{2b}\right)\left(\tan \alpha - \epsilon_s\right) + \left(\tau_{TE} - \frac{c}{2b}\right)\left(\tan \alpha - \alpha_{TE}\right) \right] \tag{18}$$

For a wing having an airfoil section such that the lifting line is at the one-quarter chord and for $\alpha_{TE} = \alpha$, equation (18) simplifies to

$$Z_s = \frac{\tau - \frac{3c}{2b}}{\tau + \frac{c}{2b}} \left[\left(\tau - \frac{c}{2b} \right) (\tan \alpha - \epsilon_s) + \left(\frac{c}{b} \right) (\tan \alpha - \alpha) \right] \quad (19)$$

For many practical cases, the last term of equation (19) can be neglected.

Correction for the Effect of the Rolling-Up of the Sheet

General analysis.- If the vorticity shed from the wing is now considered to make up a weakened sheet and two tip vortices, as discussed earlier, then the correction, $\Delta\epsilon$, to be added to the downwash calculated in the foregoing sections can be written as

$$\Delta\epsilon = \epsilon_{WS} + \epsilon_c - \epsilon_{TS}$$

where ϵ_{WS} is the downwash due to a weakened vortex sheet; ϵ_c is the downwash due to a pair of tip vortices. The weakened sheet and the tip vortices extend from a longitudinal position corresponding to the quarter-chord point of wing tip, downstream to infinity. The quantity, ϵ_{TS}, is the downwash due to the portion of the flat sheet aft of the quarter chord of the tip. Letting

$$\epsilon_T = \epsilon_{TS} - \epsilon_{WS}$$

$\Delta\epsilon$ becomes

$$\Delta\epsilon = \epsilon_c - \epsilon_T \quad (20)$$

which gives $\Delta\epsilon$ equal to the downwash due to the tip vortices minus the downwash due to the loss of vortex strength in the trailing vortex sheet.

The downwash due to only a trailing sheet extending from the quarter chord of the rearmost wing section can be deduced from equation (1) by considering an unswept wing. Replacing ξ by $(\xi - \tan \Lambda)$ then refers the coordinates to the quarter chord of the wing tip. Following the same mathematical procedures as in Appendix A, it is shown in Appendix C that the downwash due to such a trailing sheet can be reduced to

$$\frac{w}{V} = \frac{C_L}{2A} \sum_{n=1}^{4} a_{Tn} K_n \tag{21}$$

The difference between $\epsilon_{\text{flat sheet}}$ and $\epsilon_{\text{weakened sheet}}$, ϵ_T, can be considered as the loss of downwash due to the weakening of the sheet. This weakening can be taken into account by multiplying K_n in equation (21) by a term called a strength factor.

Thus, ϵ_T reduces to

$$\epsilon_T = - \frac{C_L}{2A} \sum_{n=1}^{4} a_{Tn} F_{sn} K_n \tag{22}$$

where F_{sn} will be called the strength factors of the sheet and denotes a loss of strength in the trailing vortex sheet. Thus, $1 - F_{sn}$ is the proportion of vorticity left in the sheet. The a_{Tn}'s are plotted as a function of $(\xi - \tan \Lambda)/\beta$ in figure (5).

The downwash due to a pair of tip vortices is equivalent to the downwash due to a trailing sheet behind a uniformly loaded wing of span $\eta_c b$. Thus, ϵ_c can be derived from the preceding work. The circulation of the tip vortices is $F_c C_L / \eta_c A$ where F_c denotes the proportion of wing vorticity in the tip vortices. Expressions for $\epsilon_c \eta_c A / F_c C_L$ are derived in Appendix C and values are presented in figure 6. This parameter is plotted as a function of $(1/\beta\eta_c)(\xi - \tan \Lambda)$ for various values of η/η_c and Ω_c/η_c. The quantity, Ω_c (vertical height relative to the tip vortices), is equal to $\zeta - \alpha \tan \Lambda$ or $\Omega + \zeta_s - \alpha \tan \Lambda$, where $-\alpha \tan \Lambda$ is the vertical location of the tip vortex which will be presented shortly.

As yet, F_{sn} and F_c have not been determined and, as was stated earlier, one must determine the locations of the tip vortices before proceeding to find the strength factors.

Location of tip vortices.- Reference 4 presents an approximate (curve-fitting) equation for the lateral position of the tip vortices. This equation is given by

$$\eta_c = 1 - (1 - \eta_{c_\infty}) \tanh \left(\frac{\xi - \xi_o}{\xi_c - \xi_o} \right)^{2/3} \tag{23}$$

where

$$\xi_c - \xi_o = \frac{5.05\,(1 - \eta_{c_\infty})^{3/2}}{\lim_{\varphi \to 0} \frac{G(\varphi)}{\sqrt{1 - \cos\varphi}}} \tag{24}$$

where $\eta_{c_\infty} = 1/K_4$ and represents the asymptotic position of η_c, and ξ_o indicates the start of the rolling-up process. In the last part of Appendix C, ξ_c is reduced to the more convenient form

$$\xi_c - \xi_o = \frac{(1 - \eta_{c_\infty})^{3/2}\left(\frac{A}{C_L}\right)}{0.7315\,K_1 - 0.3959\,K_2 + 0.3030\,K_3 - 0.1400\,K_4} \tag{25}$$

It should be noted that equations (23) and (24) were derived for a wing having an unswept trailing edge.

It has been found from experiment that, for a swept wing, the inward movement of the tip vortices is much slower than is indicated by equation (23). The reasons for this slowness are not clear. However, the lateral positions of the tip vortices appear to be strongly dependent upon the sweep of the wing trailing edge.

The following two considered opinions of the actions of the air flow behind such a wing are given here. First, in the region between the two swept wing panels, the vortex sheet (principally near the plane of symmetry) is above both the load vortex of the wing and the wing tip vortices and thus is subjected to an inward velocity component. This inward velocity tends to keep the vorticity in the midspan region out of the tip vortices and thereby increases the roll-up distance. A second action concerns the wing tip. For a sweptback wing, an outward velocity over the wing tips is generated due to the lateral pressure gradient resulting from the staggering of wing sections. This flow over the wing tip is here assumed the primary action that results in a further outboard location of the tip vortex relative to that of an unswept wing. Similar reasoning leads to converse effects for sweptforward wings. The velocities involved in the above phenomena are difficult to determine. A problem remains, however, in that an expression for η_c (compatible with experiment) must be found.

The problem of theoretically determining η_c for a wing with swept trailing edges is even more difficult than for an unswept wing. Therefore, an empirical equation will be used herein. One approximate method that takes into account the effect of the initial outward lateral

location of the tip vortices (due to the sweep) is to multiply $(1 - \eta_{c_\infty})$ of equation (23) by

$$\frac{f + (1/10)(\xi - \tan \Lambda)}{1 + (1/10)(\xi - \tan \Lambda)}$$

where f is a function of the sweep of the wing trailing edge. At large values of $\xi - \tan \Lambda$, this factor approaches unity and η_c approaches $1/K_4$. In the midspan region as mentioned previously, there is an inward velocity imposed upon the trailing vortex sheet which results in a longer roll-up distance. It is found that this can be taken into account by multiplying the argument of tanh in equation (23) by f^2 where f here is the same as the previous f for convenience of empirical evaluation. The effect of this multiplication is to increase the roll-up distance by a factor of $(1/f)^3$. Then, assuming the tip vortex to start at the quarter chord of the wing tip[2] ($\xi_o = \tan \Lambda$), equation (23) becomes

$$\eta_c = 1 - \left[\frac{f + (1/10)(\xi - \tan \Lambda)}{1 + (1/10)(\xi - \tan \Lambda)}\right]\left(1 - \frac{1}{K_4}\right)\tanh\left[f^2\left(\frac{\xi - \tan \Lambda}{\xi_c - \tan \Lambda}\right)^{2/3}\right] \tag{26}$$

where $\xi_c - \tan \Lambda$ is given by equation (25) for $\xi_o = \tan \Lambda$.

Equation (26) can be solved for f, since, for small values of the argument in tanh, the argument itself can be taken. A cubic equation results from which f can be determined from experimental measurements of η_c. Five wings with sweep angles of the trailing edge ranging from -41.3° to 51.9° were used in determining f. To the precision of the experiments, f is given by,

$$f = 1 - 0.0075\,(\Lambda^\circ_{TE} + 7^\circ) \tag{27}$$

It has been assumed that f is independent of aspect ratio. It should be noted that f does not quite reach unity at $\Lambda^\circ_{TE} = 0$. Thus equation (26) does not quite reduce to equation (23) for wings with unswept trailing edges. The difference, however, is small and is not considered important.

[2]This is in contradistinction from reference 4 which assumes the tip vortex to start at the wing trailing edge.

It should be realized that other expressions for η_c can be obtained. Since only the numerical value of η_c is important, the use of other expressions of η_c will not affect the material following. Later in the discussion section, it is shown that values of η_c from equation (26) compare well with the limited available experimental results.

The vertical position of the tip vortices can be determined by using the fifth assumption in the previous section. Then, since the tip vortices are assumed to start at the quarter chord of the wing tip, the vertical displacement of the two tip vortices is approximately given by the vertical position of the quarter chord of the wing tip, or

$$\zeta_c \cong - \alpha \tan \Lambda \tag{28}$$

It should be noted that far behind the wing, after the rolling-up process is essentially completed, the influence of one tip vortex on the other causes a displacement that varies linearly with ξ. The use of equation (28) therefore is restricted to locations near the wing.

Strength factors of the trailing sheet and wing tip vortices.- The rolling-up trailing-vortex system is greatly simplified with the vortex system divided into two parts, (1) a pair of rolled-up wing tip vortices, and (2) a vortex sheet stretching laterally between the two wing tip vortices (see sketch (d)). The problem is to determine what proportion of the total vortex strength each should have. A method attributed to Lotz and Fabricius in reference 4 (given originally in ref. 9) is readily applicable for unswept wings. A modified and somewhat simplified procedure of this method is developed here for swept wings.

The basis of the method depends on two vortex laws applied to the rolling-up trailing-vortex system extending downstream from each half of the wing. These laws will apply aft of the quarter-chord point of the rearmost wing section where the trailing system may be considered free and two-dimensional. These laws are:

(1) The total vortex strength shed from each half of the wing is invariant with distance downstream.

(2) The total lateral moment of the trailing vortices shed from each half of the wing (or the total lift impulse) is invariant with distance downstream.

Let $F_s(\eta)$ denote a proportional loss of strength in the trailing vortex sheet, then $1 - F_s(\eta)$ is the proportion of strength remaining in the sheet. Also let F_c denote the proportion of strength in the trailing tip vortex.

The vortex laws yield two results. First, since the total vorticity is constant, the amount of vorticity in the tip vortices equals the total amount lost by the sheet, or

$$F_c = \int_0^1 \frac{d}{d\eta}\left[F_s(\eta)\,\frac{K(\eta)}{K(o)} \right] d\eta = F_s(o) \tag{29}$$

Second, the moment gained by the tip vortices equals that lost by the sheet, or

$$F_c\eta_c = \int_0^1 \frac{d}{d\eta}\left[F_s(\eta)\,\frac{K(\eta)}{K(o)} \right] \eta d\eta = \int_0^1 F_s(\eta)\,\frac{K(\eta)}{K(o)}\, d\eta \tag{30}$$

Equations (29) and (30) are not sufficient to determine F_c and $F_s(\eta)$. However, the form of $F_s(\eta)$ can be selected so as to represent the physical actions of the rolling-up sheet to a reasonable approximation. In any rolling-up problem involving two main vortices, the vortex sheet in the outer span regions is acted on by the tip vortices more than by those in the inner regions. The outer vortex sheet rolls up at a faster rate than the inner. For these reasons the decrease of vorticity in the sheet, denoted by $F_s(\eta)$ should become larger as η becomes larger. A simple expression for $F_s(\eta)$ which approximates these phenomena is

$$F_s(\eta) = F_s(o) + \lambda\eta^2 \tag{31}$$

$F_s(\eta)$ at $\eta = \cos \varphi_n$ can be written as F_{sn}, thus

$$F_{sn} = F_{s4} + \lambda \cos^2\varphi_n \tag{32}$$

where F_{s4} is evaluated by equation (29). The parameter, λ, can be evaluated by using equation (30). Thus

$$F_{s4} = F_c$$

$$\lambda = \left(\frac{\eta_c - \eta_{c_\infty}}{\int_0^1 \eta^2 \frac{K(\eta)}{K(o)}\, d\eta} \right) F_c \tag{33}$$

The integral can be evaluated numerically by use of equation (C23) and has the value

$$\int_0^1 \eta^2 \frac{K(\eta)}{K(o)}\, d\eta = 0.1283 \frac{K_1}{K_4} + 0.1388 \frac{K_2}{K_4} + 0.0531 \frac{K_3}{K_4} \tag{34}$$

Combining equations (32), (33), and (34) results in

$$F_{sn} = F_c \left[1 + \frac{(\eta_c K_4 - 1)\cos^2\left(\frac{n\pi}{8}\right)}{0.1283\, K_1 + 0.1388\, K_2 + 0.0531\, K_3} \right] \tag{35}$$

The strength factor of the wing tip vortices is assumed to be dependent upon the wing loading distribution and the lateral position of the tip vortices, η_c. The latter gives a measure of the extent the sheet is rolled-up. Near the wing, the tip vortex would (at least) equal the wing circulation at $\eta = \eta_c$, the center of the tip vortex. At most, the tip vortex would equal the wing circulation at the span station corresponding to the inner edge of the tip vortex. The inner edge, here, is roughly estimated as twice the distance from the tip to η_c, thus located at $\eta = 2\eta_c - 1$.

Now, in the derivation of the sheet strength factors, some sheet strength is left in these outer regions. Therefore, the strength of the tip vortices will not be taken as the larger of the above two values, but will be taken as the sum of the vortices inboard to $\eta = (3\eta_c - 1)/2$ which is midway between η_c and $2\eta_c - 1$. Thus (again, near the wing),

$$F_c = -\int_{\left(\frac{3\eta_c - 1}{2}\right)}^{1} \frac{d\left(\frac{K(\eta)}{K(o)}\right)}{d\eta}\, d\eta = \frac{K\left(\frac{3\eta_c - 1}{2}\right)}{K(o)} \tag{36}$$

Far downstream, when the rolling-up is completed

$$F_c = 1 \tag{37}$$

Between the above asymptotic values, assume F_c to vary as the product of wing loading at $(3\eta_c - 1)/2$ and a linear function of η_c.

Then

$$F_c = \frac{K\left(\frac{3\eta_c - 1}{2}\right)}{K(o)} (k_1 + k_2\eta_c) \tag{38}$$

The two constants, k_1 and k_2, are evaluated by the two conditions given by equations (36) and (37). The resulting equation for F_c is

$$F_c = \frac{K\left(\frac{3\eta_c - 1}{2}\right)}{K(o)} \left[1 + \frac{\frac{K(o)}{K\left(\frac{3\eta_c - 1}{2}\right)} - 1}{1 - \eta_{c_\infty}} (1 - \eta_c) \right] \tag{39}$$

where

$K\left(\frac{3\eta_c - 1}{2}\right)$ is the value of $\frac{c_l c}{C_L c_{av}}$ at $\eta = \frac{3\eta_c - 1}{2}$,

$K\left(\frac{3\eta_{c_\infty} - 1}{2}\right)$ is the value of $\frac{c_l c}{C_L c_{av}}$ at $\eta = \frac{3\eta_{c_\infty} - 1}{2}$,

and

$$\eta_{c_\infty} = \frac{1}{K(o)}$$

It should be recognized that other procedures that might determine the strength factors more accurately can be used in the present calculations. However, it should be borne in mind that a fair amount of approximation in the strength factors can be tolerated since a small percentage change in the factors results in an even smaller percentage change in the computed downwash. In a later discussion, it is shown for an example wing that experiment and the above theory compare well with regard to the vortex strength in the tip region. The expressions presented also have the merit of being computationally simple.

Vertical location of the sheet during the rolling-up process.- When the sheet is rolling up, both the downwash induced at the sheet ($\Omega = 0$) and the location of the sheet, ζ_s, will be different from the flat-sheet results. As an approximation for the rolling-up sheet, the downwash due

to the rolling-up sheet is computed at $\Omega = 0$ using the ζ_s value given by the flat-sheet method. Substitution of this value of downwash in the displacement equation evaluates the ζ_s for the rolling-up sheet. This value of ζ_s is used throughout the balance of the rolling-up computation, replacing also the ζ_s in the flat-sheet downwash; that is, Ω for the flat sheet is then the same as Ω for the rolling-up sheet.

The rolling-up correction procedure, including the recomputation of ζ_s, is illustrated in a computing form to be presented shortly. The change in location of the vortex sheet is generally quite small in the inboard region, becoming larger in the outboard region.

Special loadings.- Span loadings which have maximum values at span stations other than at the plane of symmetry cause the equations for the strength factors to break down and in some cases to predict the lateral tip vortex location as being outboard of the wing tips. Such span loadings would have complicated rolling-up characteristics since each change in sign of the slope of a loading distribution indicates the possibility of a rolled-up vortex eventually appearing. At the wing-tip region the loading gradient is very large, approaching infinity at the wing tip; hence, the rolling-up is more pronounced at the tips. The loading gradient in the wing region between two maximum values of loading in general never becomes comparable to that at the tips, or even large. Hence, the rolling-up in this region will be very slow as compared to that at the wing tips. Thus it can be assumed for these special loadings that only the vortex sheet outboard of the maximum loading positions will roll up.

Then, when determining a rolling-up correction, the loading distribution to be used will be that with a straight faired line connecting the two maximum values of loading. The ordinates of the entire curve are then proportionately reduced so that the area under the curve is equal to the original unit area, as is illustrated below.

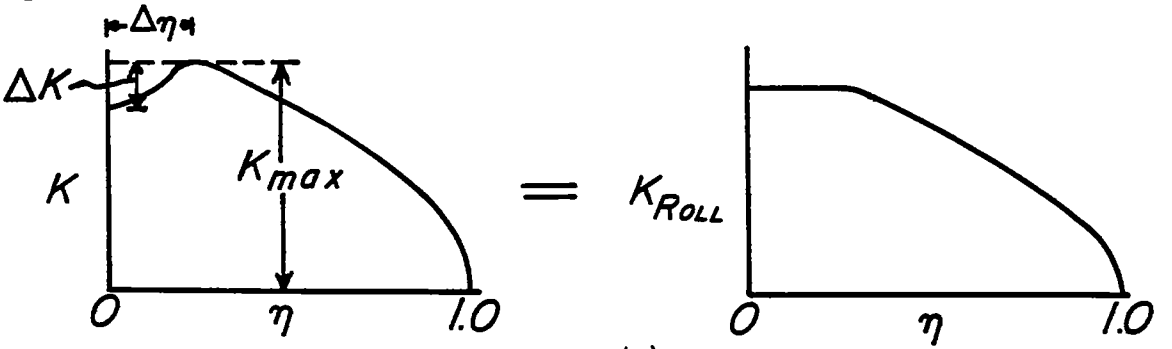

Sketch (h)

The area under the new faired loading is made a unit area by dividing the loading distribution by $1 + \int_0^{\Delta\eta} \Delta K \, d\eta$. The lift coefficient

used for the rolling-up method increases to the value

$$C_{L_{roll}} = \left(1 + \int_0^{\Delta\eta} \Delta K \, d\eta\right) C_L \qquad (40)$$

where the subscript, roll, indicates the value of lift coefficient and loading used to compute the rolling-up correction.

Effect of Fuselage

While a large part of the downwash at the tail is due to the wing, the presence of a fuselage will alter the downwash to a sufficient degree so that downwash due to the fuselage should be considered. For computational purposes, downwash due to a fuselage at the tail of an airplane can be separated into two parts: that due to the fuselage at an angle of attack and that due to the fuselage at zero angle of attack. Two effects are present for the fuselage at an angle of attack. The span loading for the wing-body combination will be somewhat different than for the wing alone. This altered loading, together with the corresponding distribution of "image" vortices will affect the downwash in the region of the tail. If the fuselage diameter is not too large, the loading can often be approximated by the wing-alone span loading. However, in view of the pronounced effect of span loading upon the downwash, it would be preferable to use the span loading corresponding to a wing-plus-fuselage combination. The other effect of the fuselage at angle of attack is that resulting from the "crossflow" component normal to the axis of the fuselage in the region of the tail. The importance of these effects depends largely on the ratio of fuselage diameter to wing span. A further discussion is given in reference 10. At zero angle of attack, there is a disturbance of the flow field due to tapering of the fuselage. The influence of the fuselage on the downwash is further complicated by flow separation on the after portion of the fuselage, but this effect will not be considered.

The relative importance of the above effects depends largely on the particular configuration being investigated and the spanwise region of interest. For the experimental data available for the present investigation, a calculation of the influence of the fuselage at zero angle of attack appeared adequate.

Since the fuselage diameters of most airplanes are small compared to the length, slender-body theory will be used to approximate the flow near the fuselage. Equation (10) of reference 11 gives the complex potential in the cross plane (normal to the longitudinal axis of the fuselage) of a slender body at an angle of attack. For a body of

revolution at zero angle of attack, the real part of this equation reduces to

$$\varphi_o = a_o \ln r$$

where $a_o = R_f(dR_f/dx)$. The radial velocity is then given by

$$\frac{d\varphi_o}{dr} = \frac{v_r}{V} = \frac{a_o}{r} = \frac{R_f(dR_f/dx)}{r}$$

The downward vertical component gives the downwash.

$$\frac{w_f}{V} = \frac{-zR_f(dR_f/dx)}{r^2} = \frac{-zR_f(dR_f/dx)}{y^2 + z^2} \tag{41}$$

where y and z are measured from the center line of the body. It should be noted that at the after part of the body dR_f/dx is negative for a tapering body and that the equations are for bodies of revolution.

Effects of Compressibility

The effect of compressibility on downwash is taken into account by use of the Prandtl-Glauert rule. That is, the longitudinal coordinates are simply stretched by a factor $1/\beta$ and c_l is replaced by βc_l.

The compressible and incompressible parameters are listed below.

Incompressible	Compressible (replace the incompressible values by:)
c_l, C_L, or C_{L_α}	βc_l, βC_L, or βC_{L_α}
A	βA
Λ	$\Lambda_\beta = \tan^{-1}[(\tan \Lambda)/\beta]$
ξ or τ	ξ/β or τ/β
η	η
ζ	ζ
c (chord)	c/β

(42)

The displacement values, ζ_s or Z_s, are not affected by β except insofar as ϵ_s is affected by compressibility. This ϵ_s can be calculated by making the above substitutions. The τ values in the ζ_s or Z_s equations are then not replaced by τ/β. The downwash for the case of sonic speeds is calculated by taking the limit as $\beta \longrightarrow 0$. The resulting simplified downwash equations are given in the rear portion of Appendix A. The values of downwash when $\beta = 0$ are not here represented as the true downwash but rather as a simple limit point that aids in fairing a Mach number curve of downwash.

Computation Forms

It is expedient to summarize the present calculations in a simple computation form. The forms for the computation of downwash angle due to a flat sheet, and the correction due to a rolling-up sheet, are presented as follows:

Flat-sheet procedure.-

Flat-sheet downwash **Vertical displacement**

$\eta =$ $\tau =$

Column no.		1	2	3	4	5	6	7	8	9	10
Column definition	Ω	a_{s1}	a_{s2}	a_{s3}	a_{s4}	ϵ/C_L	A_1	A_2	$A_2\frac{c_a}{C_L}$	Z_s/C_L	ζ_s/C_L
Operation to be performed		From figures 3 & 4 for given $\Lambda, \tau, \eta, \Omega$				$\frac{1}{2A}\sum_{n=1}^{4} a_{sn}K_n$	Eq. below	Eq. below	⑤⑦	⑥+⑧	$\frac{⑨-(\tau+\eta\tan\Lambda)}{C_L/\tan\alpha}$
	0										
	±0.5										

Span loading coefficients

K_1	K_2	K_3	K_4

For $\alpha = \alpha_{TE}$ and τ measured from $\frac{c}{4}$; A_1 and A_2 are:

$$A_1 = \frac{\left(\tau-\frac{3c}{2b}\right)\left(\tau-\frac{c}{2b}\right)\tan\alpha}{C_L\left(\tau+\frac{c}{2b}\right)} \qquad A_2 = -\frac{C_L\ A_1}{\tan\alpha}$$

For $\alpha \neq \alpha_{TE}$ see equation (18)

Vertical interpolation of flat-sheet downwash

11	12	13	14	15	16	17	18	19	20	21	22
Ω	D_1	D_2	D_3	D_4		C_1	C_2		ϵ/c_L	Z/c_L	ζ/c_L
	From Table II for given η				$\frac{1}{2A}\sum_{n=1}^{4} D_n K_n$	Constant with η		(17)$\left[\frac{\epsilon}{c_L}\right]_{\Omega=0}$ + (18)$\left[\frac{\epsilon}{c_L}\right]_{\Omega=.5}$ from (5)	(16)+(19)	(9)$\pm\frac{\Omega}{C_L}$	(10)$\pm\frac{\Omega}{C_L}$
0	x	x	x	x	x	x	x	x	x (from (5)) →			
±0.1											
±0.2											
±0.3											
±0.5	x	x	x	x	x	x	x	x	x (from (5)) →			
±0.8											

K_1	K_2	K_3	K_4

Rolling-up correction procedure.-

Required information

C_{L_α} = _____ Equation (39) F_c = _____

C_L = _____

α (radians) = _____

ξ = _____

$\xi - \tan\Lambda$ = _____ Equation (35) F_{s1} = _____, F_{s2} = _____, F_{s3} = _____, F_{s4} = _____

equation (26) η_c = _____

$\frac{1}{\eta_c}(\xi - \tan\Lambda)$ = _____

Trailing-sheet loss

η = _____ $\frac{\eta}{\eta_c}$ = _____

	23	24	25	26	27
Ω	a_{T1}	a_{T2}	a_{T3}	a_{T4}	ϵ_T
	From figure 5 for given η, $\xi - \tan\Lambda$, Ω				$-\frac{C_L}{2A}\sum_{n=1}^{4} a_{Tn} F_{sn} K_n$
0.5					
0.2					
0					
-0.2	x x x x x (same as 0.2) →				
-0.5	x x x x x (same as 0.5) →				

$F_{s1}K_1$	$F_{s2}K_2$	$F_{s3}K_3$	$F_{s4}K_4$

For span loadings with maximums not at $\eta = 0$, see "Special Loadings"

Corrected vertical displacement

28	29	30	31	32	33	34	35
Ω	Ω_c	Ω_c/η_c	$\frac{\eta_c A \epsilon_c}{C_L F_c}$	ϵ_c	ϵ_s	$\epsilon_s A_2$	ζ_s
	(10) C_L + $\alpha \tan\Lambda$	$\frac{(29)}{\eta_c}$	*	(31)$\frac{C_L F_c}{\eta_c A}$	(5) C_L + (27)+(32)	(7)(33)	A_1+(34) − $\xi\tan\alpha$
0							

* Interpolated from figure 6 for given

$\frac{\eta}{\eta_c}$, $\frac{1}{\eta_c}(\xi - \tan\Lambda)$, $\frac{\Omega}{\Omega_c}$

	Tip-vortex contribution				Total downwash			
	36	37	38	39	40	41	42	43
Ω	Ω_c	Ω_c/η_c	$\frac{\eta_c A \epsilon_c}{C_L F_c}$	ϵ_c	$\Delta\epsilon_T$	ϵ flat	Total downwash	Z
	(35) + $\alpha \tan\Lambda + \Omega$	$\frac{(36)}{\eta_c}$	*	(38) $\frac{C_L F_c}{\eta_c A}$	(27)+(39)	(20) C_L	(40) + (41)	(21) C_L − ((10)C_L − (35))
0.5								
0.2								
0								
-0.2								
-0.5								

DISCUSSION

This section evaluates the prediction of downwash due to wings alone, due to wing-fuselage combinations, and due to rolling-up of the vortex sheet by comparison with experiment. Also, for a pair of plan forms, downwash contours predicted by flat-sheet theory are compared with the flat-sheet theory corrected for rolling-up effects.

Comparison With Experiment

Wing alone.- Comparison of estimations from flat-sheet theory with some measured values of downwash from reference 12 for a swept-wing plan form is given in figure 7. For this wing, the computed rolling-up correction was very small; hence, only the flat-sheet results are presented. The computed values make use of the calculated wing loading distribution obtained from reference 6 and also of the experimental loading distribution,[3] which was somewhat different. The computed downwash distributions due to both loadings are presented and the two span loadings are shown in figure 8. The general conclusion is that the downwash prediction at the plane of symmetry is critically dependent upon the local loading distribution. This is because the downwash contributions of the vorticity on either side of the plane of symmetry are additive for a symmetrical span loading. At outboard stations, the downwash is not so dependent on the local loading since the vorticity to the inboard side results in an upwash which tends to cancel the downwash from the outboard side. It is noted that at the outboard stations the experimental and theoretical vorticity (or loading) distributions are more nearly similar. The effects of loading distribution are most prominent at the sheet. Figure 7 shows the experimental downwash from contour plots and the downwash computed using the experimental span loading to be in good agreement. The experimental and computed locations of the wake center are also shown to be in good agreement.

[3]This "experimental" span loading was estimated from consideration of experimental results of numerous wings.

Wing plus fuselage.- In figure 9 a comparison of the computed downwash (wing-alone flat-sheet results plus the fuselage "taper" correction) and of experimental downwash is presented for a particular configuration. The wing is characterized by an aspect ratio of 2.88, taper ratio of 0.625, and the quarter-chord line was swept back 50°. The wing was set at 2° incidence relative to the fuselage which had a length of 3.02 wing semispans and a maximum diameter of 0.297 wing semispans. The downwash is given at 1.239 wing semispans behind the quarter chord of the $\bar{c}$. The fuselage taper (dR_f/dx) was about -0.2. In figure 9, it is shown that the downwash due to this wing-fuselage combination is predicted with reasonable accuracy by the results of the flat-sheet method plus the downwash due to the fuselage taper. At $\eta = 0$, the computed and measured downwash above the fuselage are in good agreement at the lower angles of attack. Below the fuselage, the maximum difference is of the order of 1°. The poorer agreement at $\alpha = 13°$ may be due (in part) to a change in span loading from that which existed at the lower angles of attack.

At $\eta = 0.383$, the computed and measured downwash is in similar agreement. At $\alpha = 13°$, the possible change in span loading results in some discrepancy. However, as was pointed out in the comparisons of wing-alone downwash, this change in span loading does not result in as large a change in downwash at $\eta = 0.383$ as occurs at $\eta = 0$. At $\eta = 0.383$, the fuselage correction is quite small.

In summary, in figure 9 it is shown that good predictions can be made by adding the downwash due to fuselage taper with the downwash due to wing alone.

Rolling-up correction.- In figure 10 are presented measured values of downwash from reference 13 together with three methods of prediction for a wing with $\Lambda = 60°$, $A = 3.5$, $\lambda = 0.25$, and $C_L \simeq 0.5$. The three methods are: flat-sheet theory, rolling-up corrected flat-sheet theory, and a completely rolled-up theory. The latter is simply the downwash due to the swept bound portion plus two concentrated tip vortices located at $\eta_{c_\infty} = 0.864$. It is seen that the rolling-up method agrees well with experiment and that the agreement is best at the more outboard and at the more rearward positions. It is interesting to note that only the rolling-up correction method agrees well with experiment. For ξ equal to 2.71 and 3.43, neither the flat-sheet results nor the results for the completely rolled-up vortex yield maximum downwash angles within 10 percent of the experimental values. At $\xi = 2.02$ and $\eta = 0.383$, the experimental downwash angles appear questionable because the rolling-up method gave virtually exact agreement with experiment at $C_L = 0.25$.

In applying the rolling-up correction, it is important that the lateral position of the tip vortices be closely approximated. In figure 11 is presented a comparison of measured (refs. 12, 13, and 14) and computed locations of the tip vortices. The computed locations of the tip vortices are based on empirical equation (26). Figure 11 shows good agreement for a number of downstream positions for several swept wings.

The agreement is within the precision of the experiments. It should be noted that these are the same wings which were used in determining the empirical constant, f, at one-half semispan behind the quarter chord of the wing tip.

It is also important that the method yield a reasonable estimate of the strength factor of the tip vortices. It is difficult to determine the precise strength of the tip vortex from experiment because the vortex sheet is connected to the tip vortex. An approximate check can be obtained by determining the total vorticity in the region of the tip vortex. The experimental total can then be compared to the theoretical total. To check the totals for the 60° swept wing, the downwash contour plots of reference 13 were used.

Very near the tip vortex (just outside of the maximum ϵ values where the sheet contributes little), the downwash due to the tip vortex is approximately given by

$$\frac{w}{V} \cong \frac{G_{vortex}}{\pi(\eta_c - \eta)}$$

Let

$$p = \frac{G_{vortex}}{(C_L/2A)}$$

Values of p ranging from 0.57 to 0.63 were obtained from the experimental downwash contour plots for $\xi = 3.43$ and $\alpha = 12^\circ$ by using various η's.

The theoretical total is taken as the theoretical F_c plus the theoretical amount of vorticity left in the weakened flat sheet in the region between $\eta = (3\eta_c - 1)/2$ and 1.0. At $\xi = 3.43$ and $\alpha = 12^\circ$, the computed F_c is 0.48 and the computed total in the weakened sheet from $\eta = (3\eta_c - 1)/2$ to 1.0 is 0.136. This theoretical total of 0.616 is compatible with the experimental total and is considered a reasonably good check on this phase of the method.

Comparison of the Downwash Due to a Flat Sheet and That Due to a Rolling-Up Vortex Sheet

The foregoing has indicated that the rolling-up correction method gives an accurate picture of the downwash fields behind swept wings. As is shown in reference 4, C_L and A are important parameters in the rolling-up. Hence, it would be of interest to compare the flat-sheet results and the rolling-up results for a few combinations of C_L and A.

For this comparison the following wing-tail combinations were selected.

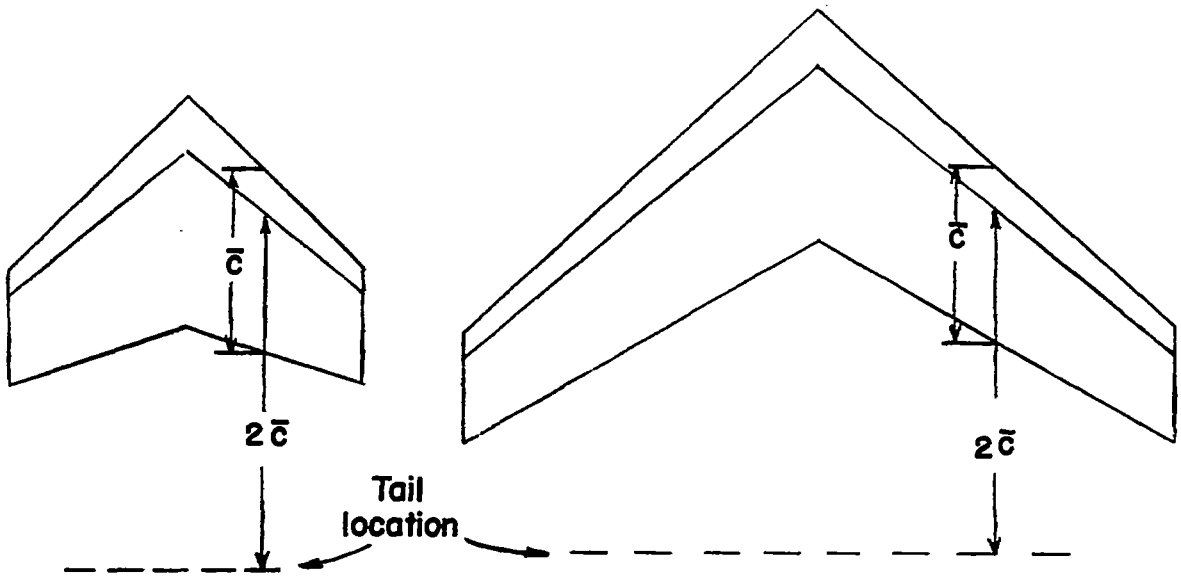

Sketch (i)

Contoured downwash fields at the tail location as predicted by flat-sheet theory and by the rolling-up corrected flat-sheet theory are shown in figure 12 for two values of C_L, 0.4 and 0.6.

In figure 12(a) (A = 2.0), the rolling-up is prominent and three principal effects are noteworthy: (1) in general, there is an upward shift of the downwash field in the more outboard areas; (2) the magnitude of the downwash around $\eta = 0$ is reduced; (3) in the mid-semispan region (around $\eta = 0.5$), the vertical distribution of downwash is more uniform than for the flat sheet. In general, the maximum values of the downwash for the two systems are not greatly different, but their locations do differ appreciably.

In figure 12(b) (A = 4.0), it is apparent that the amount of rolling-up present is quite small and the three effects mentioned above are scarcely discernible. In fact, these two cases, $C_L = 0.4$ and 0.6, could be considered as borderline cases. It is realized, of course, that near the tips (viz, $\eta = 0.9$), the rolling-up may have a sizable effect. The discussion here is limited to the more inboard locations as shown in the figure.

For other wings with the same C_L, sweep, tail position, and taper ratio, calculations indicate that for aspect ratios about one (or less), the trailing-vortex system is, in effect, rolled-up into two tip vortices. For aspect ratios larger than four, the rolling-up present is even less than that present in figure 12(b).

Thus, the general range of aspect ratios for which the rolling-up correction should be computed is roughly bounded by $A = 1.0$ and $A = 4.0$ at $C_L = 0.6$; that is, $(3/2)<(A/C_L)<6$.

CONCLUDING REMARKS

An influence-coefficient-type method is presented for the rapid estimation of the nonrolling-up downwash fields behind swept-wing airplanes. Using similar techniques, an additive correction for the effects of rolling-up is also presented. For the cases compared, the downwashes predicted by the above procedures agreed well with experiment.

To facilitate computations, charts and graphs of pertinent functions are presented together with tested computing forms. It is believed that the procedures set forth will require less time than procedures employing horseshoe vortices or discrete vortices. To obtain a simple and rapid method, a number of approximations and assumptions were made. Each approximation and assumption was investigated by various means and the range of applicability is discussed. Some findings of the present research are as follows.

By approximating the longitudinal variation of downwash behind surface-loaded wings by a simple function, a very simple expression has been derived for the vertical location of the wake center. It is shown that the location of the wake can then be written as a linear function of the downwash at the center of the wake. This downwash is easy to determine and thus the wake location can be determined very rapidly. A comparison of experimental wake locations and computed locations indicates that satisfactory predictions are made.

In the mid-wing region (around $\eta = 0$), it is found that the computed downwash near the wake is critically dependent upon the span loading used in the calculations. Thus, one should obtain the best available span loading before computing the downwash at the tail.

The experimentally determined paths of the tip vortices trailing behind several wings have been considered. It has been found that wing sweep had an appreciable effect upon the mechanics of the rolling-up and slowed the inward motion of the tip vortices to a considerable extent. An empirical correction has been developed which allows one to determine the tip vortex locations with due allowance for the effect of wing sweep.

Aside from an effect of the fuselage upon the wing span loading, it appears that an important effect of the fuselage upon the downwash at the tail can be considered as an additive correction to the wing-alone downwash for wing-fuselage combinations. This effect (due to the tapering of the rear portion of the fuselage) appears to be valid for combinations wherein the diameter of the fuselage is fairly small compared to both the length of the fuselage and the span of the wing. The correction (obtained by slender-body theory) is expressed in a simple form and has been shown to be in good agreement with experimental results on one airplane model.

Ames Aeronautical Laboratory
National Advisory Committee for Aeronautics
Moffett Field, Calif., Sept. 16, 1954

APPENDIX A

INTEGRATION OF EQUATION (3) TO OBTAIN DOWNWASH

A general equation for the flat-sheet downwash is presented in the section "ANALYSIS AND DEVELOPMENT OF METHOD." The purpose of the present section is to reduce the downwash integrals of equation (3) to the form of equation (6). It will be shown in the later part of this section that in the special case of sonic speeds, the downwash integrals simplify considerably. The downwash due to a completely rolled-up vortex system can be considered as a special case of the flat sheet; namely, that of a wing with rectangular span loading. Thus, the first portion of Appendix A is concerned with the general flat-sheet system, whereas the second portion considers specific cases.

General Solution

Representing the arbitrary loading distribution by a series and replacing the lateral integration variable by a trigonometric variable allows the first integral of equation (3) to be evaluated analytically. However, the second integral of equation (3) can only be evaluated numerically and may be evaluated in the same manner as that of reference 6. The first portion of the following will be concerned with the analytical integration of the first integral of equation (3).

It can be shown that $G'(\varphi)$ can be represented as

$$G'(\varphi) = \frac{2}{m+1} \sum_{n=1}^{m} G_n \sum_{\mu_1=1}^{m} \mu_1 \sin \mu_1 \varphi_n \cos \mu_1 \varphi \tag{A1}$$

Then, the first integral becomes

$$\frac{1}{\pi} \int_0^{\pi} \frac{(\cos \varphi - \eta) G'(\varphi) d\varphi}{\Omega^2 + (\cos \varphi - \eta)^2} = \sum_{n=1}^{m} 2 b_{sn} G_n \tag{A2}$$

where

$$b_{sn} = \frac{1}{m+1} \sum_{\mu_1=1}^{m} \mu_1 \sin \mu_1 \varphi_n \left(\frac{1}{\pi}\right) \int_0^{\pi} \frac{(\cos \varphi - \eta) \cos \mu_1 \varphi \, d\varphi}{\Omega^2 + (\cos \varphi - \eta)^2} \tag{A3}$$

Equation (A2) gives the integration to the same degree of accuracy as the vorticity distribution is given by the series of equation (A1). It remains to evaluate the integral of equation (A3). Define

$$I_{\mu_1} = \frac{1}{\pi} \int_0^{\pi} \frac{(\cos \varphi - \eta)\cos \mu_1 \varphi \, d\varphi}{\Omega^2 + (\cos \varphi - \eta)^2} \tag{A4}$$

With the relation for odd μ_1

$$\cos \mu_1 \varphi = 2^{\mu_1 - 1} \cos^{\mu_1} \varphi - \sum_{l=1}^{\frac{\mu_1 - 1}{2}} \frac{\mu_1!}{l!(\mu_1 - l)!} \cos(\mu_1 - 2l)\varphi$$

equation (A4) can be written as a recursion formula. Thus

$$I_{\mu_1} = 2^{\mu_1 - 1}\left(J_{\mu_1 + 1} - \eta J_{\mu_1}\right) - \sum_{l=1}^{\frac{\mu_1 - 1}{2}} \frac{\mu_1!}{l!(\mu_1 - l)!} I_{\mu_1 - 2l} \tag{A5}$$

where

$$J_{\mu_1} = \frac{1}{\pi} \int_0^{\pi} \frac{\cos^{\mu_1} \varphi \, d\varphi}{(\cos \varphi - \eta)^2 + \Omega^2} \tag{A6}$$

Now J_{μ_1} can be expressed in a recursion formula, by dividing the denominator of the integrand into the numerator, then

$$J_{\mu_1} = \begin{bmatrix} \left(\frac{{}^{n}C_r}{2}\right), & \text{for } \mu_1 = \text{even} \\ 0, & \text{for } \mu_1 = \text{odd} \end{bmatrix} + 2\eta J_{\mu_1 - 1} - (\eta^2 + \Omega^2) J_{\mu_1 - 2} \tag{A7}$$

where ${}^{n}C_r$ are binomial coefficients where

$$n = \mu_1 - 2$$

and

$$r = \frac{\mu_1 - 2}{2}$$

The integrations represented by J_0 and J_1 are found as follows: Let $u = \tan\frac{\varphi}{2}$ then $\cos\varphi = \frac{1-u^2}{1+u^2}$, $d\varphi = \frac{2du}{1+u^2}$. With these substitutions, equation (A6) for $\mu_1 = 0$ takes the form

$$J_0 = \frac{1}{\pi}\left\{\int_0^\infty \frac{d(u^2)}{[p+(q)(u^2)+(r)(u^2)^2]\sqrt{(u^2)}} + \int_0^\infty \frac{\sqrt{(u^2)}\,d(u^2)}{p+(q)(u^2)+(r)(u^2)^2}\right\}$$

These definite integrals are tabulated in reference 15 and give the value for J_0 as

$$\left.\begin{aligned} J_0 &= \frac{(1/\sqrt{p})+(1/\sqrt{r})}{\sqrt{q+2\sqrt{pr}}} \\ &\text{where} \\ p &= \Omega^2 + (1-\eta)^2 \\ q &= 2(\Omega^2 + \eta^2 - 1) \\ r &= \Omega^2 + (1+\eta)^2 \end{aligned}\right\} \qquad \text{(A8)}$$

A similar procedure gives

$$J_1 = \frac{(1/\sqrt{p}) - (1/\sqrt{r})}{\sqrt{q+2\sqrt{pr}}} \qquad \text{(A9)}$$

where the p's and q's and r's are the same as those in equation (A8).

With tabulated values of J_{μ_1} (from eqs. (A7) through (A9)), the application of the recursion formula of equation (A5) evaluates the desired integral of equation (A4). For symmetric loading, values of I_{μ_1} for odd μ_1 are given in the following equations:

$$
\left.
\begin{aligned}
I_1 &= 1 - (\Omega^2 + \eta^2)J_0 + \eta J_1 \\
I_3 &= -(1 - 4\eta^2 + 4\Omega^2) - (\eta^2 + \Omega^2)(-3 + 4\eta^2 - 4\Omega^2)J_0 + \eta(-3 + 4\eta^2 - 12\Omega^2)J_1 \\
I_5 &= [1 - 12\eta^2 + 16\eta^4 + (12 - 96\eta^2)\Omega^2 + 16\Omega^4] - \\
&\quad (\eta^2 + \Omega^2)[5 - 20\eta^2 + 16\eta^4 + (20 - 96\eta^2)\Omega^2 + 16\Omega^4]J_0 + \\
&\quad \eta[5 - 20\eta^2 + 16\eta^4 + (60 - 160\eta^2)\Omega^2 + 80\Omega^4]J_1 \\
I_7 &= [-1 + 24\eta^2 - 80\eta^4 + 64\eta^6 - (24 - 480\eta^2 + 960\eta^4)\Omega^2 + \\
&\quad (-80 + 960\eta^2)\Omega^4 - 64\Omega^6] - (\eta^2 + \Omega^2)[-7 + 56\eta^2 - 112\eta^4 + \\
&\quad 64\eta^6 - (56 - 672\eta^2 + 960\eta^4)\Omega^2 + (-112 + 960\eta^2)\Omega^4 - 64\Omega^6]J_0 + \\
&\quad \eta[-7 + 56\eta^2 - 112\eta^4 + 64\eta^6 - (168 - 1120\eta^2 + 1344\eta^4)\Omega^2 + \\
&\quad (-560 + 2240\eta^2)\Omega^4 - 448\Omega^6]J_1
\end{aligned}
\right\} \quad (A10)
$$

For numerically evaluating I_{μ_1} for high μ_1, it may be simpler to use equation (A5) directly; that is, to tabulate numerical values of J_{μ_1} from equation (A7), then with a numerical value of I_1 to tabulate successive I_{μ_1}.

With I_{μ_1} defined, equation (A3) becomes

$$b_{sn} = \frac{1}{m+1} \sum_{\mu_1=1}^{m} \mu_1 \sin \mu_1 \varphi_n I_{\mu_1} \qquad (A11)$$

The coefficients b_{sn} can be found for arbitrary Ω and η. The value of the integrals of equation (A2) is the summation of the arbitrary loading, G_n, and the b_{sn} values. The integral of equation (A2) gives the downwash due to a continuous trailing vortex sheet at an infinite distance aft of any wing and also twice the downwash at the load line for unswept wings. For the case of elliptic loading, the downwash is given directly by I_1 alone, a result derived by other procedures in the past (e.g., see ref. 7). For symmetric loading ($G_{m+1-n} = G_n$, and only odd μ_1), equation (A2) becomes

$$\frac{1}{\pi} \int_0^{\pi} \frac{(\cos \varphi - \eta)G'(\varphi)\,d\varphi}{\Omega^2 + (\cos \varphi - \eta)^2} = \sum_{n=1}^{\frac{m+1}{2}} 2B_{sn}G_n \qquad (A12)$$

where with μ_1 odd

$$\left.\begin{aligned} B_{sn} &= 2b_{sn}, \qquad n \neq \frac{m+1}{2} \\ &= b_{sn}, \qquad n = \frac{m+1}{2} \end{aligned}\right\} \tag{A13}$$

The numerical integration of the second integral of equation (3) is obtained from the appendix of reference 6 by substituting $L_{s\mu}$ given by equations (4) and (5) for $L(\eta,\bar{\eta})$ in reference 6.

In summary, for symmetric loading, the downwash integral of equation (3) becomes

$$\epsilon = \frac{w}{V} = \sum_{n=1}^{\frac{m+1}{2}} a_{sn} G_n \tag{A14}$$

where

$$a_{sn} = 2B_{sn} + \frac{-1}{2(M+1)} \sum_{\mu=0}^{\frac{M-1}{2}} \bar{f}_{n\mu} \Delta L_{s\mu}$$

$$B_{sn} = \frac{2}{m+1} \sum_{\mu_1=1,\text{odd}}^{m} \mu_1 \sin \mu_1 \varphi_n I_{\mu_1}, \qquad n \neq \frac{m+1}{2}$$

$$B_{s,\frac{m+1}{2}} = \frac{B_{sn}}{2} \quad \text{for} \quad n = \frac{m+1}{2}$$

and I_{μ_1} is given by equations (A10) and (A5)

$$\begin{aligned} \bar{f}_{n\mu} &= 2f_{n\mu}, \quad \text{for} \quad n \neq \frac{m+1}{2}, \quad \mu > 0 \\ &= f_{n\mu}, \qquad n = \frac{m+1}{2}, \quad \mu > 0 \\ &= f_{n\mu}, \qquad n \neq \frac{m+1}{2}, \quad \mu = 0 \\ &= \frac{f_{n\mu}}{2}, \qquad n = \frac{m+1}{2}, \quad \mu = 0 \end{aligned}$$

$$f_{n\mu} = \frac{2}{m+1} \sum_{\mu_1=1,\text{odd}}^{m} \mu_1 \sin \mu_1\varphi_n \cos \mu_1\varphi_\mu$$

where $\varphi_n = \frac{n\pi}{m+1}$, and $\varphi_\mu = \frac{\mu\pi}{m+1}$. Table III lists values of $\bar{f}_{n\mu}$ for several values of M and m.

$$\Delta L_{s\mu} = \frac{\dfrac{(\eta-\bar{\eta}_\mu)[\tau + (\eta-\bar{\eta}_\mu)\tan\Lambda]}{\Omega^2 + (\eta-\bar{\eta}_\mu)^2} + \dfrac{\tau(\eta-\bar{\eta}_\mu + \tau \sin\Lambda \cos\Lambda)}{\Omega^2 + \tau^2 \cos^2\Lambda}}{\sqrt{[\tau + (\eta-\bar{\eta}_\mu)\tan\Lambda]^2 + (\eta-\bar{\eta}_\mu)^2 + \Omega^2}} -$$

$$\frac{\dfrac{(\eta+\bar{\eta}_\mu)[\tau+(\eta-\bar{\eta}_\mu)\tan\Lambda]}{\Omega^2+(\eta+\bar{\eta}_\mu)^2} - \dfrac{(\tau+2\eta\tan\Lambda)(\eta-\bar{\eta}_\mu+\tau\sin\Lambda\cos\Lambda-2\eta\cos^2\Lambda)}{\Omega^2+(\tau+2\eta\tan\Lambda)^2\cos^2\Lambda}}{\sqrt{[\tau + (\eta-\bar{\eta}_\mu)\tan\Lambda]^2 + (\eta+\bar{\eta}_\mu)^2 + \Omega^2}} -$$

$$\frac{\dfrac{\tau(\eta+\tau\sin\Lambda\cos\Lambda)}{\Omega^2+\tau^2\cos^2\Lambda} + \dfrac{(\tau+2\eta\tan\Lambda)(\eta+\tau\sin\Lambda\cos\Lambda-2\eta\cos^2\Lambda)}{\Omega^2+(\tau+2\eta\tan\Lambda)^2\cos^2\Lambda}}{\sqrt{(\tau+\eta\tan\Lambda)^2+\eta^2+\Omega^2}} - \frac{\eta-\bar{\eta}_\mu}{\Omega^2+(\eta-\bar{\eta}_\mu)^2} + \frac{\eta+\bar{\eta}_\mu}{\Omega^2+(\eta+\bar{\eta}_\mu)^2}$$

where

$$\bar{\eta}_\mu = \cos\frac{\mu\pi}{M+1} = \cos\varphi_\mu$$

A convenient closed form of $f_{n\mu}$ is given by:

$$f_{n\mu} = \frac{-2(-1)^n \sin \varphi_n}{(m+1)(\cos 2\varphi_n - \cos 2\varphi_\mu)^2} [\sin \varphi_\mu \sin (m+1)\varphi_\mu (2 + \cos 2\varphi_n + \cos 2\varphi_\mu) -$$

$$(m+1) \cos \varphi_\mu \cos (m+1)\varphi_\mu (\cos 2\varphi_n - \cos 2\varphi_\mu)]$$

for

$$\varphi_\mu = \varphi_n$$

$$f_{n\mu} = \frac{-1}{2 \sin 2\varphi_n}$$

for

$$M = m$$

$$f_{n\mu} = \frac{2(-1)^{n+\mu} \sin \varphi_n \cos \varphi_\mu}{\cos 2\varphi_n - \cos 2\varphi_\mu}$$

Special Cases

Compressibility considerations and downwash at sonic speeds.- The effects of compressibility, subject to the limitations of the linearized compressible flow equation, can be included in the previous work by the substitution of the parameters $\frac{\xi}{\beta}$ and $\Lambda_\beta = \tan^{-1}\left(\frac{\tan \Lambda}{\beta}\right)$, for ξ and Λ, respectively. It can be seen that since the B_{sn} coefficients are independent of ξ and Λ, they are unaffected by compressibility and that only the $L_{s\mu}$ function is affected by compressibility.

The limit value of the downwash at sonic speeds can be found by substituting into equations (3), (4), and (5) the parameters τ/β and Λ_β which replace τ and Λ, respectively, then determining the limit as $\beta \to 0$. With the limit

$$\lim_{\beta \to 0} \frac{\beta}{\cos \Lambda_\beta} \longrightarrow \tan \Lambda \qquad \text{(A15)}$$

equation (3) at sonic speeds becomes

$$\frac{w}{V} = \frac{1}{2\pi}\left\{\int_{-1}^{1}\left[1 + \frac{\tau + (|\eta| - |\bar{\eta}|)\tan\Lambda}{|\tau + (|\eta| - |\bar{\eta}|)\tan\Lambda|}\right]\frac{\eta - \bar{\eta}}{\Omega^2 + (\eta - \bar{\eta})^2}G'(\bar{\eta})\,d\bar{\eta} - \right.$$

$$\frac{[\tau + (|\eta| - \eta)\tan\Lambda]\tan\Lambda}{[\tau + (|\eta| - \eta)\tan\Lambda]^2 + \Omega^2\tan^2\Lambda}\int_{0}^{1}\left[\frac{\tau + |\eta|\tan\Lambda}{|\tau + |\eta|\tan\Lambda|} - \frac{\tau + (|\eta| - |\bar{\eta}|)\tan\Lambda}{|\tau + (|\eta| - |\bar{\eta}|)\tan\Lambda|}\right]G'(\bar{\eta})\,d\bar{\eta} +$$

$$\left.\frac{[\tau + (|\eta| + \eta)\tan\Lambda]\tan\Lambda}{[\tau + (|\eta| + \eta)\tan\Lambda]^2 + \Omega^2\tan^2\Lambda}\int_{-1}^{0}\left[\frac{\tau + |\eta|\tan\Lambda}{|\tau + |\eta|\tan\Lambda|} - \frac{\tau + (|\eta| - |\bar{\eta}|)\tan\Lambda}{|\tau + (|\eta| - |\bar{\eta}|)\tan\Lambda|}\right]G'(\bar{\eta})\,d\bar{\eta}\right\} \quad (A16)$$

The form of equation (A16) can be simplified by considering three longitudinal regions of downwash. These regions can be pictured as follows:

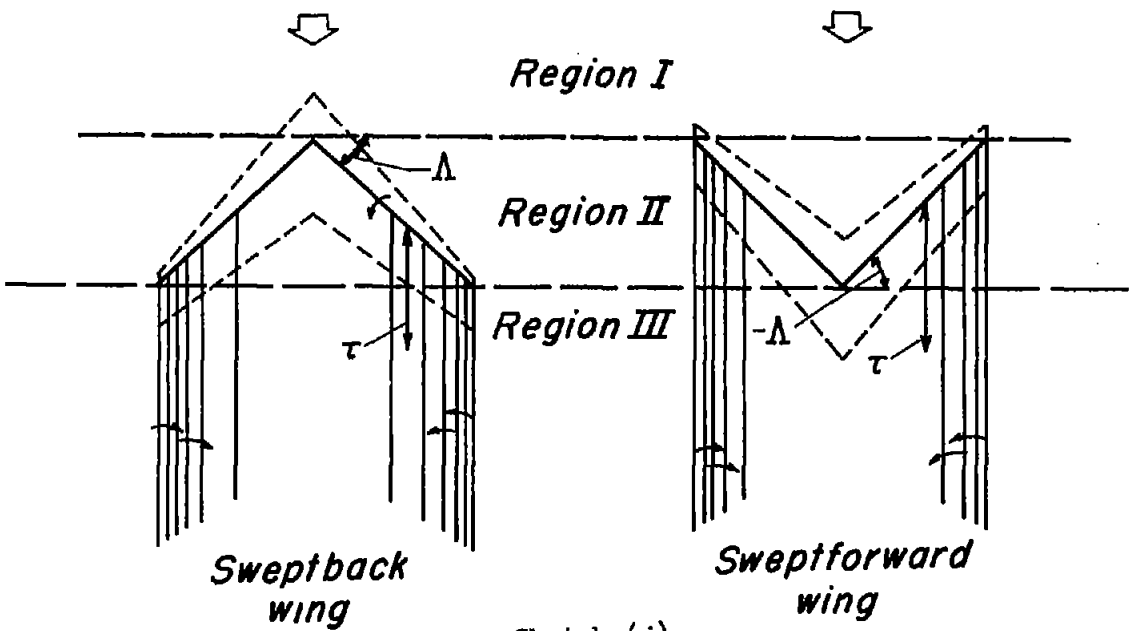

Sketch (j)

For the three regions, equation (A16) gives

Region I:

$$\frac{w}{V} = 0$$

Region II (for sweepback):

$$\frac{w}{V} = \frac{1}{2\pi}\left\{\int_{-\left|\frac{\tau+|\eta|\tan\Lambda}{\tan\Lambda}\right|}^{\left|\frac{\tau+|\eta|\tan\Lambda}{\tan\Lambda}\right|} \frac{\eta-\bar{\eta}}{\Omega^2+(\eta-\bar{\eta})^2} G'(\bar{\eta})\,d\bar{\eta} + \right.$$

$$\frac{2[\tau+(|\eta|-\eta)\tan\Lambda]\tan\Lambda \; G\left(\left|\frac{\tau+|\eta|\tan\Lambda}{\tan\Lambda}\right|\right)}{[\tau+(|\eta|-\eta)\tan\Lambda]^2+\Omega^2\tan^2\Lambda} +$$

$$\left.\frac{2[\tau+(|\eta|+\eta)\tan\Lambda]\tan\Lambda \; G\left(-\left|\frac{\tau+|\eta|\tan\Lambda}{\tan\Lambda}\right|\right)}{[\tau+(|\eta|+\eta)\tan\Lambda]^2+\Omega^2\tan^2\Lambda}\right\} \qquad \text{(A17)}$$

Region II (for sweepforward):

$$\frac{w}{V} = \frac{1}{2\pi}\left\{\int_{-1}^{-\left|\frac{\tau+|\eta|\tan\Lambda}{\tan\Lambda}\right|} \frac{\eta-\bar{\eta}}{\Omega^2+(\eta-\bar{\eta})^2} G'(\bar{\eta})d\bar{\eta} + \right.$$

$$\int_{\left|\frac{\tau+|\eta|\tan\Lambda}{\tan\Lambda}\right|}^{1} \frac{\eta-\bar{\eta}}{\Omega^2+(\eta-\bar{\eta})^2} G'(\bar{\eta})d\bar{\eta} +$$

$$\frac{2[\tau+(|\eta|-\eta)\tan\Lambda]\tan\Lambda\ G\left(\left|\frac{\tau+|\eta|\tan\Lambda}{\tan\Lambda}\right|\right)}{[\tau+(|\eta|-\eta)\tan\Lambda]^2+\Omega^2\tan^2\Lambda} +$$

$$\left.\frac{2[\tau+(|\eta|+\eta)\tan\Lambda]\tan\Lambda\ G\left(-\left|\frac{\tau+|\eta|\tan\Lambda}{\tan\Lambda}\right|\right)}{[\tau+(|\eta|+\eta)\tan\Lambda]^2+\Omega^2\tan^2\Lambda}\right\}$$

Region III:

$$\frac{w}{V} = \frac{1}{\pi}\int_{-1}^{1} \frac{\eta-\bar{\eta}}{\Omega^2+(\eta-\bar{\eta})^2} G'(\bar{\eta})d\eta \qquad \text{(A18)}$$

The symbol $G\left(\pm\left|\frac{\tau+|\eta|\tan\Lambda}{\tan\Lambda}\right|\right)$ denotes the value of G at that span station.

For symmetric loading, Region II given by equation (A16) simplifies (since $G(-\eta) = G(\eta)$) to:

Region II (for sweepback):

$$\frac{w}{V} = \frac{1}{\pi}\left\{\int_{-\left|\frac{\tau+\eta\tan\Lambda}{\tan\Lambda}\right|}^{\left|\frac{\tau+\eta\tan\Lambda}{\tan\Lambda}\right|} \frac{\eta-\bar{\eta}}{\Omega^2+(\eta-\bar{\eta})^2} G'(\bar{\eta})d\bar{\eta} + \right.$$

$$\tan\Lambda\left[\frac{\tau}{\tau^2+\Omega^2\tan^2\Lambda} + \frac{\tau+2\eta\tan\Lambda}{(\tau+2\eta\tan\Lambda)^2+\Omega^2\tan^2\Lambda}\right]$$

$$\left. G\left(\left|\frac{\tau+\eta\tan\Lambda}{\tan\Lambda}\right|\right)\right\} \tag{A19}$$

Region II (for sweepforward):

$$\frac{w}{V} = \frac{1}{\pi}\left\{\int_{-1}^{-\left|\frac{\tau+\eta\tan\Lambda}{\tan\Lambda}\right|} \frac{\eta-\bar{\eta}}{\Omega^2+(\eta-\bar{\eta})^2} G'(\bar{\eta})d\bar{\eta} + \right.$$

$$\int_{+\left|\frac{\tau+\eta\tan\Lambda}{\tan\Lambda}\right|}^{1} \frac{\eta-\bar{\eta}}{\Omega^2+(\eta-\bar{\eta})^2} G'(\bar{\eta})d\bar{\eta} +$$

$$\tan\Lambda\left[\frac{\tau}{\tau^2+\Omega^2\tan^2\Lambda} + \frac{\tau+2\eta\tan\Lambda}{(\tau+2\eta\tan\Lambda)^2+\Omega^2\tan^2\Lambda}\right]$$

$$\left. G\left(\left|\frac{\tau+\eta\tan\Lambda}{\tan\Lambda}\right|\right)\right\} \tag{A20}$$

For the Region II for the case of sweptback wings, the downwash can be written as (symmetric loading)

$$\frac{w}{V} = \left(\frac{w}{V}\right)_{III} - \frac{1}{\pi}\int_{-1}^{-\left|\frac{\tau+\eta\tan\Lambda}{\tan\Lambda}\right|} \frac{\eta-\bar{\eta}}{\Omega^2+(\eta-\bar{\eta})^2} G'(\bar{\eta})d\bar{\eta} -$$

$$\frac{1}{\pi}\int_{\left|\frac{\tau+\eta\tan\Lambda}{\tan\Lambda}\right|}^{1} \frac{\eta-\bar{\eta}}{\Omega^2+(\eta-\bar{\eta})^2} G'(\bar{\eta})d\bar{\eta} +$$

$$\frac{\tan\Lambda}{\pi}\left[\frac{\tau}{\tau^2+\Omega^2\tan^2\Lambda} + \frac{\tau+2\eta\tan\Lambda}{(\tau+2\eta\tan\Lambda)^2+\Omega^2\tan^2\Lambda}\right]$$

$$\left[G\left(\left|\frac{\tau+\eta\tan\Lambda}{\tan\Lambda}\right|\right)\right] \qquad (A21)$$

The two integrals can be approximated by replacing the loading distribution near the wing tip by a single vortex having strength given by $G\left(\left|\frac{\tau+\eta\tan\Lambda}{\tan\Lambda}\right|\right)$ and laterally located so that the downwash at $\eta=\Omega=0$ due to elliptic loading at the wing tip equals that of a single vortex. Then the lateral location of a single vortex is at

$$\bar{\eta} = \frac{\sqrt{1-\left(\frac{\tau+\eta\tan\Lambda}{\tan\Lambda}\right)^2}}{\cos^{-1}\left(\frac{\tau+\eta\tan\Lambda}{\tan\Lambda}\right)} \cong \sqrt{\frac{1}{2}\left(1+\left|\frac{\tau+\eta\tan\Lambda}{\tan\Lambda}\right|\right)} \qquad (A22)$$

Then the downwash becomes

$$\frac{w}{V} = \left(\frac{w}{V}\right)_{III} - \frac{1}{\pi}\left\{\frac{\sqrt{\frac{1}{2}\left(1 + \left|\frac{\tau+\eta\tan\Lambda}{\tan\Lambda}\right|\right)} - \eta}{\Omega^2 + \left[\sqrt{\frac{1}{2}\left(1 + \left|\frac{\tau+\eta\tan\Lambda}{\tan\Lambda}\right|\right)} - \eta\right]^2} + \right.$$

$$\left.\frac{\sqrt{\frac{1}{2}\left(1 + \left|\frac{\tau+\eta\tan\Lambda}{\tan\Lambda}\right|\right)} + \eta}{\Omega^2 + \left[\sqrt{\frac{1}{2}\left(1 + \left|\frac{\tau+\eta\tan\Lambda}{\tan\Lambda}\right|\right)} + \eta\right]^2}\right\} G\left(\left|\frac{\tau+\eta\tan\Lambda}{\tan\Lambda}\right|\right) +$$

$$\frac{\tan\Lambda}{\pi}\left[\frac{\tau}{\tau^2 + \Omega^2\tan^2\Lambda} + \frac{\tau + 2\eta\tan\Lambda}{(\tau + 2\eta\tan\Lambda)^2 + \Omega^2\tan^2\Lambda}\right] G\left(\left|\frac{\tau+\eta\tan\Lambda}{\tan\Lambda}\right|\right) \tag{A23}$$

The downwash in Region III can be evaluated from equation (A12), then

$$\left(\frac{w}{V}\right)_{III} = \sum_{n=1}^{m} 2b_{sn}G_n \tag{A24}$$

For symmetric loading

$$\left(\frac{w}{V}\right)_{III} = \sum_{n=1}^{\frac{m+1}{2}} 2B_{sn}G_n \tag{A25}$$

where the value of $2B_{sn}$ is the value of a_{sn} at $\tau = \infty$ given by equation (A14).

Downwash due to rectangular span loading.- For rectangular span loading the equations for determining downwash simplify considerably. Since the loading is constant across the wing span, then in equations (3), (4), and (5) one can substitute $-\int_0^1 G'(\bar{\eta})d\bar{\eta} = G(0)$, and plus and minus values

of unity for $\bar{\eta}$. The downwash equation becomes

$$\frac{w/V}{2G(o)} = \frac{1}{4\pi}\left\{\frac{1-\eta}{\Omega^2+(1-\eta)^2} + \frac{1+\eta}{\Omega^2+(1+\eta)^2} + \frac{(1-\eta)[\tau-(1-\eta)\tan\Lambda]}{\Omega^2+(1-\eta)^2} - \frac{\tau\left[\tau\tan\Lambda - \dfrac{(1-\eta)}{\cos^2\Lambda}\right]}{\tau^2+\Omega^2/\cos^2\Lambda}}{\sqrt{[\tau-(1-\eta)\tan\Lambda]^2+(1-\eta)^2+\Omega^2}} + \right.$$

$$\frac{(1+\eta)[\tau-(1-\eta)\tan\Lambda]}{\Omega^2+(1+\eta)^2} + \frac{(\tau+2\eta\tan\Lambda)[\tau\tan\Lambda-2\eta-(1-\eta)/\cos^2\Lambda]}{(\tau+2\eta\tan\Lambda)^2+\Omega^2/\cos^2\Lambda}}{\sqrt{[\tau-(1-\eta)\tan\Lambda]^2+(1+\eta)^2+\Omega^2}} +$$

$$\left.\frac{\tau(\tau\tan\Lambda+\eta/\cos^2\Lambda)}{\tau^2+\Omega^2/\cos^2\Lambda} + \frac{(\tau+2\eta\tan\Lambda)(\tau\tan\Lambda-2\eta+\eta/\cos^2\Lambda)}{(\tau+2\eta\tan\Lambda)^2+\Omega^2/\cos^2\Lambda}}{\sqrt{(\tau+\eta\tan\Lambda)^2+\eta^2+\Omega^2}}\right\} \tag{A26}$$

For $\Omega = 0$ equation (A26) simplifies to

$$\frac{w/V}{2G(o)} = \frac{1}{4\pi}\left\{\frac{1}{1-\eta} + \frac{1}{1+\eta} + \frac{\sqrt{[\tau-(1-\eta)\tan\Lambda]^2+(1-\eta)^2}}{\tau(1-\eta)} + \frac{\sqrt{[\tau-(1-\eta)\tan\Lambda]^2+(1+\eta)^2}}{(\tau+2\eta\tan\Lambda)(1+\eta)} + \right.$$

$$\left.\frac{2\tan\Lambda\sqrt{(\tau+\eta\tan\Lambda)^2+\eta^2}}{\tau(\tau+2\eta\tan\Lambda)}\right\} \tag{A27}$$

Compressibility is taken into account in the same manner as in the previous section. At sonic speeds for the same regions as before, equation (A26) reduces to

Region I:

$$\frac{w/V}{2G(o)} = 0$$

Region II (for sweepback):

$$\frac{w/V}{2G(o)} = \frac{\tan\Lambda}{2\pi}\left[\frac{\tau}{\tau^2 + \Omega^2\tan^2\Lambda} + \frac{\tau + 2\eta\tan\Lambda}{(\tau + 2\eta\tan\Lambda)^2 + \Omega^2\tan^2\Lambda}\right] \tag{A28}$$

Region II (for sweepforward):

$$\frac{w/V}{2G(o)} = \frac{1}{2\pi}\left\{\frac{1-\eta}{\Omega^2 + (1-\eta)^2} + \frac{1+\eta}{\Omega^2 + (1+\eta)^2} + \tan\Lambda\left[\frac{\tau}{\tau^2 + \Omega^2\tan^2\Lambda} + \frac{\tau + 2\eta\tan\Lambda}{(\tau + 2\eta\tan\Lambda)^2 + \Omega^2\tan^2\Lambda}\right]\right\} \tag{A29}$$

Region III:

$$\frac{w/V}{2G(o)} = \frac{1}{2\pi}\left[\frac{1-\eta}{\Omega^2 + (1-\eta)^2} + \frac{1+\eta}{\Omega^2 + (1+\eta)^2}\right] \tag{A30}$$

If the trailing vortices due to rectangular loading are not at the wing tip ($\eta = 1$) but laterally located at η_c, then the downwash is obtained by substituting $\frac{G(o)}{\eta_c}$, $\frac{\tau}{\eta_c}$, $\frac{\eta}{\eta_c}$, and $\frac{\Omega}{\eta_c}$, for $G(o)$, τ, η, and Ω, respectively, in the previous equations.

APPENDIX B

VERTICAL INTERPOLATION OF DOWNWASH

An approximate vertical interpolation of downwash can be found by using the method of reference 8 for small values of Ω. In the present report, the interpolation formula for other values of Ω will be based on a fitted function of Ω that fairs through the two known values of downwash ($\Omega = 0$ and ± 0.5), approaches the function given by reference 8 for small values of Ω, and approaches the correct function for high values of Ω (e.g., ref. 7).

In reference 8 the downwash function is expanded in a Taylor series starting from the vortex sheet:

$$\epsilon(\Omega) = \epsilon(0) + \left(\frac{\partial \epsilon}{\partial \Omega}\right)_0 |\Omega| + \frac{1}{2}\left(\frac{\partial^2 \epsilon}{\partial \Omega^2}\right)_0 \Omega^2 + \cdots \tag{B1}$$

where the subscript, o, indicates evaluation at $\Omega = 0$. Assuming the trailing sheet extends fore and aft to infinity, the following relations are derived in reference 8:

$$\left(\frac{\partial \epsilon}{\partial \Omega}\right)_0 = \frac{d^2 G}{d\eta^2}, \qquad \left(\frac{\partial^2 \epsilon}{\partial \Omega^2}\right)_0 = -\frac{d^2 \epsilon}{d\eta^2} \tag{B2}$$

Now, for large values of Ω, if τ is small relative to Ω, the downwash for any loading distribution is given by

$$\epsilon(\Omega) \approx \frac{\Omega^2 - \eta^2}{2(\Omega^2 + \eta^2)^2} \frac{C_L}{\pi A} \tag{B3}$$

As Ω becomes very large (compared to η), equation (B3) becomes

$$\epsilon(\Omega) = \frac{1}{2\Omega^2} \frac{C_L}{\pi A} \tag{B4}$$

The derivative of equation (B4) gives

$$\frac{d\epsilon}{d\Omega} = -\frac{1}{\Omega^3} \frac{C_L}{\pi A} \tag{B5}$$

It is desired to curve-fit a function of Ω that approaches equation (B1) for small Ω, gives the known value of ϵ at $\Omega = \pm 0.5$, and

approaches equations (B3), (B4), and (B5) for large Ω. Assume the following function:

$$\epsilon(\Omega) = \epsilon(0) + C_1^* \left(\sqrt{\frac{\Omega^2}{1+\Omega^2}}\right) + C_2^* \left(\sqrt{\frac{\Omega^2}{1+\Omega^2}}\right)^2 + A_1 \left(\sqrt{\frac{\Omega^2}{1+\Omega^2}}\right)^3 + A_2 \left(\sqrt{\frac{\Omega^2}{1+\Omega^2}}\right)^4 + A_3 \left(\sqrt{\frac{\Omega^2}{1+\Omega^2}}\right)^5 + A_4 \left(\sqrt{\frac{\Omega^2}{1+\Omega^2}}\right)^6 \tag{B6}$$

Where the variable $\sqrt{\frac{\Omega^2}{1+\Omega^2}}$ is chosen since downwash can be shown (by using eq. (A10)) to be proportional to this parameter for elliptic loading at $\eta = 0$.

The coefficients C_1^* and C_2^* are evaluated by taking the first and second derivatives with respect to Ω of equation (B6), which, at $\Omega = 0$, give the values of equation (B2), that is,

$$C_1^* = \frac{d^2G}{d\eta^2}, \qquad C_2^* = -\frac{1}{2}\frac{d^2\epsilon}{d\eta^2} \tag{B7}$$

The four remaining coefficients of equation (B6) can be found by using four conditions which the equation must satisfy. One condition is that it pass through the known value of ϵ at $\Omega = 1/2$. Another is[1] that it pass through the value of ϵ at $\Omega = 2.0$ given by equation (B3). A third condition is that at very large values of Ω, the downwash must be the value given by equation (B4). A fourth condition is that the slope of the curve at very large Ω be that given by equation (B5). The four coefficients (A_1, A_2, A_3, and A_4) so determined will be in terms of ϵ_0, $\epsilon\left(\frac{1}{2}\right)$, $\frac{d^2G}{d\eta^2}$, $\frac{d^2\epsilon}{d\eta^2}$, and $\frac{C_L}{\pi A}$. The next step is to evaluate the two derivatives and $\frac{C_L}{A}$.

To find $\frac{d^2G}{d\eta^2}$:

Now

$$\frac{d^2G(\varphi)}{d\eta^2} = \frac{dG(\varphi)}{d\varphi}\frac{d^2\varphi}{d\eta^2} + \frac{d^2G(\varphi)}{d\varphi^2}\left(\frac{d\varphi}{d\eta}\right)^2 \tag{B8}$$

[1]It should be noted that at two semispans from the sheet the downwash is essentially independent of span loading (e.g., ref. 7, p. 165); however, the downwash still has enough magnitude to make it useful in the curve fitting.

where

$$\varphi = \cos^{-1}\eta$$

$$\frac{d\varphi}{d\eta} = -\frac{1}{\sin\varphi}, \qquad \frac{d^2\varphi}{d\eta^2} = -\frac{\cos\varphi}{\sin^3\varphi} \tag{B9}$$

Then

$$\frac{d^2G(\varphi)}{d\eta^2} = -\frac{\cos\varphi}{\sin^3\varphi}\frac{dG(\varphi)}{d\varphi} + \frac{1}{\sin^2\varphi}\frac{d^2G(\varphi)}{d\varphi^2} \tag{B10}$$

The derivatives of $G(\varphi)$ are obtained from equation (A1). Then equation (B8) becomes

$$\frac{d^2G(\varphi)}{d\eta^2} = -\sum_{n=1}^{m} l_{\nu_n} G_n \tag{B11}$$

where

$$l_{\nu_n} = \frac{2}{m+1}\sum_{\mu_1=1}^{m}\left(\frac{\cos\mu_1\varphi_\nu}{\tan\varphi_\nu} + \mu_1\sin\mu_1\varphi_\nu\right)\frac{\mu_1\sin\mu_1\varphi_n}{\sin^2\varphi_\nu}$$

$$= \begin{cases} \dfrac{(-1)^{n-\nu}\sin\varphi_n[2\sin^2\varphi_\nu + (\cos\varphi_n - \cos\varphi_\nu)\cos\varphi_\nu]}{\sin^3\varphi_\nu(\cos\varphi_n - \cos\varphi_\nu)^2}, & n \neq \nu \\ \dfrac{m(m+2)\sin^2\varphi_\nu - 3\cos^2\varphi_\nu}{3\sin^4\varphi_\nu}, & n = \nu \end{cases} \tag{B12}$$

For symmetric loading,

$$\frac{d^2G(\varphi)}{d\eta^2} = -\sum_{n=1}^{\frac{m+1}{2}} \bar{l}_{\nu_n} G_n \tag{B13}$$

where

$$\bar{l}_{\nu_n} = \begin{cases} l_{\nu_n} + l_{\nu_{m+1-n}}, & n \neq \frac{m+1}{2} \\ l_{\nu_n}, & n = \frac{m+1}{2} \end{cases} \tag{B14}$$

For $m = 7$, the $\bar{l}_{\nu_n}$ values are given as follows:

$\bar{l}_{\nu_n}$

n \ η	0	0.383	0.707	0.924
1	-1.7934	3.5149	-26.5029	100.7692
2	5.6568	-16.5757	40.0000	-19.1087
3	-25.2346	27.2308	-19.6374	-20.4839
4	21.0000	-13.5139	2.8284	11.7199

With $d^2G/d\eta^2$ evaluated, the next step is to evaluate $d^2\epsilon/d\eta^2$. The downwash of the two-dimensional trailing vortex sheet is given by equation (A2). For $\Omega = 0$, equations (A2) and (A3) simplify and become (e.g., ref. 6, eq. (A19))

$$\epsilon(\varphi) = \sum_{n=1}^{m} G_n \frac{2}{m+1} \sum_{\mu_1=1}^{m} \frac{\mu_1 \sin \mu_1\varphi_n \sin \mu_1\varphi}{\sin \varphi} \tag{B15}$$

Then similar to equation (B10)

$$\frac{d^2\epsilon}{d\eta^2} = -\frac{\cos \varphi}{\sin^3\varphi} \frac{d\epsilon}{d\varphi} + \frac{1}{\sin^2\varphi} \frac{d^2\epsilon}{d\varphi^2} \tag{B16}$$

The derivatives occurring in equation (B16) are obtained by differentiating equation (B15); then after summing up several resulting summations, equation (B16) becomes

$$\frac{d^2\epsilon_\nu}{d\eta^2} = \sum_{n=1}^{m} E_{\nu_n} G_n \tag{B17}$$

where

$$\left.\begin{aligned} E_{\substack{\nu_n \\ n=\nu}} &= \frac{m+1}{4\sin^5\varphi_\nu}\left[15-(m^2+2m+12)\sin^2\varphi_\nu\right] \\ E_{\substack{\nu_n \\ n\neq\nu}} &= \frac{-3\sin\varphi_n}{(m+1)\sin^2\varphi_\nu(\cos\varphi_n-\cos\varphi_\nu)}\left\{\frac{(m+1)^2(-1)^{n-\nu}\cos\varphi_\nu}{\sin^2\varphi_\nu}+\right. \\ &\left.\frac{(m+1)^2(-1)^{n-\nu}}{\cos\varphi_n-\cos\varphi_\nu}+\frac{2[1-(-1)^{n-\nu}]\sin^2\varphi_\nu}{(\cos\varphi_n-\cos\varphi_\nu)^3}\right\} \end{aligned}\right\} \quad \text{(B18)}$$

For symmetric loading

$$\frac{d^2\epsilon_\nu}{d\eta^2} = \sum_{n=1}^{\frac{m+1}{2}} \bar{E}_{\nu_n} G_n \quad \text{(B19)}$$

where

$$\bar{E}_{\nu_n} = \begin{cases} E_{\nu_n} + E_{\nu_{m+1-n}}, & n \neq \frac{m+1}{2} \\ E_{\nu_n}, & n = \frac{m+1}{2} \end{cases} \quad \text{(B20)}$$

For $m = 7$, the $\bar{E}_{\nu_n}$ values are given as follows

$\bar{E}_{\nu_n}$

n \ η	0	0.383	0.707	0.924
1	19.945	-48.262	241.673	1174.743
2	-67.883	128.450	-237.586	-1791.706
3	173.641	-174.776	81.739	1890.134
4	-120.000	89.112	0	-929.163

The lift coefficient can also be given as a summation of G_n.

Thus

$$\frac{C_L}{A} = \sum_{n=1}^{\frac{m+1}{2}} \begin{pmatrix} \frac{2\pi \sin \varphi_n}{m+1}, & n \neq \frac{m+1}{2} \\ \frac{\pi}{m+1}, & n = \frac{m+1}{2} \end{pmatrix} G_n \tag{B21}$$

For $m = 7$, the factors of G_n in equation (B21) are as follows:

n	1	2	3	4
factor	0.3006	0.5554	0.7256	0.3927

As mentioned before, the coefficients of equation (B6) (A_1, A_2, A_3, and A_4) are in terms of $\epsilon(0)$, $\epsilon(1/2)$, $d^2G/d\eta^2$, $d^2\epsilon/d\eta^2$, and $C_L/\pi A$. It has just been seen that $d^2G/d\eta^2$, $d^2\epsilon/d\eta^2$, and $C_L/\pi A$ can be expressed in terms of summations with G_n. Thus, equation (B6) can be written in terms of $\sqrt{\Omega^2/1+\Omega^2}$, $\epsilon(0)$, $\epsilon(1/2)$, and summations of G_n. The equation can now be algebraically rewritten into the form

$$\epsilon(\Omega) = C_1\, \epsilon(0) + C_2\, \epsilon\left(\frac{1}{2}\right) + \sum_{n=1}^{\frac{m+1}{2}} D_n G_n \tag{B22}$$

where the constants C_1, C_2, and D_n contain the $\sqrt{\Omega^2/1+\Omega^2}$ terms and the integration coefficients of $d^2G/d\eta^2$, $d^2\epsilon/d\eta^2$, and C_L/A. Letting $X = \sqrt{\Omega^2/1+\Omega^2}$, the constants are:

$$C_1 = 1 - \frac{172+111\sqrt{5}}{8} X^3 + \frac{539+282\sqrt{5}}{8} X^5 - \frac{610+231\sqrt{5}}{8} X^5 + \frac{235+60\sqrt{5}}{8} X^6 \tag{B23}$$

$$C_2 = \frac{25}{4}(5+3\sqrt{5})X^3 + \frac{25}{8}(35+17\sqrt{5})X^4 + 25(5+2\sqrt{5})X^5 - \frac{25}{8}(15+5\sqrt{5})X^6 \tag{B24}$$

$$D_n = -\left(X - \frac{47+12\sqrt{5}}{4} X^3 + \frac{98+39\sqrt{5}}{4} X^4 - \frac{75+42\sqrt{5}}{4} X^5 + \frac{20+15\sqrt{5}}{4} X^6\right) \bar{l}_{\nu_n} +$$

$$\left(-\frac{1}{2} X^2 + \frac{4+3\sqrt{5}}{4} X^3 - \frac{7+6\sqrt{5}}{4} X^4 + \frac{10+3\sqrt{5}}{4} X^5 - \frac{5}{4} X^6\right) \bar{E}_{\nu_n} +$$

$$\left\{\left[\frac{7+3\sqrt{5}}{2} X^3 - \frac{59+27\sqrt{5}}{4} X^4 + (20+9\sqrt{5}) X^5 - \frac{35+15\sqrt{5}}{4} X^6\right] +\right.$$

$$\left[-\frac{25}{16}(20+9\sqrt{5}) X^3 + \frac{25}{16}(85+38\sqrt{5}) X^4 - \frac{25}{16}(110+49\sqrt{5}) X^5 +\right.$$

$$\left.\left.\frac{125}{16}(9+4\sqrt{5}) X^6\right] \frac{(4-\eta^2)}{(4+\eta^2)^2}\right\} \begin{pmatrix} \frac{2 \sin \varphi_n}{m+1}, & n \neq \frac{m+1}{2} \\ \frac{1}{m+1}, & n = \frac{m+1}{2} \end{pmatrix} \qquad \text{(B25)}$$

For $m = 7$, values of C_1, C_2, and D_n are presented in table II for various values of Ω.

APPENDIX C

DEVELOPMENT OF EQUATIONS PERTAINING TO THE ROLLING-UP CORRECTION

This appendix includes the downwash due to a flat trailing sheet alone, downwash due to a pair of trailing wing-tip vortices, and a reduction to more convenient form of the "rolling-up distance" of reference 4.

Downwash Due to a Flat Trailing Vortex Sheet Extending From the Quarter Chord of the Wing Tip to Infinity

The downwash can be obtained from equation (1) by setting

$$\cos \theta_1 = \frac{x - (b/2) \tan \Lambda}{\sqrt{\left(x - \frac{b}{2} \tan \Lambda\right)^2 + (y-\bar{y})^2 + (z-z_s)^2}} \tag{C1}$$

In dimensionless coordinates, the downwash becomes

$$\frac{w}{V} = \frac{1}{\pi} \int_{-1}^{1} \frac{(\eta-\bar{\eta})G'(\bar{\eta})d\bar{\eta}}{\Omega^2 + (\eta-\bar{\eta})^2} -$$

$$\frac{1}{2\pi} \int_{-1}^{1} \frac{\eta - \bar{\eta}}{\Omega^2 + (\eta-\bar{\eta})^2} \left[1 - \frac{\xi - \tan \Lambda}{\sqrt{(\xi-\tan \Lambda)^2 + (\eta-\bar{\eta})^2 + \Omega^2}}\right] G'(\bar{\eta})d\bar{\eta} \tag{C2}$$

The first integral is integrated analytically in Appendix A, and is given by equation (A12).

The numerical integration of the second integral can be performed by following the procedure of Appendix A. Let

$$L_{T\mu} = \frac{\eta - \bar{\eta}}{\Omega^2 + (\eta-\bar{\eta})^2} \left[1 - \frac{\xi - \tan \Lambda}{\sqrt{(\xi-\tan \Lambda)^2 + (\eta-\bar{\eta})^2 + \Omega^2}}\right] \tag{C3}$$

then the second integral of equation (C2) becomes $\left(\bar{\eta} = \cos \varphi_\mu = \cos \frac{\mu\pi}{m+1}\right)$

$$- \frac{1}{2\pi} \int_0^\pi L_{T\mu} G'(\varphi) d\varphi = \sum_{n=1}^{\frac{m+1}{2}} \bar{g}_{Tn} G_n \tag{C4}$$

where

$$\bar{g}_{Tn} = - \frac{1}{2(M+1)} \sum_{\mu=0}^{\frac{M-1}{2}} \bar{f}_{n\mu} (L_{T\mu} - L_{T,M+1-\mu}) \tag{C5}$$

where $\bar{f}_{n\mu}$ values are given under equation (A14).

For the case of $\eta = \Omega = 0$, the second integral of equation (C2) can be handled in much the same fashion as equation (A2) and with the same limitations. The vorticity distribution is given by equation (A1) which for symmetrical loadings becomes

$$\frac{dG(\varphi)}{d\varphi} = \frac{2}{m+1} \left[G_{\left(\frac{m+1}{2}\right)} \sum_{\mu_1=1,\text{odd}}^{m} \mu_1 (-1)^{\left(\frac{\mu_1-1}{2}\right)} \cos \mu_1 \varphi + 2 \sum_{n=1}^{\frac{m-1}{2}} G_n \sum_{\mu_1=1,\text{odd}}^{m} \mu_1 \sin \mu_1 \varphi_n \cos \mu_1 \varphi \right] \tag{C6}$$

With equation (C6), the second integral can be written as

$$- \frac{1}{2\pi} \int_0^\pi L_{T\mu} G'(\varphi) d\varphi = G_{\left(\frac{m+1}{2}\right)} \left[\frac{-1}{(m+1)\pi} \sum_{\mu_1=1,\text{odd}}^{m} \mu_1 (-1)^{\left(\frac{\mu_1-1}{2}\right)} \int_0^\pi L_{T\mu} \cos \mu_1 \varphi \, d\varphi \right] + \sum_{n=1}^{\frac{m-1}{2}} G_n \left[\frac{-2}{(m+1)\pi} \sum_{\mu_1=1,\text{odd}}^{m} \mu_1 \sin \mu_1 \varphi_n \int_0^\pi L_{T\mu} \cos \mu_1 \varphi \, d\varphi \right] \tag{C7}$$

Now, for $\Omega = \eta = 0$

$$\int_0^{\pi} L_{\mp\mu} \cos \mu_1\varphi \, d\varphi = \int_0^{\pi} \frac{1}{\cos \varphi}\left[1 - \frac{\xi - \tan \Lambda}{\sqrt{(\xi - \tan \Lambda)^2 + \cos^2\varphi}}\right] \cos \mu_1\varphi \, d\varphi$$

$$= \pi \sin \mu_1\left(\frac{\pi}{2}\right) - (\xi - \tan \Lambda) \int_0^{\pi} \frac{\cos \mu_1\varphi \, d\varphi}{\cos \varphi\sqrt{(\xi - \tan \Lambda)^2 + \cos^2\varphi}} \tag{C8}$$

The integral remaining in equation (C8) can be written as[1]

$$\int_0^{\pi} \frac{\cos \mu_1\varphi \, d\varphi}{\cos \varphi\sqrt{(\xi - \tan \Lambda)^2 + \cos^2\varphi}} = 2k \int_0^{\pi/2} \frac{\cos \mu_1\varphi \, d\varphi}{\cos \varphi\sqrt{1 - k^2\sin^2\varphi}} \tag{C9}$$

where

$$k = \frac{1}{\sqrt{1 + (\xi - \tan \Lambda)^2}}$$

This integral is evaluated by a recursion method.

For odd values of μ_1

$$\frac{\cos \mu_1\varphi}{\cos \varphi} = 2^{\mu_1 - 1} \cos^{\mu_1 - 1} \varphi - \sum_{l=1}^{\frac{\mu_1 - 1}{2}} \frac{\mu_1! \cos (\mu_1 - 2l)\varphi}{l!(\mu_1 - l)! \cos \varphi} \tag{C10}$$

Hence,

$$D_{\mu_1} = 2^{\mu_1} k \, R\left(\frac{\mu_1 - 1}{2}\right) - \sum_{l=1}^{\frac{\mu_1 - 1}{2}} \frac{\mu_1! \, D_{\mu_1 - 2l}}{l! \, (\mu_1 - l)!} \tag{C11}$$

[1]The integration of equation (C9) was obtained with the aid of reference 16.

where

$$D_{\mu_1} = 2k \int_0^{\pi/2} \frac{\cos \mu_1 \varphi \, d\varphi}{\cos \varphi \sqrt{1-k^2 \sin^2 \varphi}} \tag{C12}$$

$$R_{\left(\frac{\mu_1-1}{2}\right)} = \int_0^{\pi/2} \frac{\cos^{\mu_1-1} \varphi \, d\varphi}{\sqrt{1-k^2 \sin^2 \varphi}} \tag{C13}$$

For $\mu_1 = 1$ and $\mu_1 = 3$, equation (C13) integrates directly to

$$R_0 = \frac{D_1}{2k} = K$$

$$R_1 = \frac{1}{k^2} [E - (1-k^2)K] \tag{C14}$$

where K and E are complete elliptic integrals of the first and second kind, respectively. Higher terms of $R_{\left(\frac{\mu_1-1}{2}\right)}$ can now be obtained from the recursion formula:

$$R_{\left(\frac{\mu_1-1}{2}\right)} = \frac{1}{(\mu_1-2)k^2} \left[(\mu_1-4)(1-k^2) R_{\left(\frac{\mu_1-5}{2}\right)} + (\mu_1-3)(2k^2-1) R_{\left(\frac{\mu_1-3}{2}\right)} \right] \tag{C15}$$

With values of $R_{\left(\frac{\mu_1-1}{2}\right)}$ determined, the values of D_{μ_1} are obtained from the recursion formula of equation (C11). Then

$$\left.\begin{aligned} D_1 &= 2kK \\ D_3 &= -\frac{2}{k}[(4 - k^2)K - 4E] \\ D_5 &= \frac{2}{3k^3}[(32 - 20k^2 + 3k^4)K - 4(8 - k^2)E] \\ D_7 &= -\frac{2}{15k^5}[(512 - 608k^2 + 216k^4 - 15k^6)K - (512 - 352k^2 + 72k^4)E] \end{aligned}\right\} \tag{C16}$$

where k follows equation (C9).

Thus the second integral is evaluated exactly for $\Omega = \eta = 0$ and, in summary, is given by

$$-\frac{1}{2\pi}\int_0^{\pi} L_{T\mu}G'(\varphi)\,d\varphi =$$

$$G_{\left(\frac{m+1}{2}\right)}\left\{\frac{-1}{(m+1)\pi}\sum_{\mu_1=1,\text{odd}}^{m}\mu_1(-1)^{\left(\frac{\mu_1-1}{2}\right)}\left[\pi(-1)^{\left(\frac{\mu_1-1}{2}\right)} - (\xi-\tan\Lambda)D_{\mu_1}\right]\right\} +$$

$$\sum_{n=1}^{\frac{m-1}{2}} G_n\left\{\frac{-2}{(m+1)\pi}\sum_{\mu_1=1,\text{odd}}^{m}\mu_1\sin\mu_1\varphi_n\left[\pi\sin\mu_1\frac{\pi}{2} - (\xi-\tan\Lambda)D_{\mu_1}\right]\right\} \qquad (C17)$$

where the D_{μ_1} values are given by equation (C16) and for higher values of μ_1 by the recursion formula of equation (C11).

Similar to the work of Appendix A the downwash, given by equation (C3), can be expressed as the sum of the products of influence coefficients and values of the loading distribution, or

$$\frac{w}{V} = \sum_{n=1}^{\frac{m+1}{2}} a_{Tn}G_n \qquad (C18)$$

where

$$a_{Tn} = 2B_{sn} + \frac{-1}{2(M+1)}\sum_{\mu=0}^{\frac{M-1}{2}}\bar{f}_{n\mu}\Delta L_{T\mu}$$

The coefficient, B_{sn}, follows equation (A14). Similarly, $\bar{f}_{n\mu}$ also

follows equation (A14)

$$\Delta L_{T\mu} = \frac{\eta - \bar{\eta}_\mu}{\Omega^2 + (\eta-\bar{\eta}_\mu)^2}\left[1 - \frac{\xi - \tan\Lambda}{\sqrt{(\xi-\tan\Lambda)^2 + (\eta-\bar{\eta}_\mu)^2 + \Omega^2}}\right] -$$

$$\frac{\eta + \bar{\eta}_\mu}{\Omega^2 + (\eta+\bar{\eta}_\mu)^2}\left[1 - \frac{\xi - \tan\Lambda}{\sqrt{(\xi-\tan\Lambda)^2 + (\eta+\bar{\eta}_\mu)^2 + \Omega^2}}\right]$$

$$\bar{\eta}_\mu = \cos\frac{\mu\pi}{m+1}$$

For $\eta = \Omega = 0$, the analytical integration which evaluates a_{Tn} is

$$a_{Tn} = B_{sn} + \begin{cases} \dfrac{2(\xi-\tan\Lambda)}{(m+1)\pi} \displaystyle\sum_{\mu_1=\text{odd}}^{m} \mu_1 D_{\mu_1} \sin \mu_1\varphi, & n \neq \dfrac{m+1}{2} \\ \dfrac{\xi-\tan\Lambda}{(m+1)\pi} \displaystyle\sum_{\mu_1=\text{odd}}^{m} \mu_1 D_{\mu_1} (-1)^{\frac{\mu_1-1}{2}}, & n = \dfrac{m+1}{2} \end{cases} \qquad \text{(C19)}$$

where D_{μ_1} values are given in equation (C16).

Downwash Due to Two Trailing Vortices

Let the lateral position of the two vortices be at $\bar{\eta} = \pm\eta_c$ where η_c is the fraction of wing semispan from mid-wing to the center of the wing tip vortex. The downwash equation is obtained by substituting

$$-\int_0^{\eta_c} G'(\bar{\eta})\,d\bar{\eta} = G(0)$$

plus and minus values of η_c for $\bar{\eta}$, and $\eta_c b$ for b in equation (C3). Then

$$\frac{w}{V} = \frac{G(0)}{2\pi}\left\{\frac{\eta_c - \eta}{\Omega^2 + (\eta_c-\eta)^2}\left[1 + \frac{\xi - \tan\Lambda}{\sqrt{(\xi-\tan\Lambda)^2 + (\eta_c-\eta)^2 + \Omega^2}}\right] + \right.$$

$$\left.\frac{\eta_c + \eta}{\Omega^2 + (\eta_c+\eta)^2}\left[1 + \frac{\xi - \tan\Lambda}{\sqrt{(\xi-\tan\Lambda)^2 + (\eta_c+\eta)^2 + \Omega^2}}\right]\right\} \qquad \text{(C20)}$$

Now, η_c can be absorbed into coordinate parameters, then

$$\frac{w/V}{2\frac{G(0)}{\eta_c}} = \frac{1}{4\pi}\left\{\frac{1-\frac{\eta}{\eta_c}}{\left(\frac{\Omega}{\eta_c}\right)^2+\left(1-\frac{\eta}{\eta_c}\right)^2}\left[1+\frac{\left(\frac{\xi-\tan\Lambda}{\eta_c}\right)}{\sqrt{\left(\frac{\xi-\tan\Lambda}{\eta_c}\right)^2+\left(1-\frac{\eta}{\eta_c}\right)^2+\left(\frac{\Omega}{\eta_c}\right)^2}}\right]+\right.$$

$$\left.\frac{1+\frac{\eta}{\eta_c}}{\left(\frac{\Omega}{\eta_c}\right)^2+\left(1+\frac{\eta}{\eta_c}\right)^2}\left[1+\frac{\left(\frac{\xi-\tan\Lambda}{\eta_c}\right)}{\sqrt{\left(\frac{\xi-\tan\Lambda}{\eta_c}\right)^2+\left(1+\frac{\eta}{\eta_c}\right)^2+\left(\frac{\Omega}{\eta_c}\right)^2}}\right]\right\} \tag{C21}$$

Roll-Up Distance, $\xi_c - \xi_o$

The longitudinal distance at which the vortex sheet is essentially rolled-up is a function of wing loading, lift coefficient, aspect ratio, and sweep. The roll-up distance given in reference 4 is given by (when the coordinates are changed to the present notation),

$$\xi_c - \xi_o = \frac{5.05(1-\eta_{c_\infty})^{3/2}}{\lim\limits_{\varphi\to o}\frac{G(\varphi)}{\sqrt{1-\cos\varphi}}} \tag{C22}$$

where ξ_o represents the start of the rolling-up process.

A simple numerical method for evaluating the denominator of equation (C22) is as follows. The loading distribution is given by the series

$$G(\varphi) = \frac{2}{m+1}\sum_{n=1}^{m} G_n \sum_{\mu_1=1}^{m} \sin\mu_1\varphi_n \sin\mu_1\varphi \tag{C23}$$

With equation (C23), the denominator of equation (C22) becomes

$$\lim_{\varphi \to 0} \frac{G(\varphi)}{\sqrt{1-\cos\varphi}} = \frac{2}{m+1} \sum_{n=1}^{m} G_n \sum_{\mu_1=1}^{m} \sin \mu_1 \varphi_n \left(\lim_{\varphi \to 0} \frac{\sin \mu_1 \varphi}{\sqrt{1-\cos\varphi}} \right)$$

$$= \sum_{n=1}^{m} G_n \frac{2\sqrt{2}}{m+1} \sum_{\mu_1=1}^{m} \mu_1 \sin \mu_1 \varphi_n \qquad (C24)$$

For symmetric loading for which $G_n = G_{m+1-n}$ and μ_1 is only odd, equation (C24) becomes

$$\lim_{\varphi \to 0} \frac{G(\varphi)}{\sqrt{1-\cos\varphi}} = \left(\frac{2\sqrt{2}}{m+1} \sum_{\mu_1=\text{odd}}^{m} \mu_1 \sin \mu_1 \frac{\pi}{2} \right) G_{\left(\frac{m+1}{2}\right)} +$$

$$\sum_{n=1}^{\frac{m-1}{2}} \left(\frac{4\sqrt{2}}{m+1} \sum_{\mu_1=\text{odd}}^{m} \mu_1 \sin \mu_1 \varphi_n \right) G_n \qquad (C25)$$

The summation, $\sum_{\mu_1=1}^{m} \mu_1 \sin \mu_1 \varphi_n$, in equation (C25) can be evaluated as follows:

let

$$Z = e^{i\varphi_n} = \cos \varphi_n + i \sin \varphi_n$$

then,

$$\sum_{\mu_1=\text{odd}}^{m} \mu_1 \sin \mu_1 \varphi_n = \text{imaginary part of} \left[Z \frac{d \sum_{\mu_1 \text{odd}}^{m} Z^{\mu_1}}{dZ} \right] = \frac{-(m+1)(-1)^n}{2 \sin \varphi_n} \qquad (C26)$$

With equation (C26), equation (C25) becomes

$$\lim_{\varphi \to o} \frac{G(\varphi)}{\sqrt{1 - \cos \varphi}} = - \sqrt{2}\, G_{\left(\frac{m+1}{2}\right)} - 2\sqrt{2} \sum_{n=1}^{\frac{m-1}{2}} \frac{(-1)^n G_n}{\sin \varphi_n} \qquad (C27)$$

Equation (C27) inserted into equation (C22) gives

$$\xi_c - \xi_o = \frac{5.05(1 - \eta_{c_\infty})^{3/2}}{-\sqrt{2}\, G_{\left(\frac{m+1}{2}\right)} - 2\sqrt{2} \sum_{n=1}^{\frac{m-1}{2}} \frac{(-1)^n G_n}{\sin \varphi_n}} \qquad (C28)$$

For $m = 7$ equation (C28) simplifies to the following:

$$\xi_c - \xi_o = \frac{(1 - \eta_{c_\infty})^{3/2}}{1.4630\, G_1 - 0.7917\, G_2 + 0.6060\, G_3 - 0.2799\, G_4}$$

$$= \frac{(1 - \eta_{c_\infty})^{3/2} \left(\frac{A}{C_L}\right)}{0.7315\, K_1 - 0.3959\, K_2 + 0.3030\, K_3 - 0.1400\, K_4}$$

where the subscripts pertain to span stations $n = 1, 2, 3$, and 4; or $\eta = \cos \frac{n\pi}{8} = 0.9239, 0.7071, 0.3827$, and 0, respectively.

REFERENCES

1. Silverstein, Abe, and Katzoff, S.: Design Charts for Predicting Downwash Angles and Wake Characteristics Behind Plain and Flapped Wings. NACA Rep. 648, 1939.

2. Silverstein, Abe, Katzoff, S., and Bullivant, W. Kenneth: Downwash and Wake Behind Plain and Flapped Airfoils. NACA Rep. 651, 1939.

3. DeYoung, John: Theoretical Symmetric Span Loading Due to Flap Deflection for Wings of Arbitrary Plan Form at Subsonic Speeds. NACA Rep. 1071, 1952. (Supersedes NACA TN 2278)

4. Spreiter, John R., and Sacks, Alvin H.: The Rolling Up of the Trailing Vortex Sheet and its Effect on the Downwash Behind Wings. Jour. Aero. Sci. (preprint 250), vol. 18, no. 1, Jan. 1951, pp. 21-32.

5. Multhopp, H.: Methods for Calculating the Lift Distribution of Wings (Subsonic Lifting Surface Theory). Rep. Aero. 2353, British R.A.E., 1950.

6. DeYoung, John, and Harper, Charles W.: Theoretical Symmetric Span Loading at Subsonic Speeds for Wings Having Arbitrary Plan Form. NACA Rep. 921, 1949.

7. Glauert, Hermann: The Elements of Aerofoil and Airscrew Theory. The MacMillan Co., New York, 1943.

8. Holstein, H.: The Downwash. Part 3.6 of AVA Monographs, A. Betz, ed., F_1. Theory of the Three-Dimensional Aerofoil, I. Ginzel, ed. M.A.P., Volkenrode, VG 326 (Rep. & Translations 1026), British, 1948.

9. Lotz, I., and Fabricius, W.: Die Berechnung des Abwindes hinter einem Tragflügel bei Berüchsinchtigung des Aufwichelns der Unstetigkeitsfläche. Luftfahrtforschung Bd 14, Lfg 11, 1937, pp. 552-557.

10. Rogers, Arthur W.: Application of Two-Dimensional Vortex Theory to the Prediction of Flow Fields Behind Wings of Wing-Body Combinations at Subsonic and Supersonic Speeds. NACA TN 3227, 1954.

11. Ward, G. N.: Supersonic Flow Past Slender Pointed Bodies. Quart. Jour. Mech. and Appl. Math., vol. II, pt. 1, 1949, pp. 75-97.

12. Furlong, G. Chester, and Bollech, Thomas V.: Downwash, Sidewash, and Wake Surveys Behind a 42° Sweptback Wing at a Reynolds Number of 6.8×10^6 with and without a Simulated Ground. NACA RM L8G22, 1948.

13. Tolhurst, William H., Jr.: Downwash Characteristics and Vortex-Sheet Shape Behind a 63° Swept-Back Wing-Fuselage Combination at a Reynolds Number of 6.1×10^6. NACA TN 3175, 1954.

14. Luetgebrune, H.: Nachlauf-und Widerstandsuntersuchungen an Gepfeilten und Ungepfeilten Tragflugeln. Zentrale für Wissenschaftliches Berichtswesen der Luftfahrtforschung, FB 1672, Berlin, Sept. 1942.

15. Bierens de Hann, David: Examen des Nouvelles Tables D'Integrales Definies. G. E. Stechert and Company, New York, 1944.

16. Byrd, P. E., and Friedman, M. D.: Handbook of Elliptic Integrals for Engineers and Physicists. (Grundlehren der mathematischen wissenshaften in Einzeldarstellungen, Bd. LXVII.) Springer-Verlag, Berlin, 1954.

TABLE I.- LATERAL INTERPOLATION FACTORS

H_n \ η	0.098	0.195	0.290	0.556	0.831	0.981
H_1	0.0030	0.0089	0.0102	-0.0449	0.3378	1.6982
H_2	-.0178	-.0538	-.0645	.4365	.9777	-1.3604
H_3	.1086	.3916	.7361	.8790	-.5861	1.3155
H_4	.9061	.6533	.3182	-.2706	.2706	-.6533
H_1+H_2	-.0148	-.0449	-.0543	.3916	---	---

NACA

TABLE II.- VERTICAL INTERPOLATION FACTORS

Ω	±0.1	±0.2	±0.3	±0.8
	For all η			
C_1	0.9611	0.7819	0.5005	-0.1947
C_2	.0522	.2784	.5986	.9978
n	D_n, η = 0			
1	.0973	.0932	.0559	-.0029
2	-.2957	-.2788	-.1699	.0591
3	1.6725	1.9224	1.3752	-.5490
4	-1.4618	-1.7412	-1.2816	.5816
n	D_n, η = 0.383			
1	-.1667	-.1392	-.0734	.0125
2	1.0587	1.1846	.8303	-.3137
3	-1.8423	-2.1540	-1.5653	.6952
4	.9066	1.0512	.7570	-.8976

Ω	±0.1	±0.2	±0.3	±0.8
n	D_n, η = 0.707			
1	1.5928	1.7007	1.1502	-0.4075
2	-2.7584	-3.2636	-2.3921	1.0580
3	1.4504	1.7888	1.3447	-.6115
4	-.2506	-.3236	-.2566	.1384
n	D_n, η = 0.924			
1	-11.8776	-17.8814	-15.0373	8.4886
2	6.6138	11.9406	10.8359	-6.7796
3	-3.5043	-7.9690	-7.7815	5.3097
4	1.5814	3.7283	3.6751	-2.5254

NACA

TABLE III.- $\bar{f}_{n\mu}$, FOR SEVERAL VALUES OF m AND M

μ(for m = 7)						
M = 7	M = 15	M = 31	n = 1	n = 2	n = 3	n = 4
0	0	0	2.6131	-1.4142	1.0824	-0.5000
---	---	1	4.5889	-2.1053	1.5663	-.7193
---	1	2	2.8844	-.2363	.0751	-.0253
---	---	3	.6573	2.0046	-1.5402	.7109
1	2	4	-1.4142	3.6955	-2.4142	1.0824
---	---	5	-2.7625	4.1506	-2.0037	.8553
---	3	6	-3.1207	3.1958	-.3621	.1005
---	---	7	-2.5843	1.2224	1.8601	-.8209
2	4	8	-1.5307	-1.0000	3.6955	-1.4142
---	---	9	-.4383	-2.6609	4.2950	-1.2844
---	5	10	.3114	-3.2465	3.3216	-.3367
---	---	11	.5651	-2.7288	1.1207	1.1492
3	6	12	.4142	-1.5307	-1.4142	2.6131
---	---	13	.1016	-.2939	-3.2260	3.4397
---	7	14	-.1258	.4372	-3.5579	3.2212
---	---	15	-.1444	.4635	-2.2904	1.9416

m = M = 15

μ	n = 1	n = 2	n = 3	n = 4	n = 5	n = 6	n = 7	n = 8
0	5.1258	-2.6131	1.800	-1.4142	1.2027	-1.0824	1.0196	-0.5000
1	-2.6131	6.9258	-4.0273	3.0027	-2.4966	2.2223	-2.0824	1.0196
2	-3.3258	-1.4142	6.3285	-3.6955	2.8196	-2.4142	2.2223	-1.0824
3	1.1989	-3.9231	-1.0824	6.1454	-3.6131	2.8196	-2.4966	1.2027
4	-.5973	1.5307	-4.1062	-1.0000	6.1454	-3.6955	3.0027	-1.4142
5	.3318	-.7804	1.6131	-4.1062	-1.0824	6.3285	-4.0273	1.8000
6	-.1831	.4142	-.7804	1.5307	-3.9231	-1.4142	6.9258	-2.6131
7	.0824	-.1831	.3318	-.5973	1.1989	-3.3258	-2.6131	5.1258

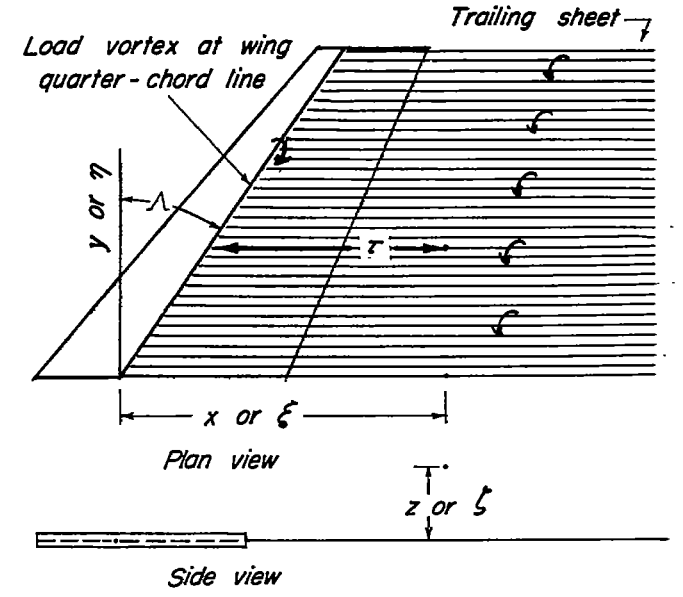

Coordinates of flat-sheet vortex system

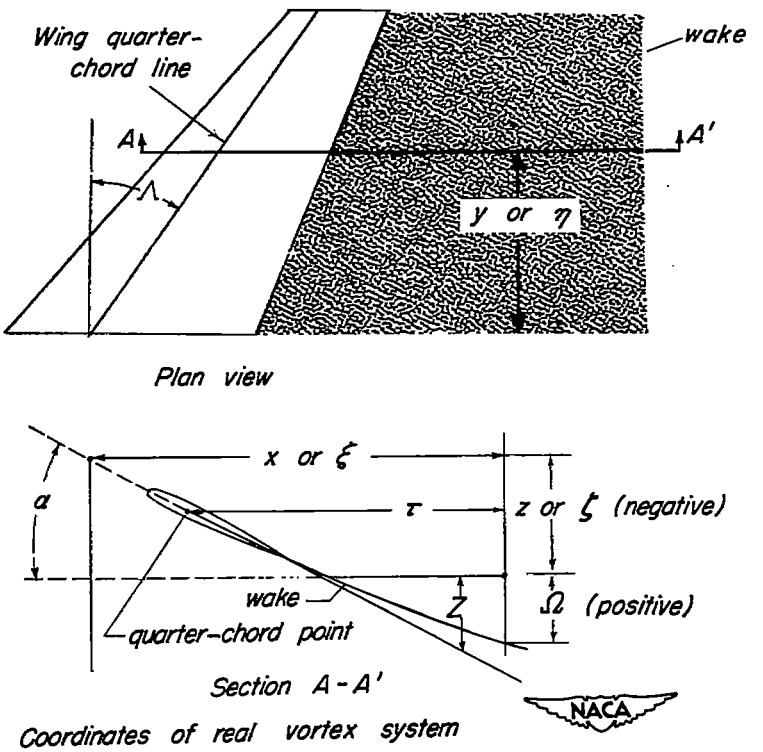

Coordinates of real vortex system

Figure 1.- Illustration of coordinates.

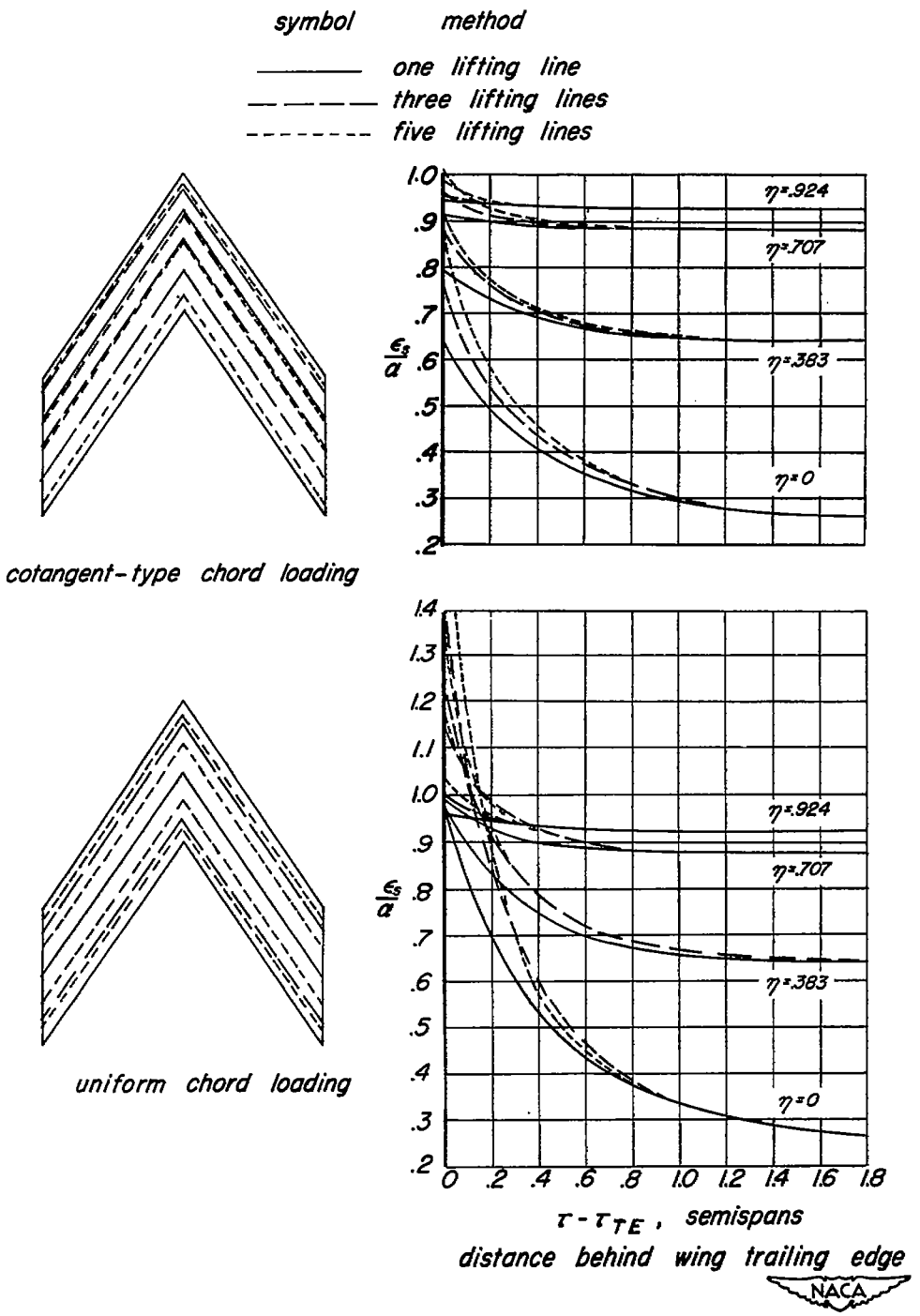

(a) $\lambda = 1.0$

Figure 2.- Comparison of the downwash field due to a lifting line with that due to a lifting surface composed of several lifting lines. ($A = 2.0$, $\Lambda = 56^\circ$, $\Omega = 0$)

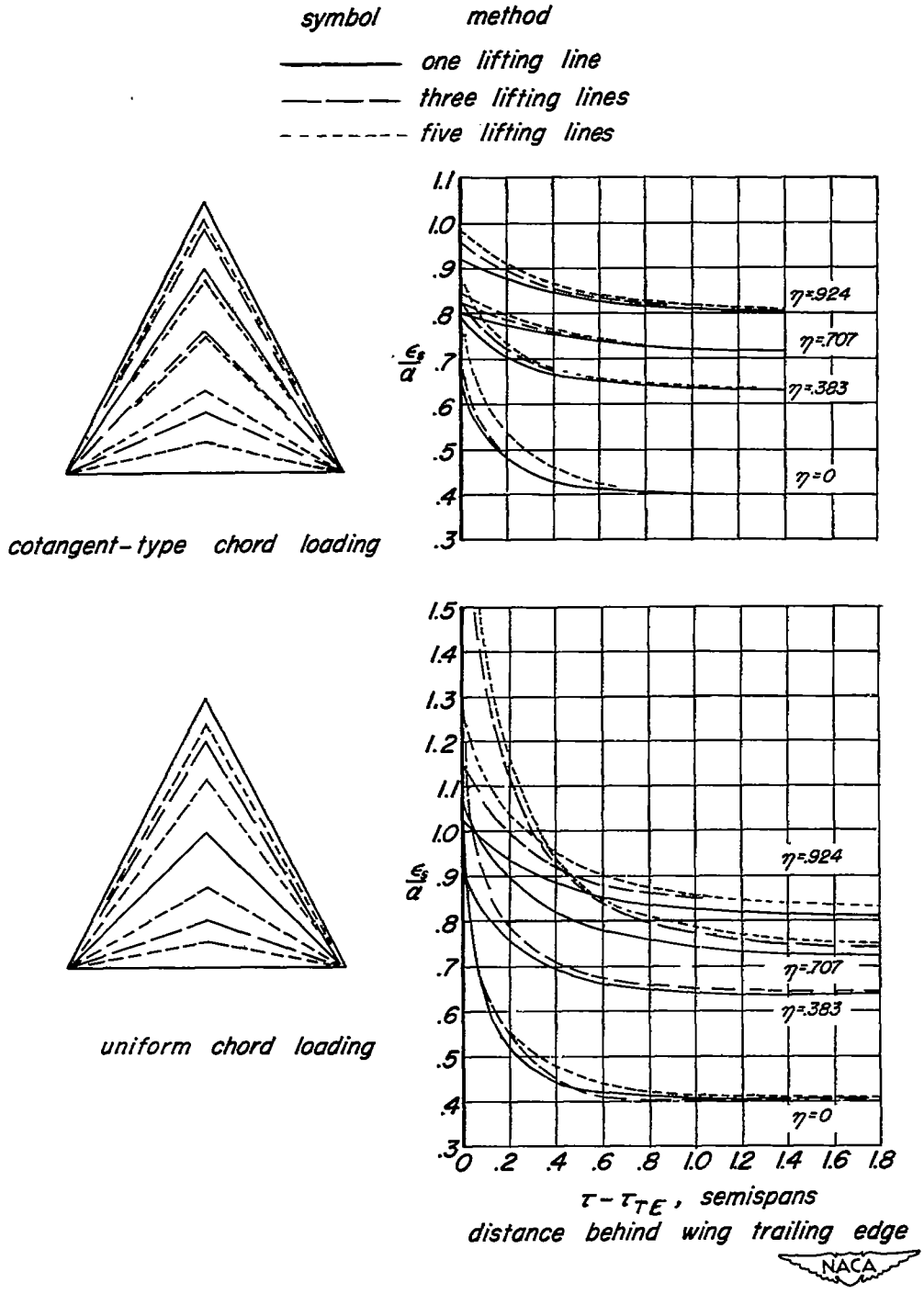

(b) $\lambda = 0$

Figure 2.- Concluded.

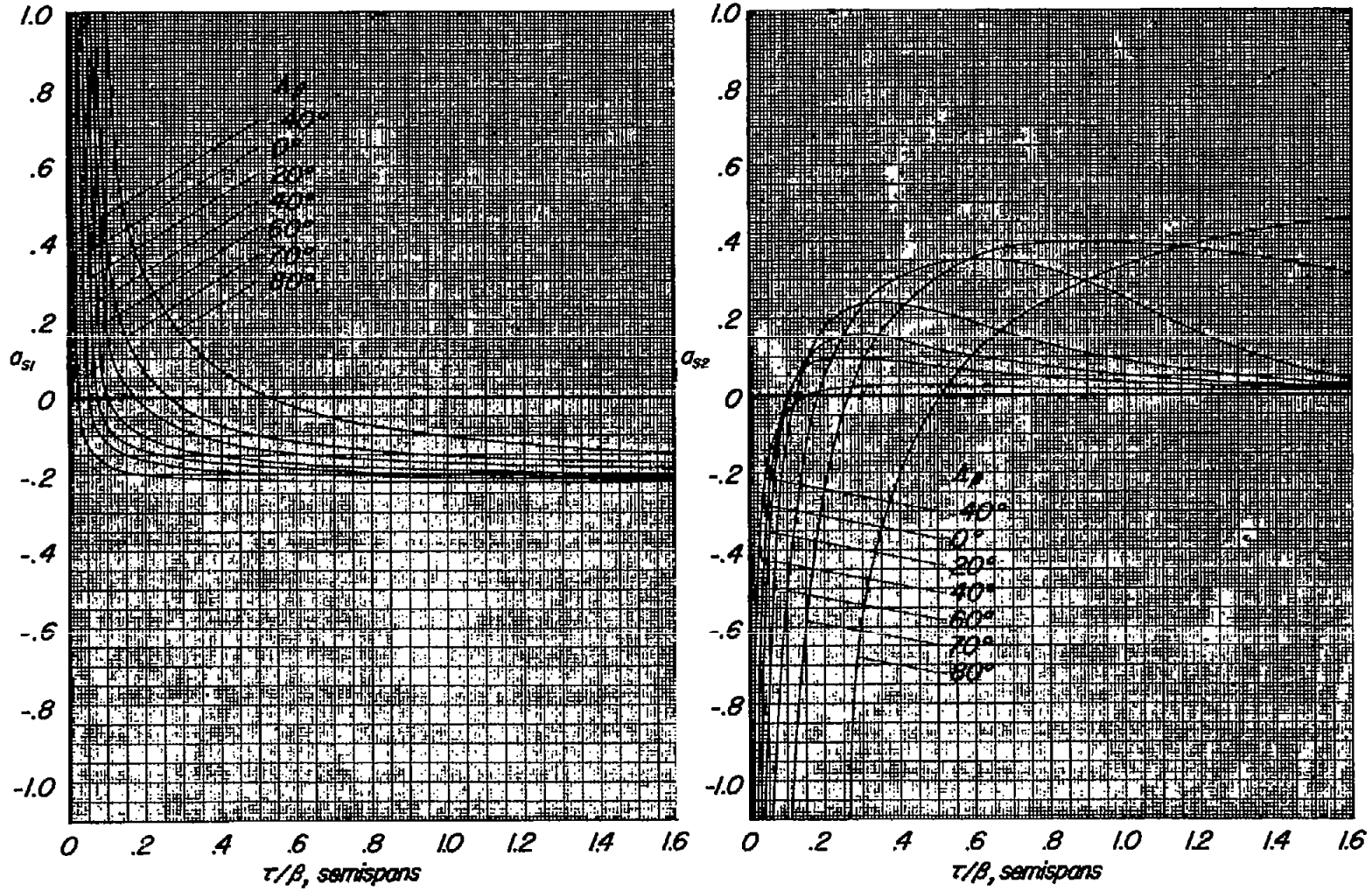
1.0
.8
.6
.4
.2
0
-.2
-.4
-.6
-.8
-1.0
a_{s1}
a_{s2}
Λ_f
40°
0°
20°
40°
60°
70°
80°
0
.2
.4
.6
.8
1.0
1.2
1.4
1.6
τ/β, semispans

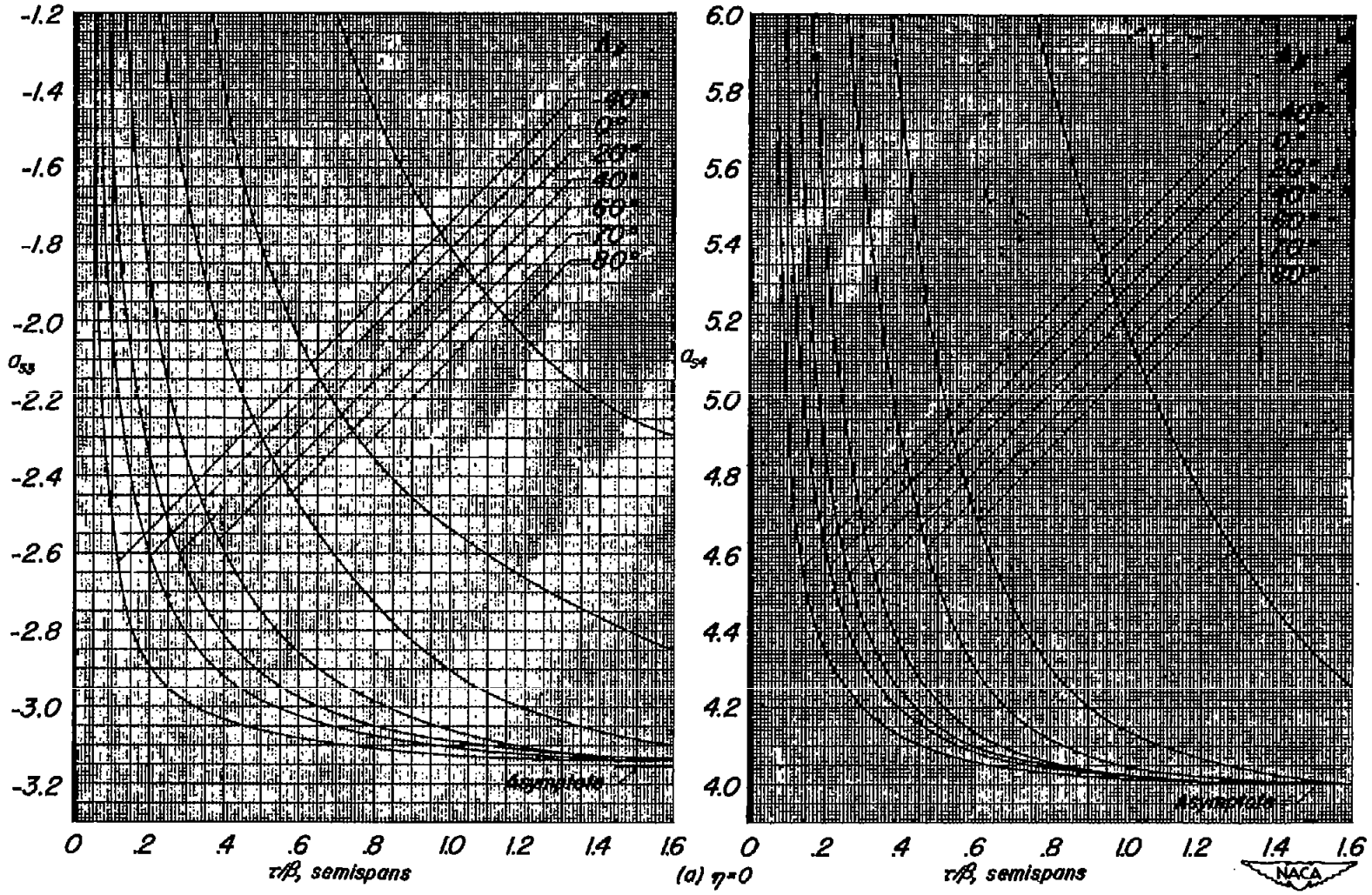

(a) $\eta = 0$

Figure 3.- Downwash influence coefficient, a_{sn}, due to total flat-sheet vortex system; τ/β aft of c/4, $\Omega_s = 0$.

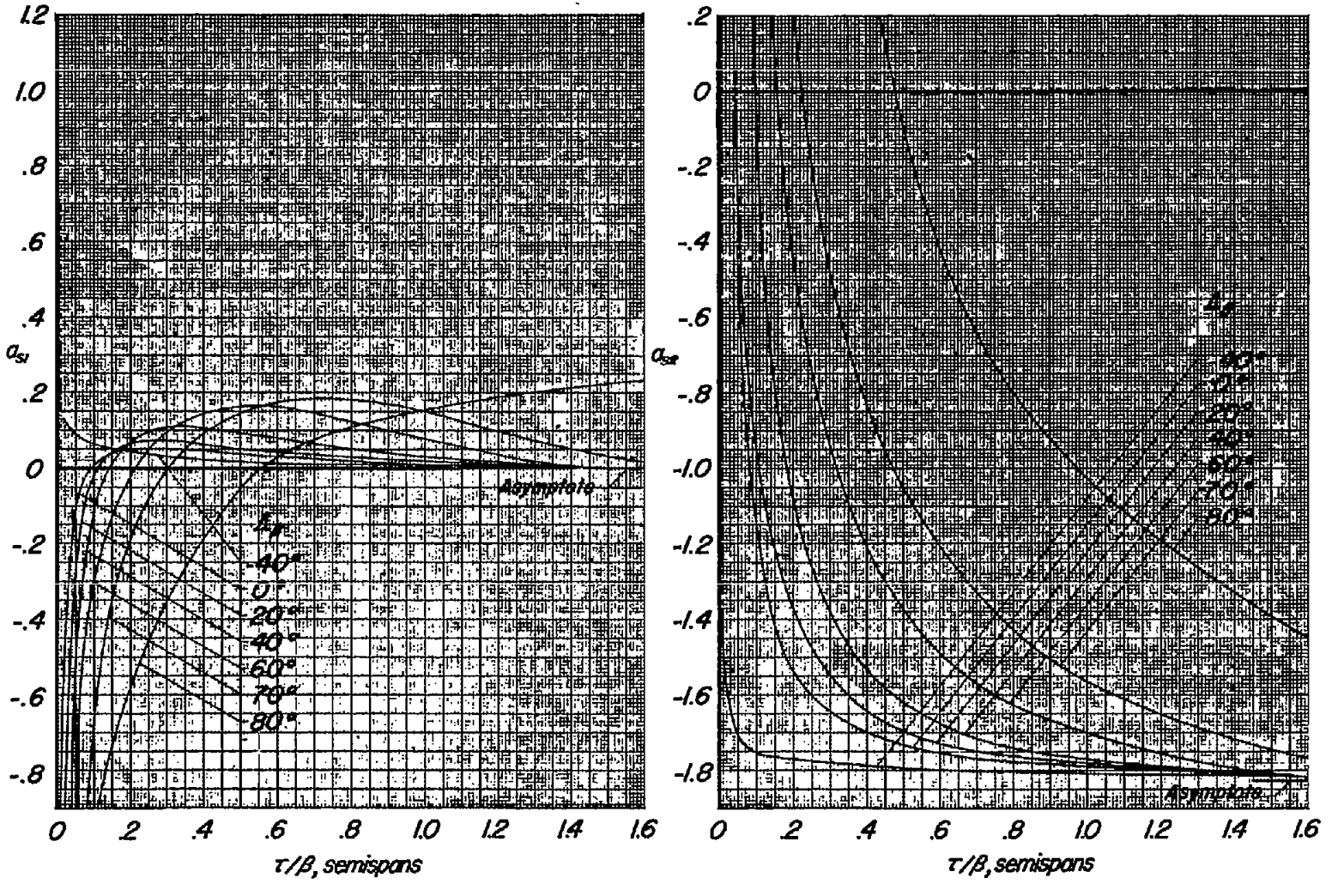
1.2
1.0
.8
.6
.4
.2
0
-.2
-.4
-.6
-.8
a_{si}
Asymptote
Λ_T
-40°
0
20°
40°
60°
70°
80°
0 .2 .4 .6 .8 1.0 1.2 1.4 1.6
τ/β, semispans
.2
0
-.2
-.4
-.6
-.8
-1.0
-1.2
-1.4
-1.6
-1.8
a_{se}
Asymptote
Λ_T
-40°
0
20°
40°
60°
70°
80°
0 .2 .4 .6 .8 1.0 1.2 1.4 1.6
τ/β, semispans

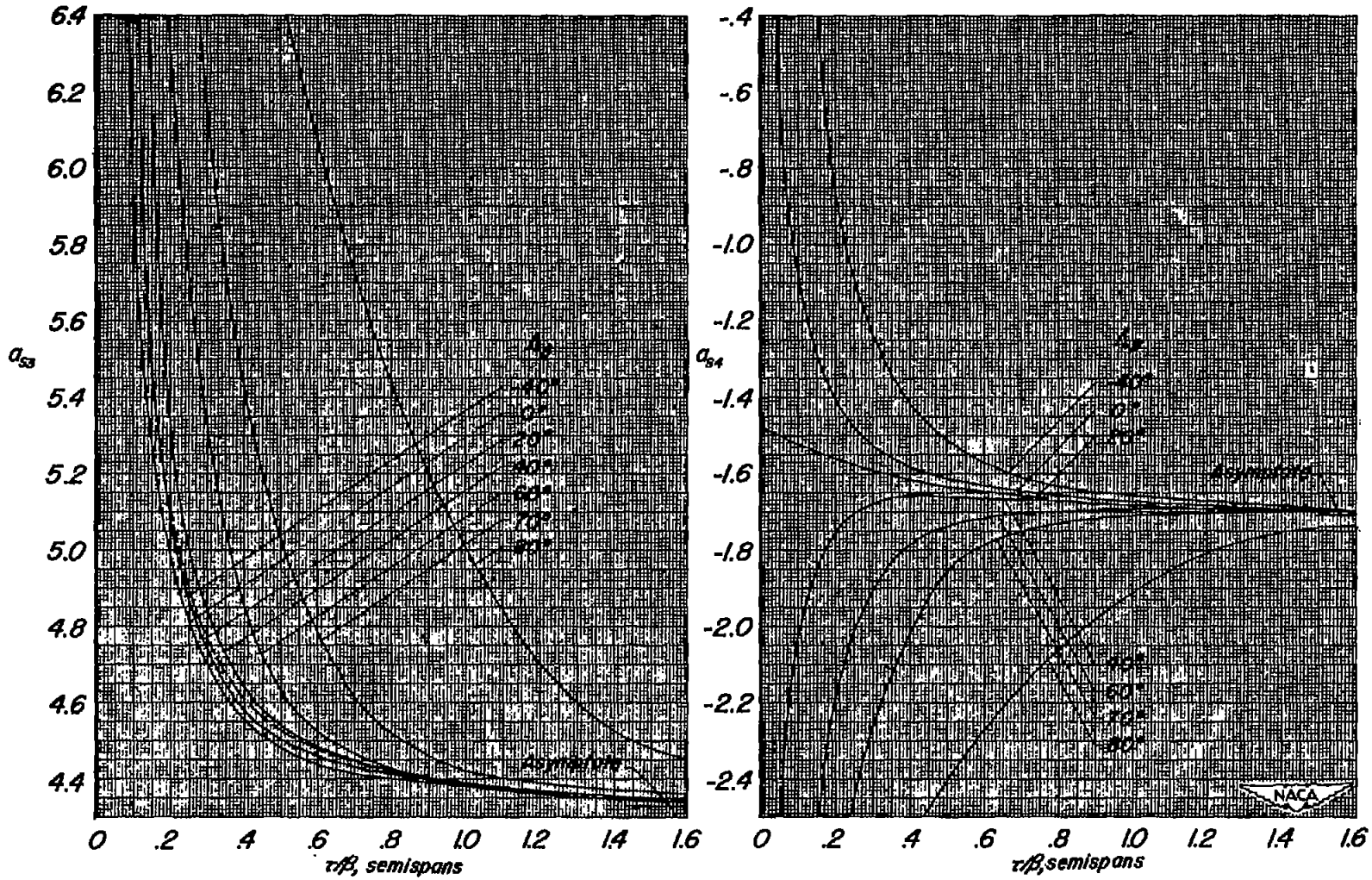

(b) $\eta = 0.383$

Figure 3.- Continued.

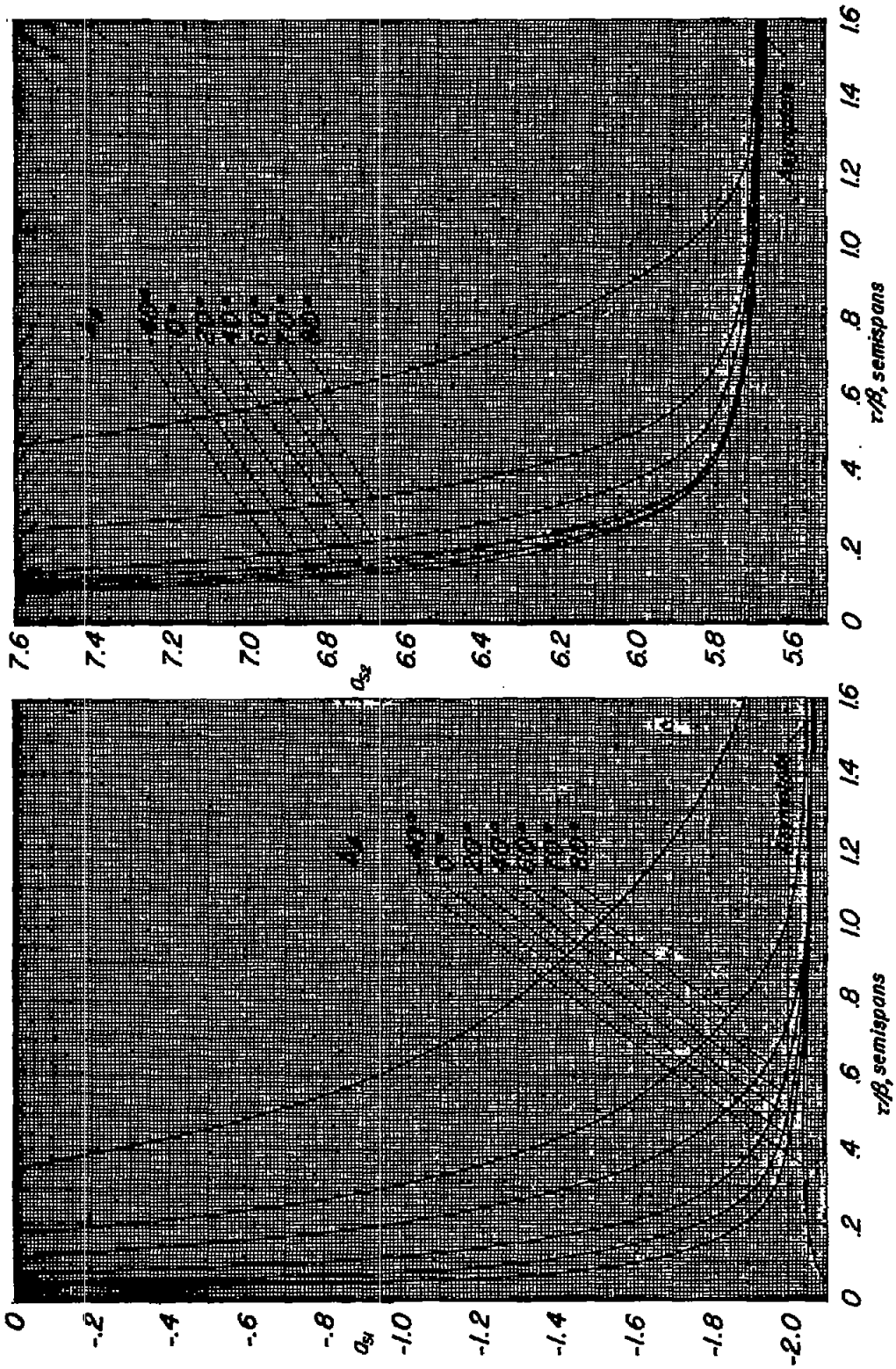
7.6
7.4
7.2
7.0
6.8
6.6
6.4
6.2
6.0
5.8
5.6
a_{3x}
0
.2
.4
.6
.8
1.0
1.2
1.4
1.6
r/β, semispans
0
-.2
-.4
-.6
-.8
-1.0
-1.2
-1.4
-1.6
-1.8
-2.0
a_{3l}
r/β, semispans

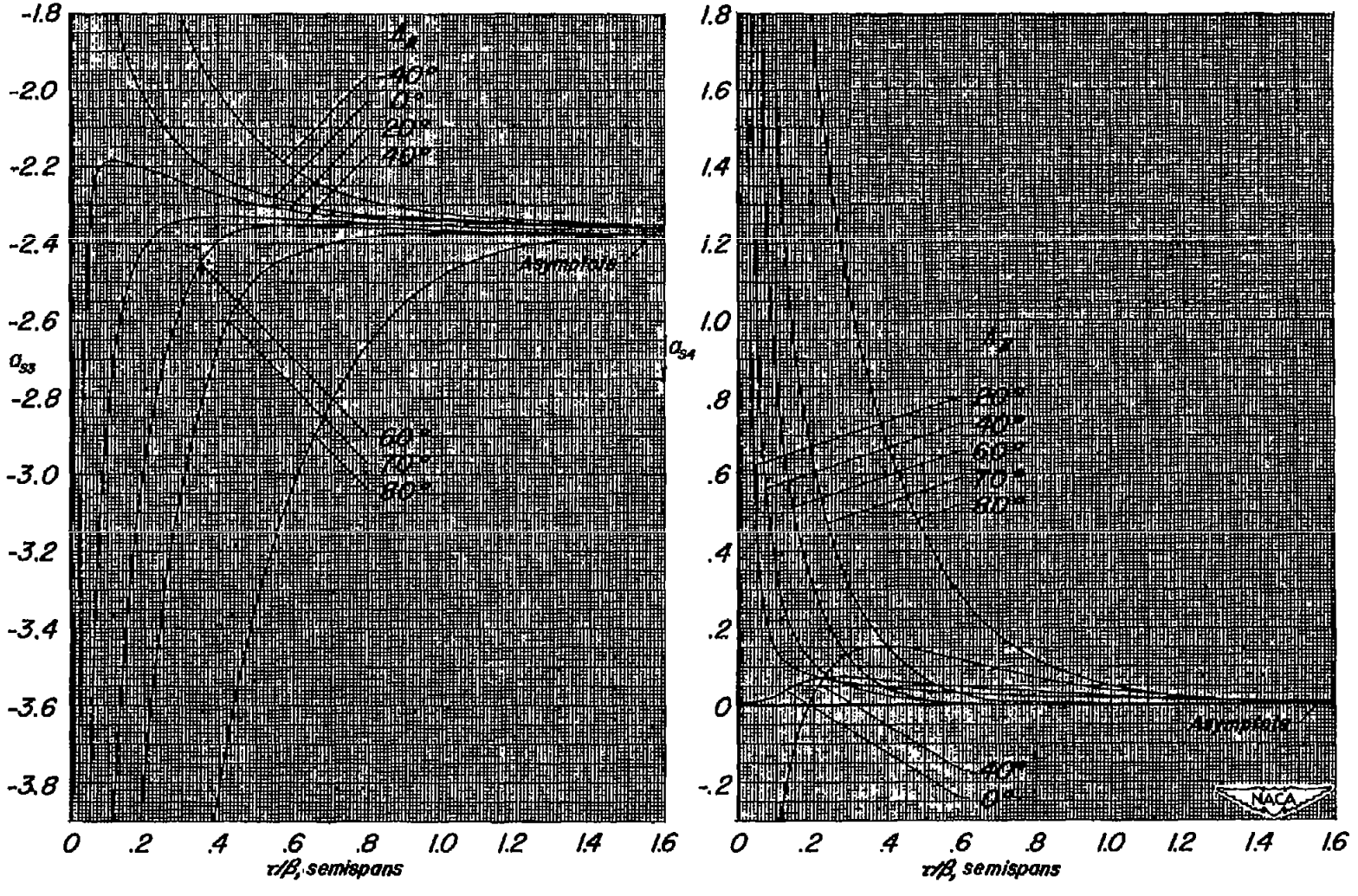

(c) η = 0.707

Figure 3.- Continued.

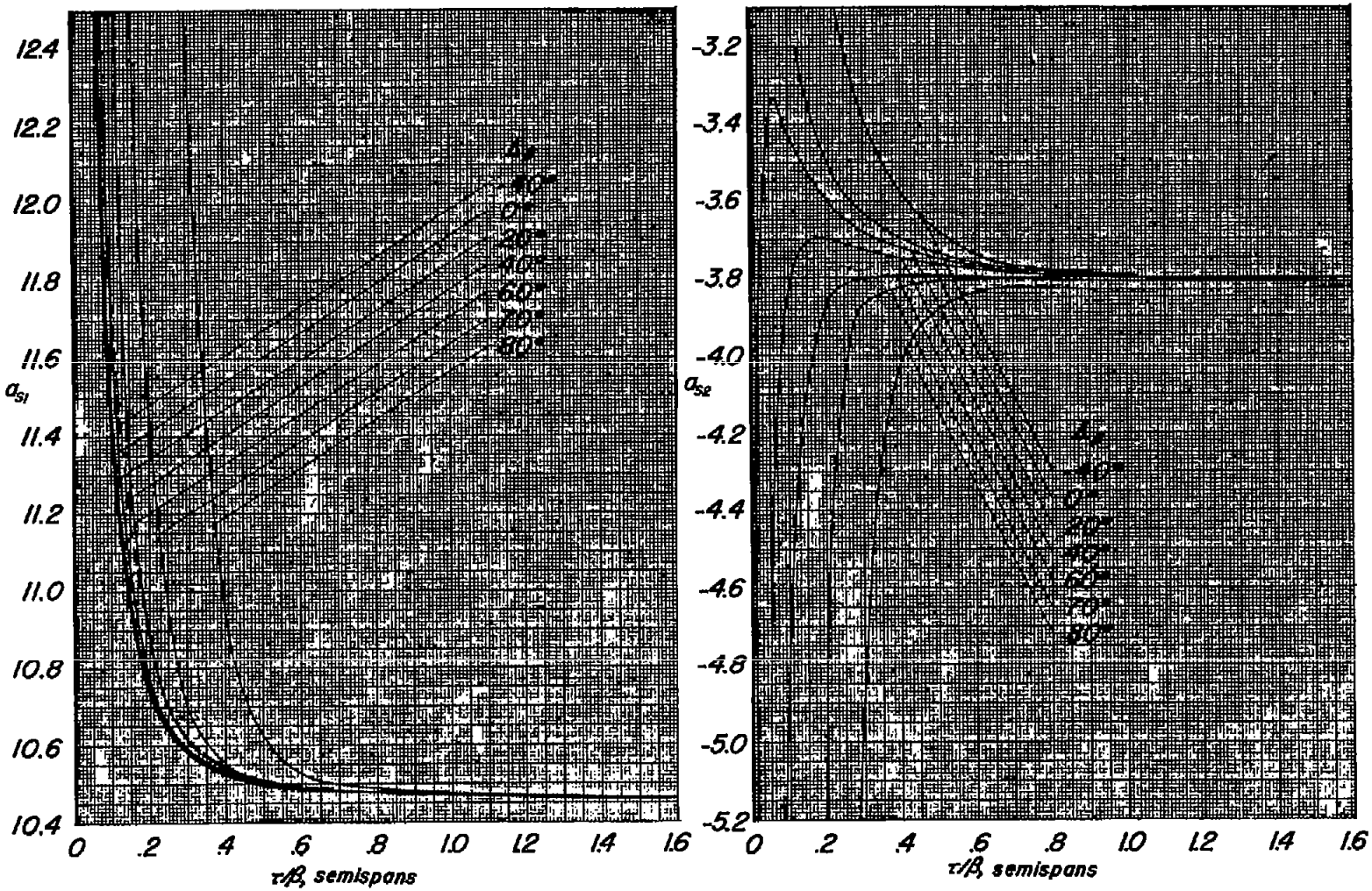
12.4
12.2
12.0
11.8
11.6
11.4
11.2
11.0
10.8
10.6
10.4
a_{s1}
-3.2
-3.4
-3.6
-3.8
-4.0
-4.2
-4.4
-4.6
-4.8
-5.0
-5.2
a_{s2}
$\Delta\psi$
-40°
0°
20°
40°
60°
70°
80°
0 .2 .4 .6 .8 1.0 1.2 1.4 1.6
τ/β, semispans

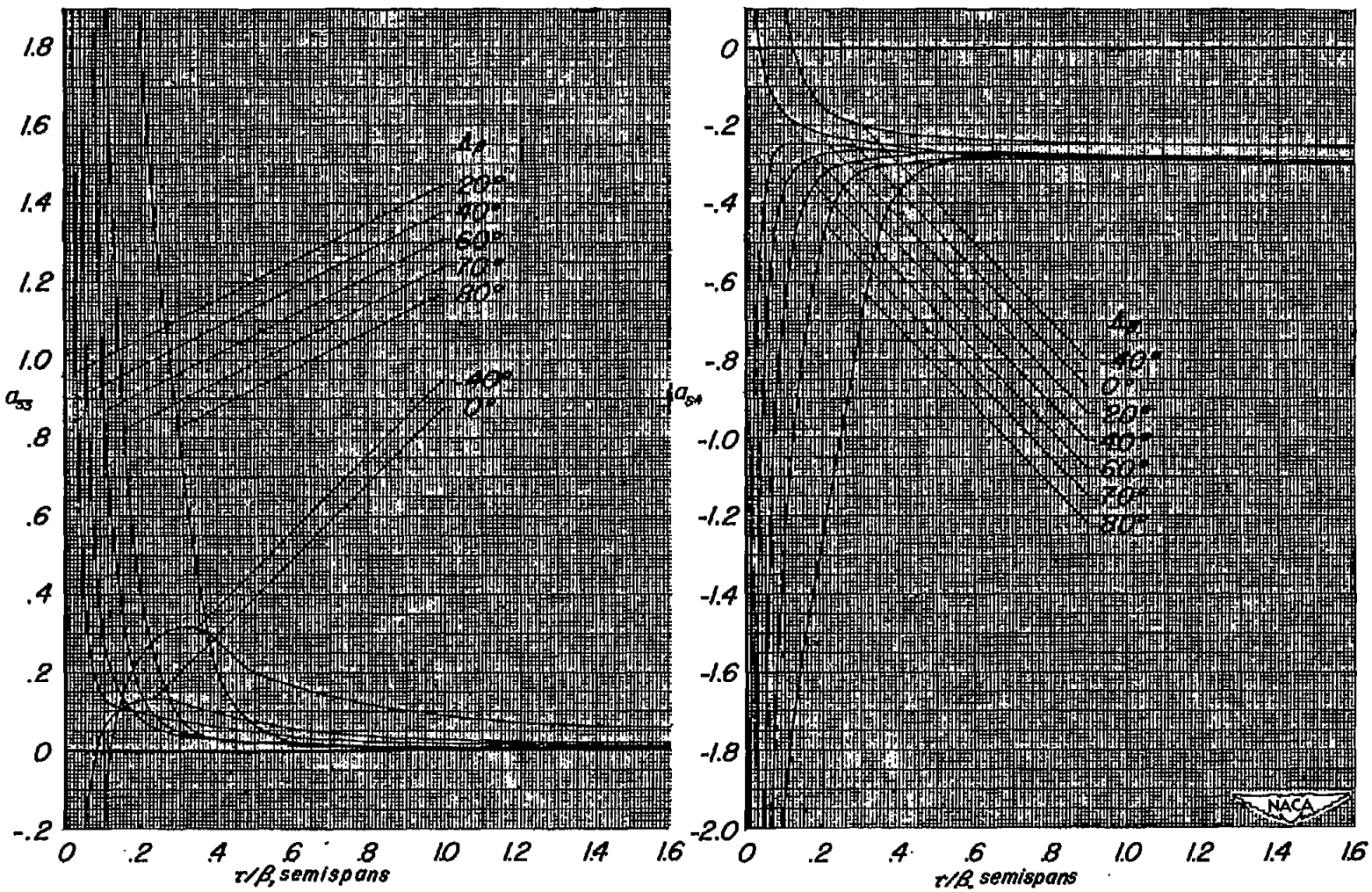

(d) $\eta = 0.924$

Figure 3.- Concluded.

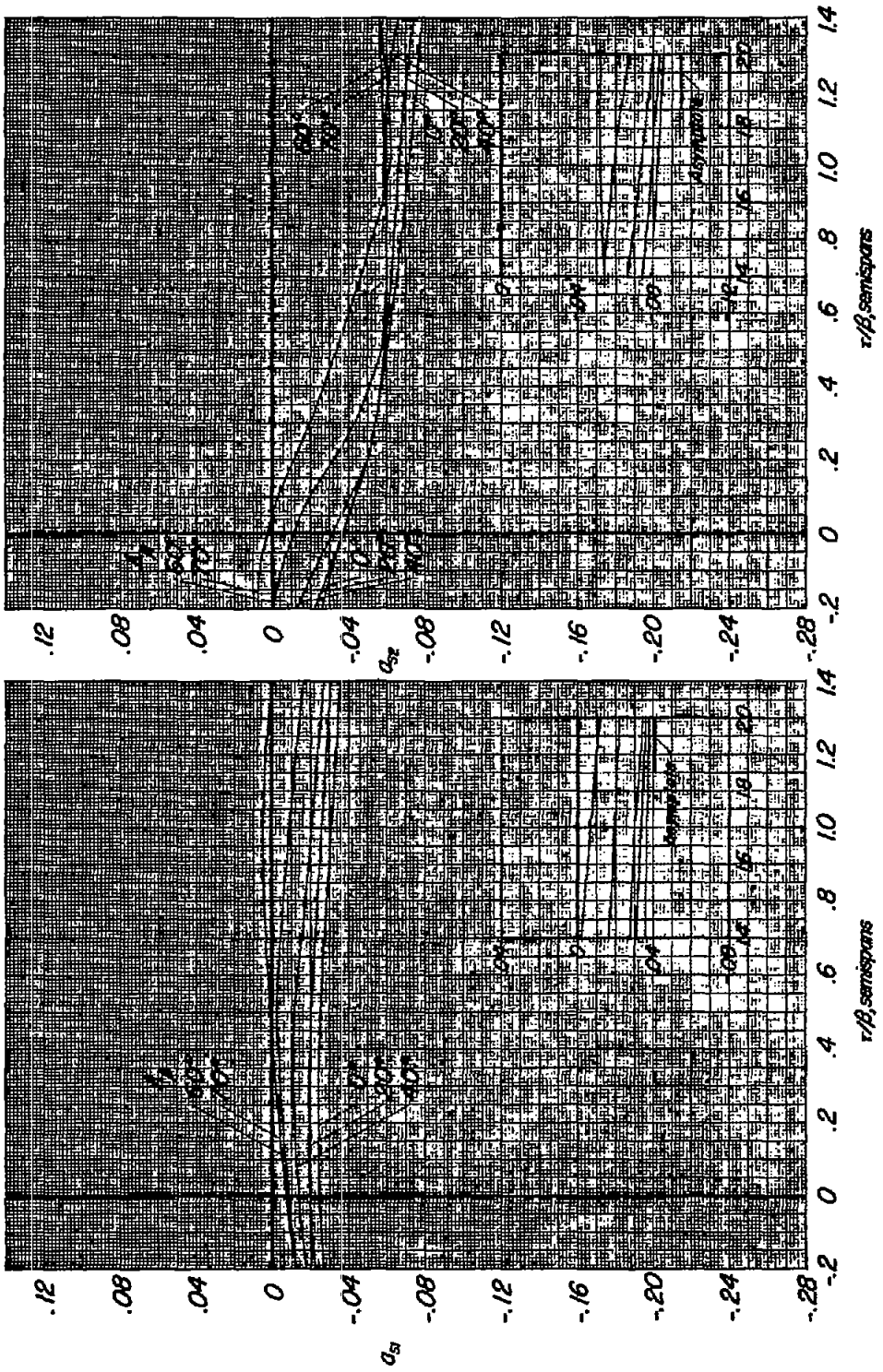
.12
.08
.04
0
-.04
-.08
-.12
-.16
-.20
-.24
-.28
a_{sz}
a_{sy}
-.2
0
.2
.4
.6
.8
1.0
1.2
1.4
r/B, semispans

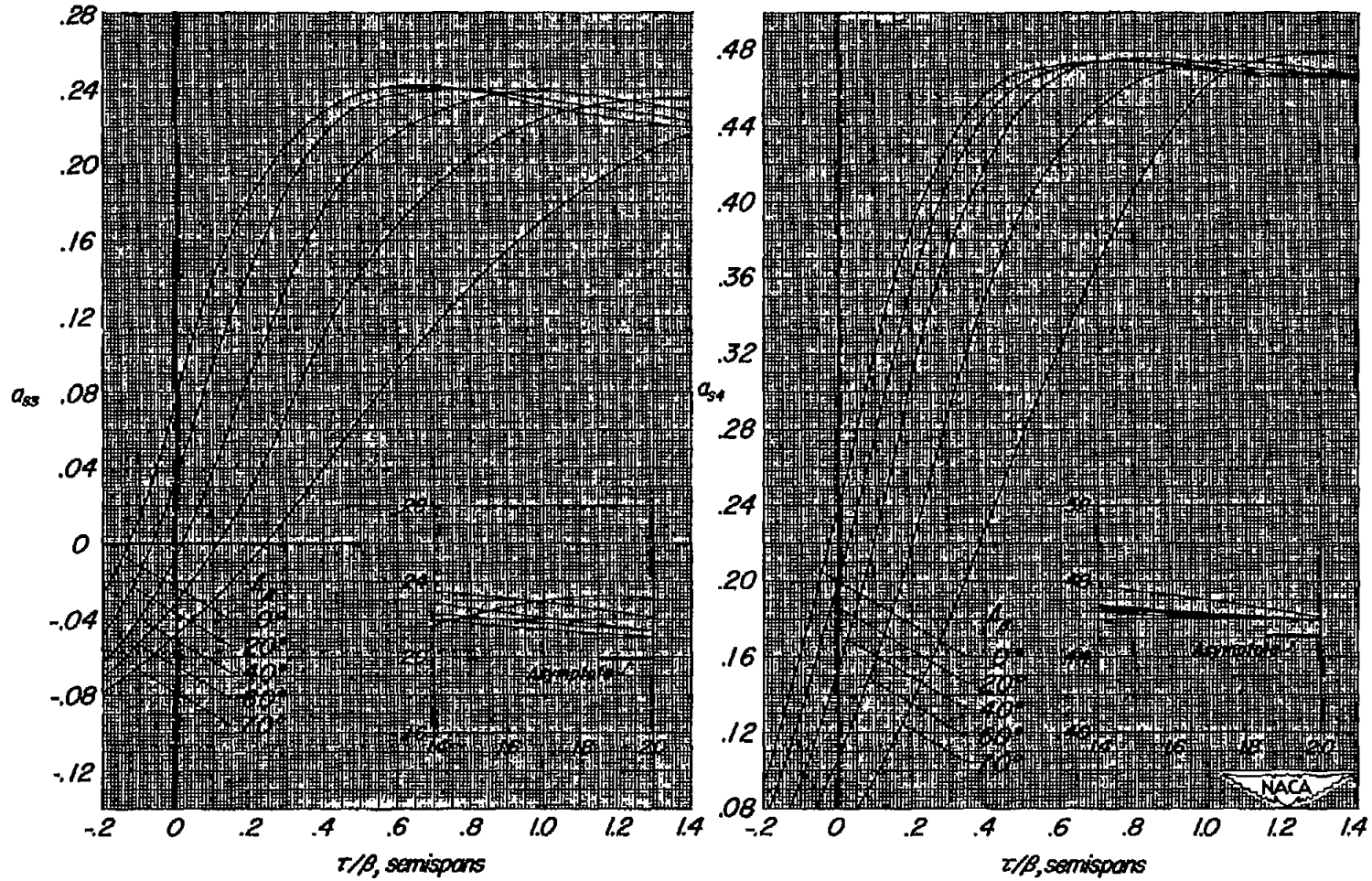

(a) $\eta = 0$

Figure 4.- Downwash influence coefficient, a_{sn}, due to total flat-sheet vortex system; τ/β aft of $c/4$, $\Omega_s = 0.5$.

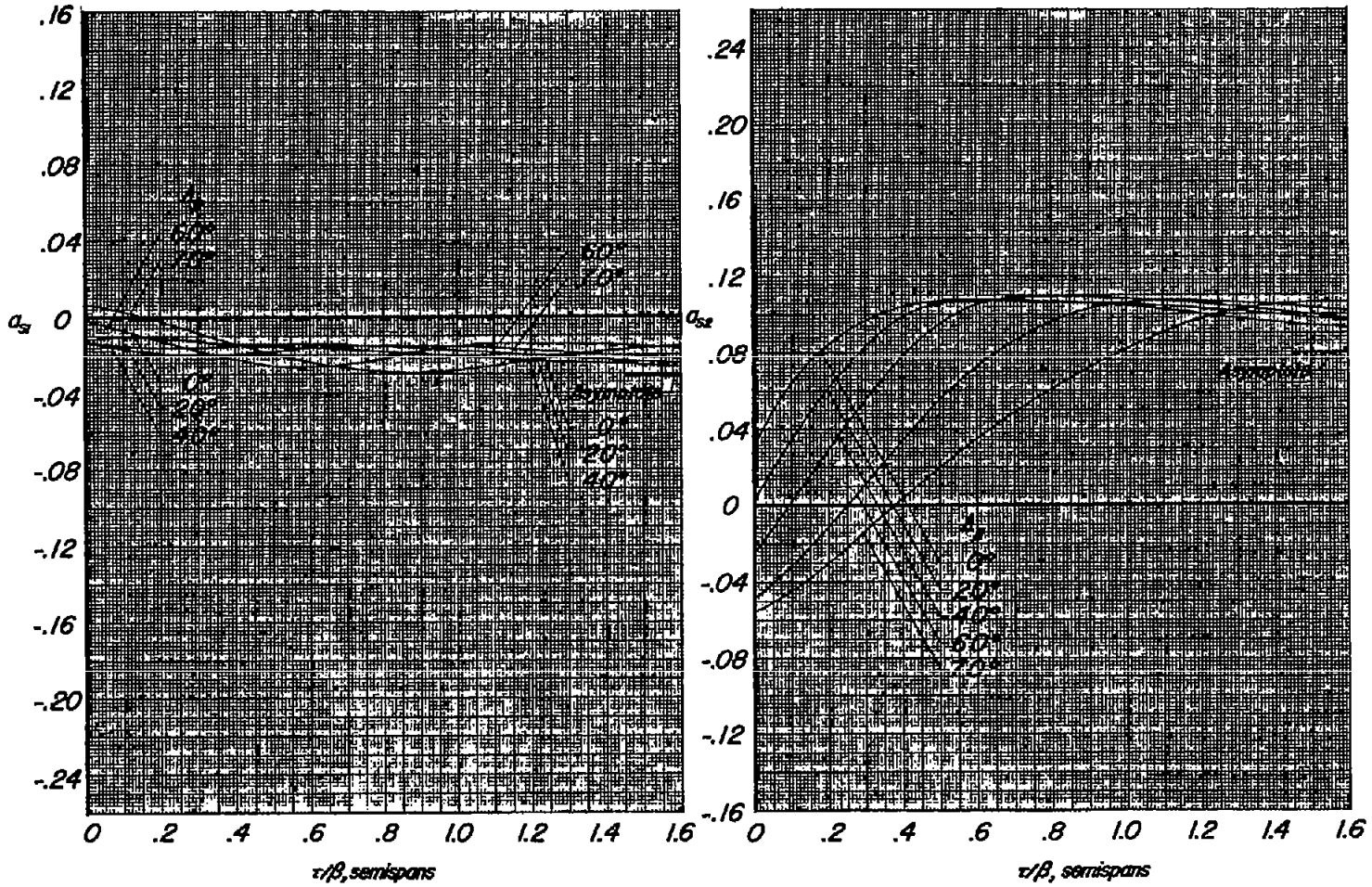
.16
.12
.08
.04
0
-.04
-.08
-.12
-.16
-.20
-.24
a_{s2}
0 .2 .4 .6 .8 1.0 1.2 1.4 1.6
r/β, semispans
.24
.20
.16
.12
.08
.04
0
-.04
-.08
-.12
-.16
a_{s2}
0 .2 .4 .6 .8 1.0 1.2 1.4 1.6
r/β, semispans

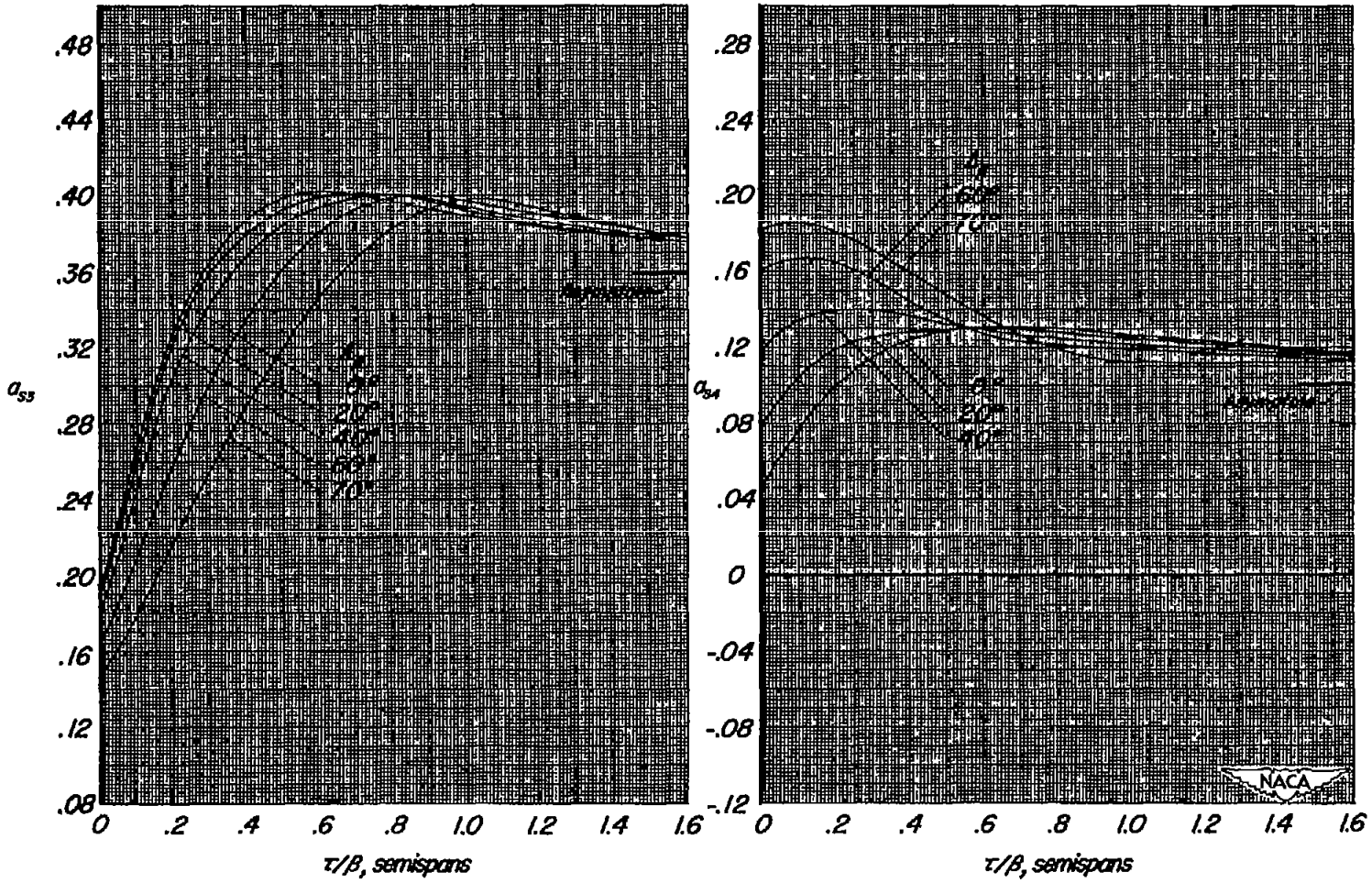

(b) $\eta = 0.383$

Figure 4.- Continued.

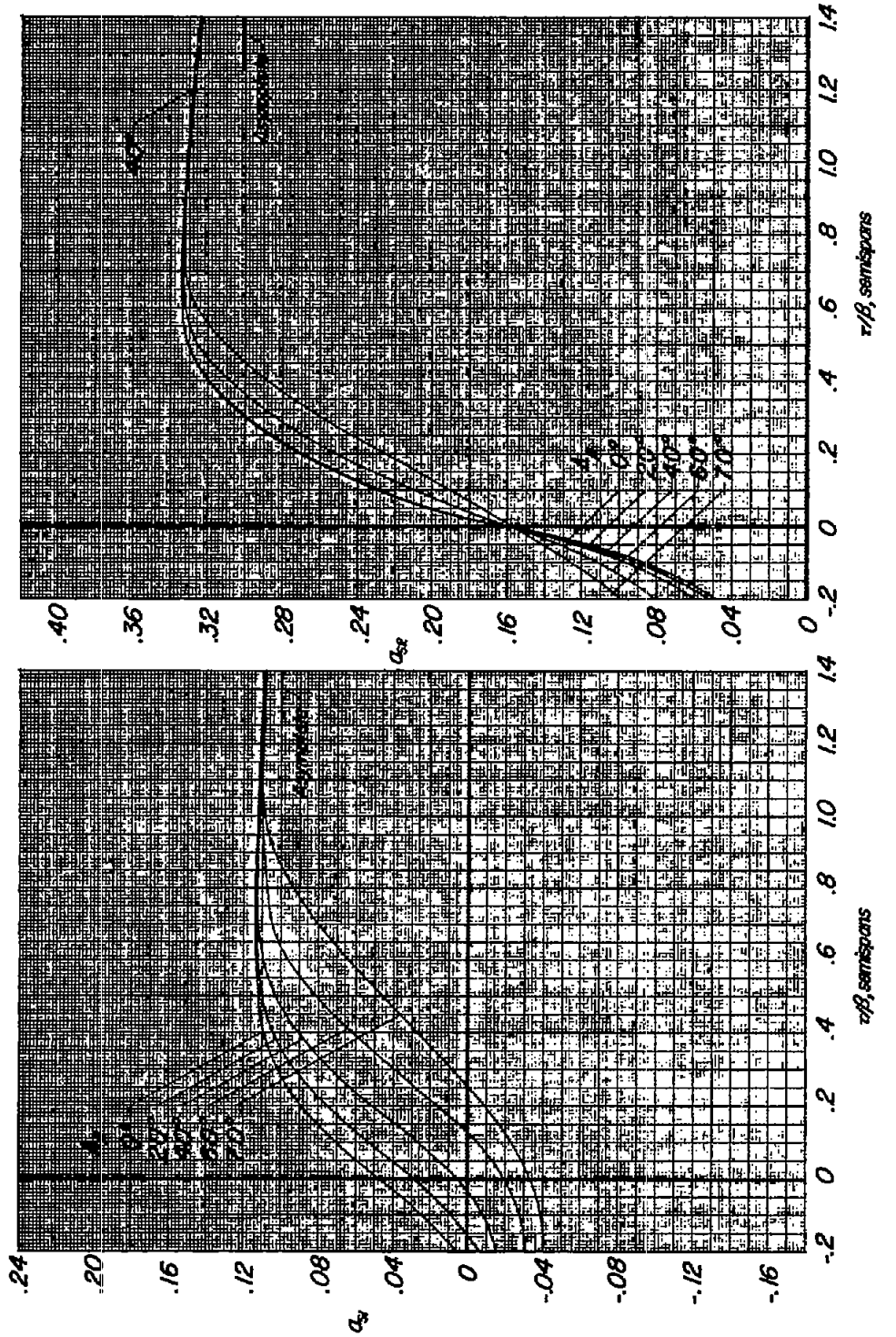
a_{sx}
a_{sy}
r/β, semispans
r/β, semispans

(c) $\eta = 0.707$

Figure 4.- Continued.

.32
.28
.24
.20
.16
.12
.08
.04
0
-.04
-.08
a_{s1}
a_{s2}
0° to 80°
70°
40°
20°
0°
0
.2
.4
.6
.8
1.0
1.2
1.4
1.6
x/β, semispans

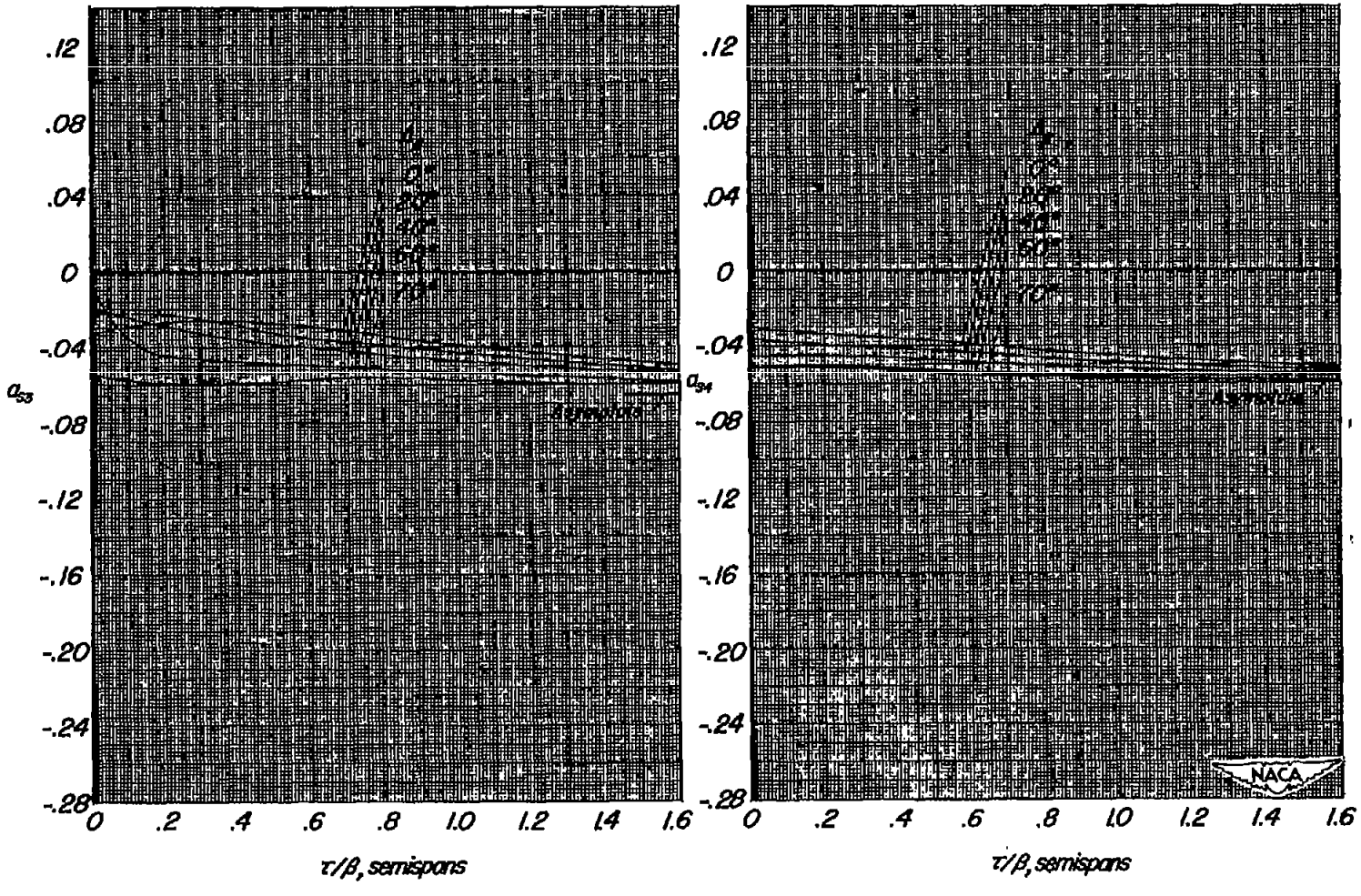

(d) $\eta = 0.924$

Figure 4.- Concluded.

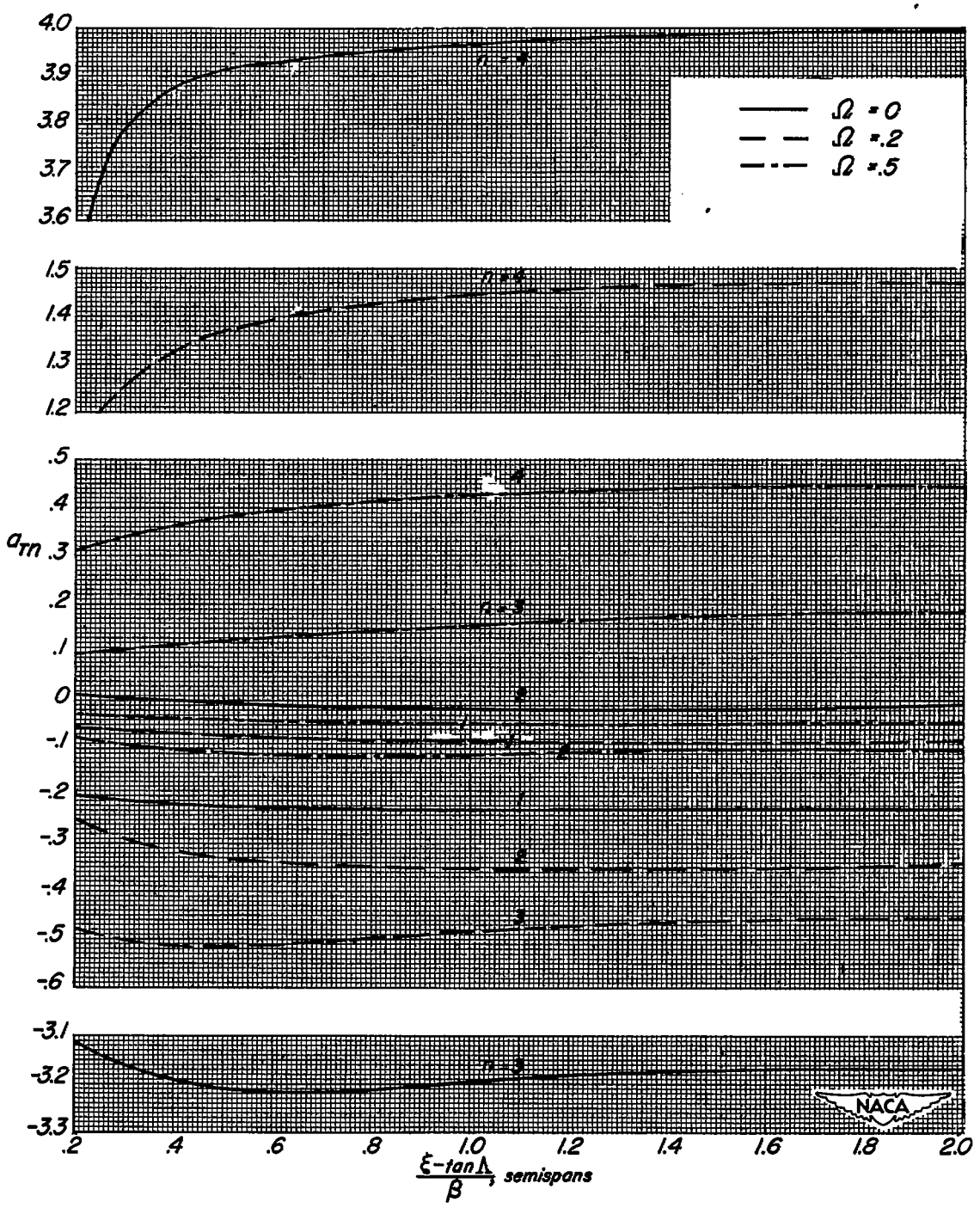

(a) $\eta = 0$

Figure 5.- Downwash influence coefficient, a_{Tn}, due to trailing vortex sheet.

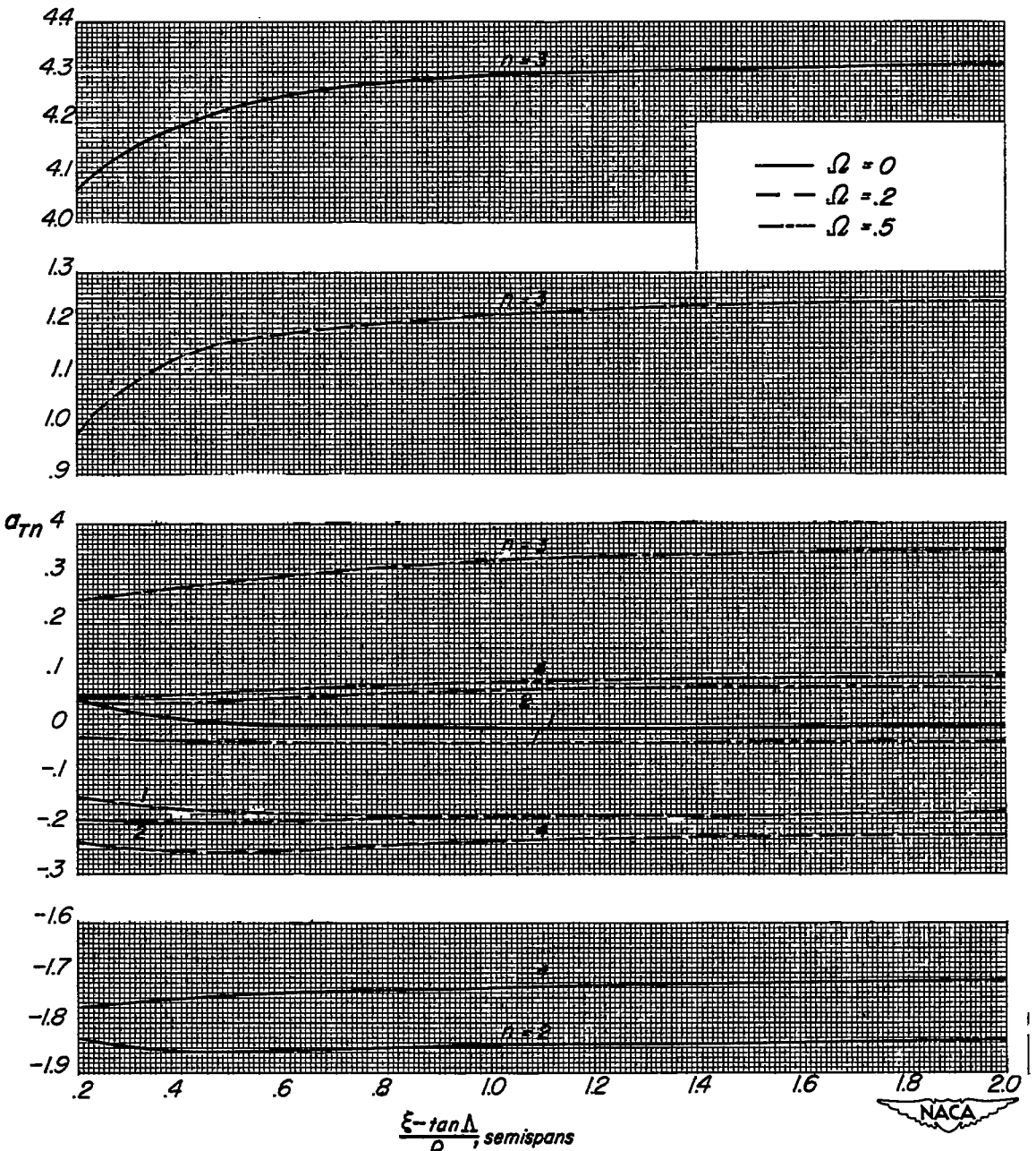

(b) $\eta = 0.383$

Figure 5.- Continued.

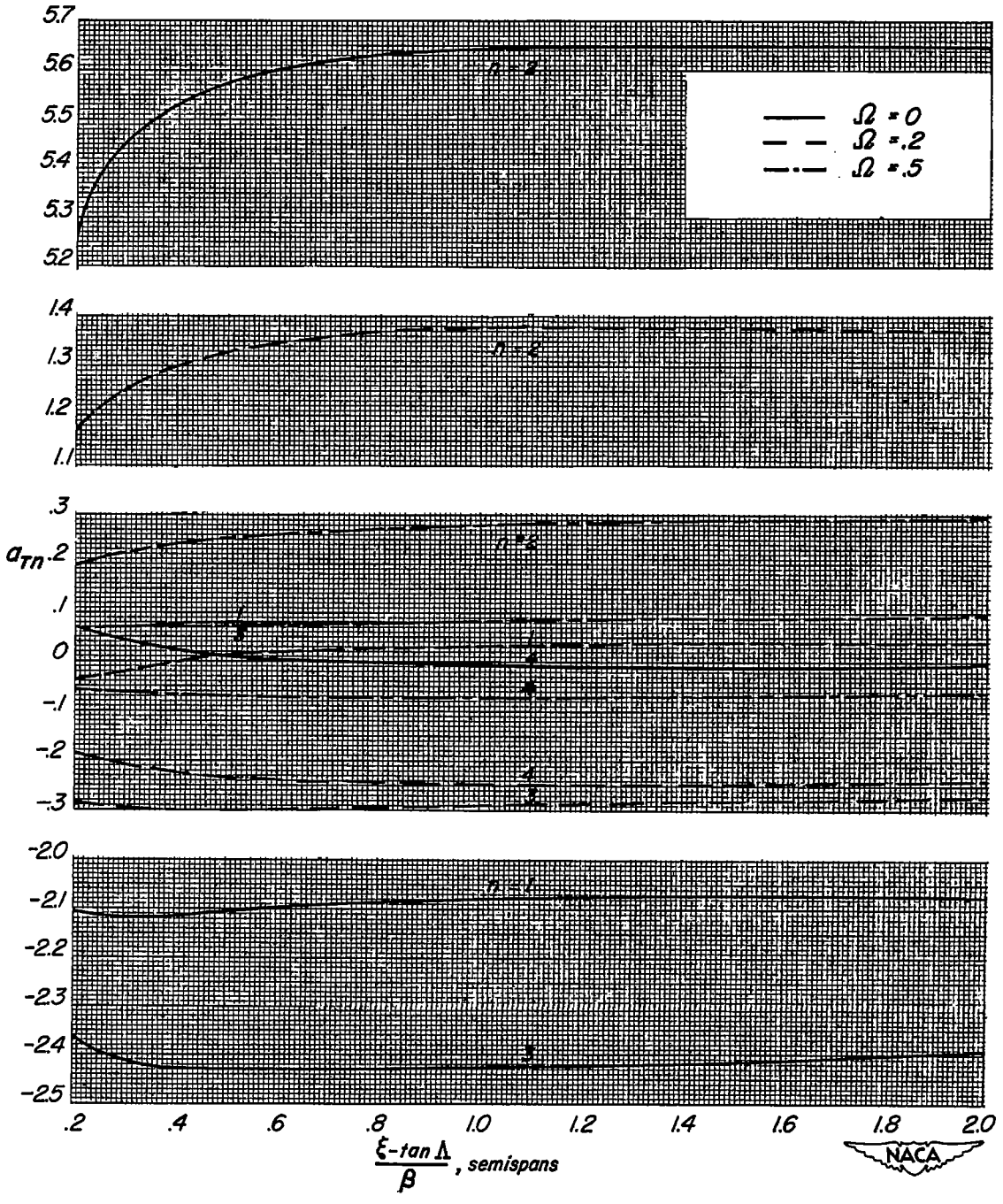

(c) $\eta = 0.707$

Figure 5.- Concluded.

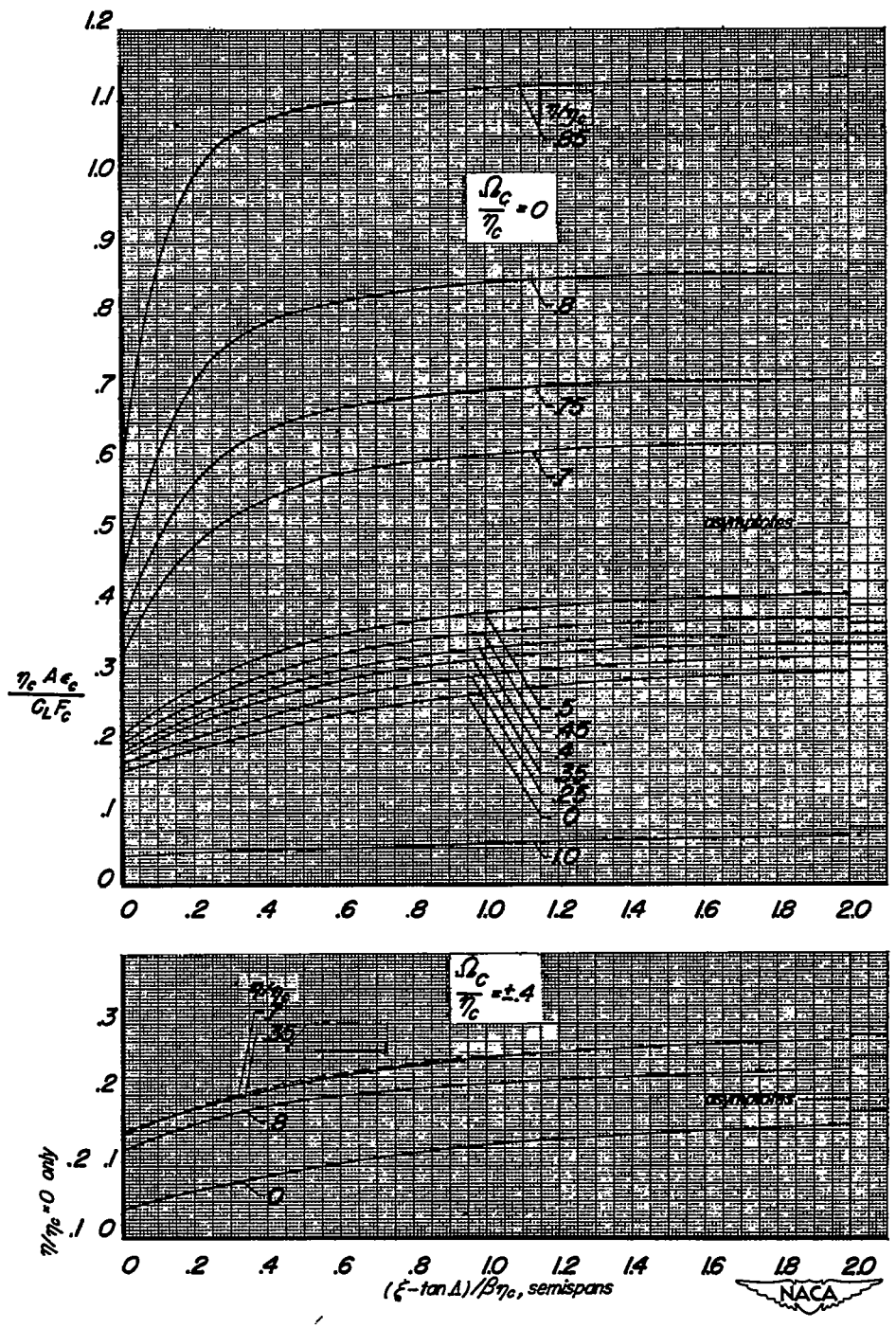

(a) $\frac{\Omega_c}{\eta_c} = 0$ and ± 0.4

Figure 6.- Downwash parameter for two trailing vortex cores that extend downstream from the quarter chord of the wing tip.

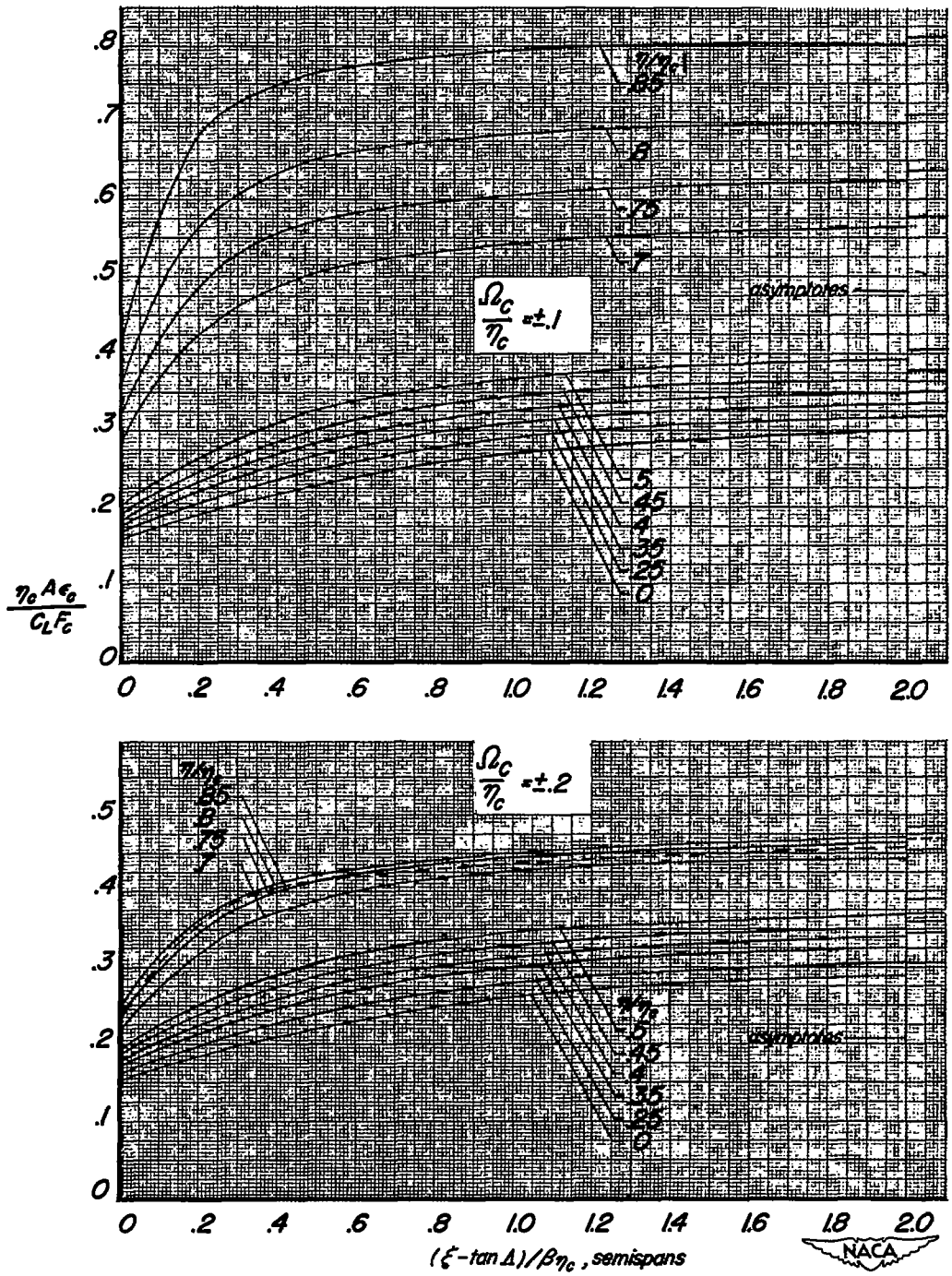

(b) $\frac{\Omega_c}{\eta_c} = \pm 0.1$ and ± 0.2

Figure 6.- Concluded.

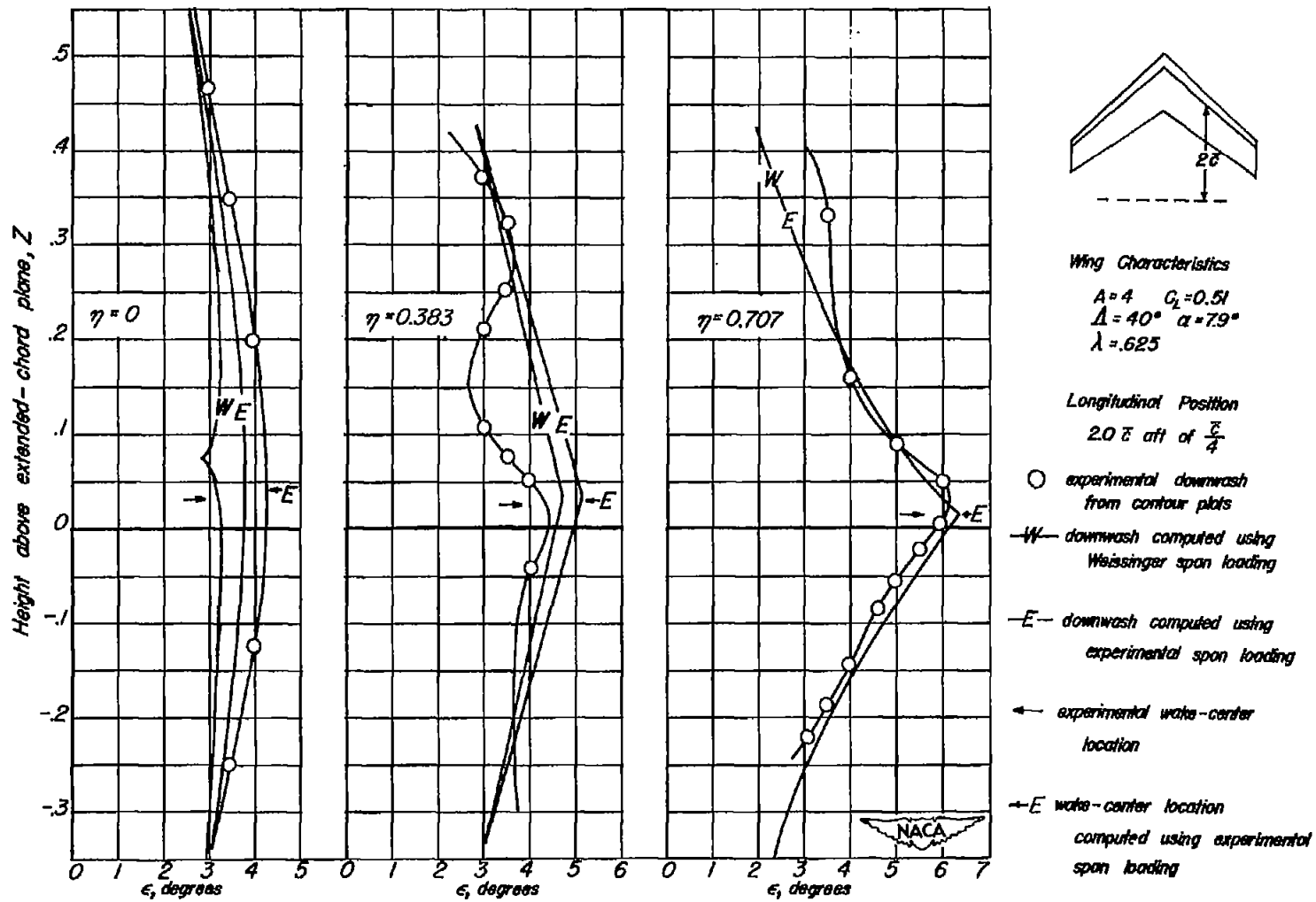

Figure 7.- Comparison of downwash angles obtained experimentally with those computed by flat-sheet theory.

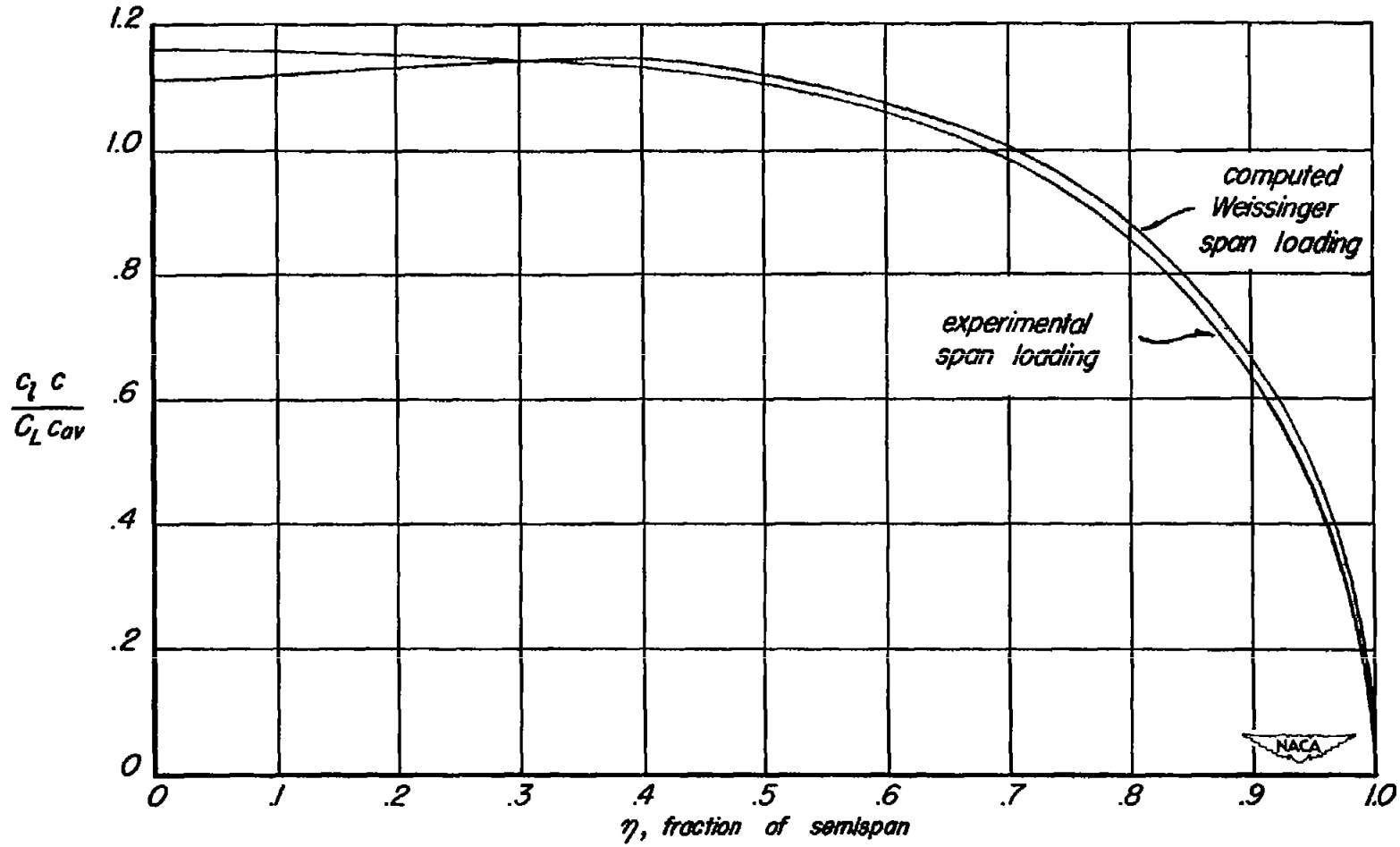

Figure 8.- Comparison of Weissinger span loading and experimental span loading for the configuration of figure 7.

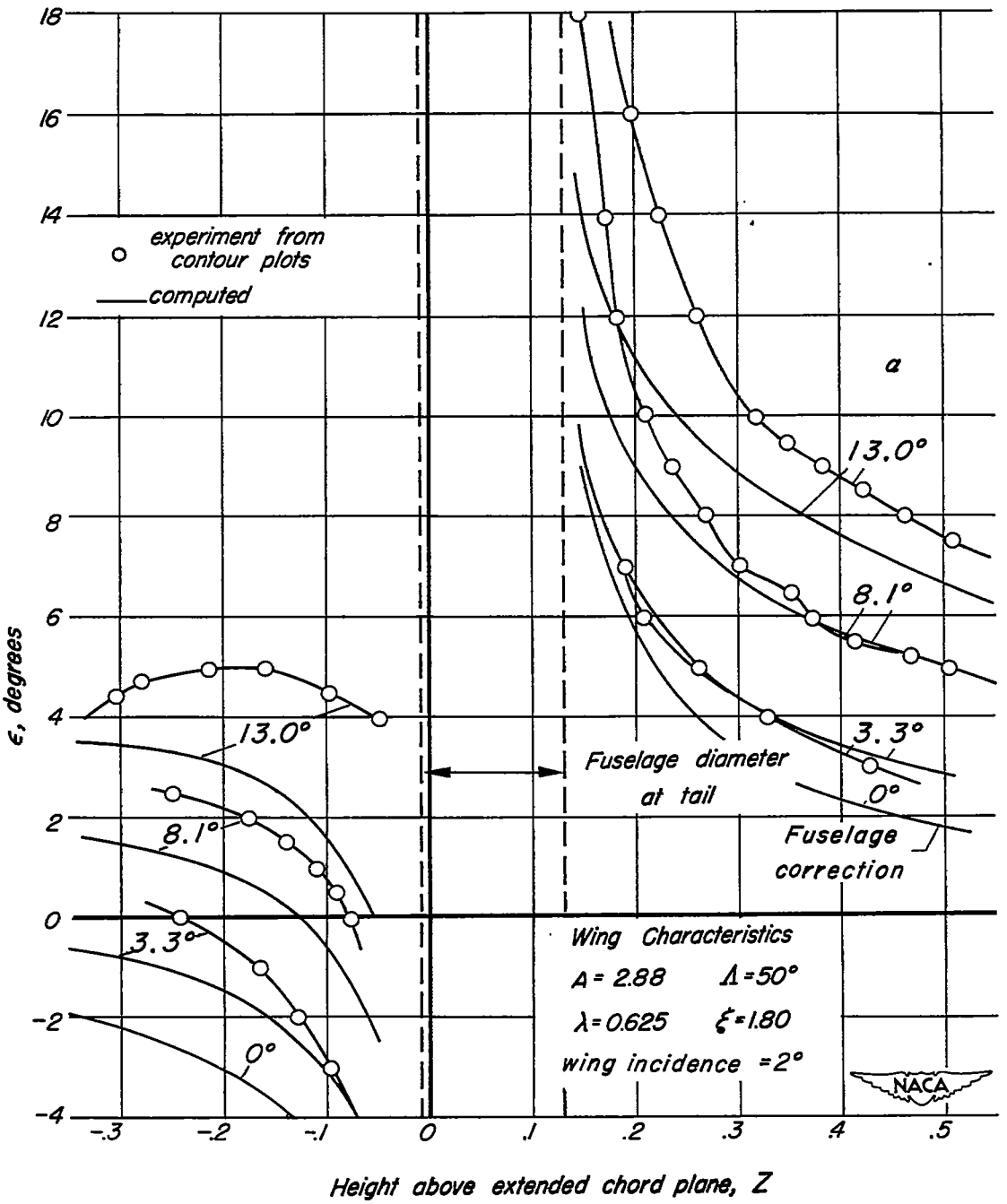

(a) $\eta = 0$

Figure 9.- Comparison of experimentally obtained downwash angles for a wing-fuselage combination with those computed by the flat-sheet method plus a fuselage correction.

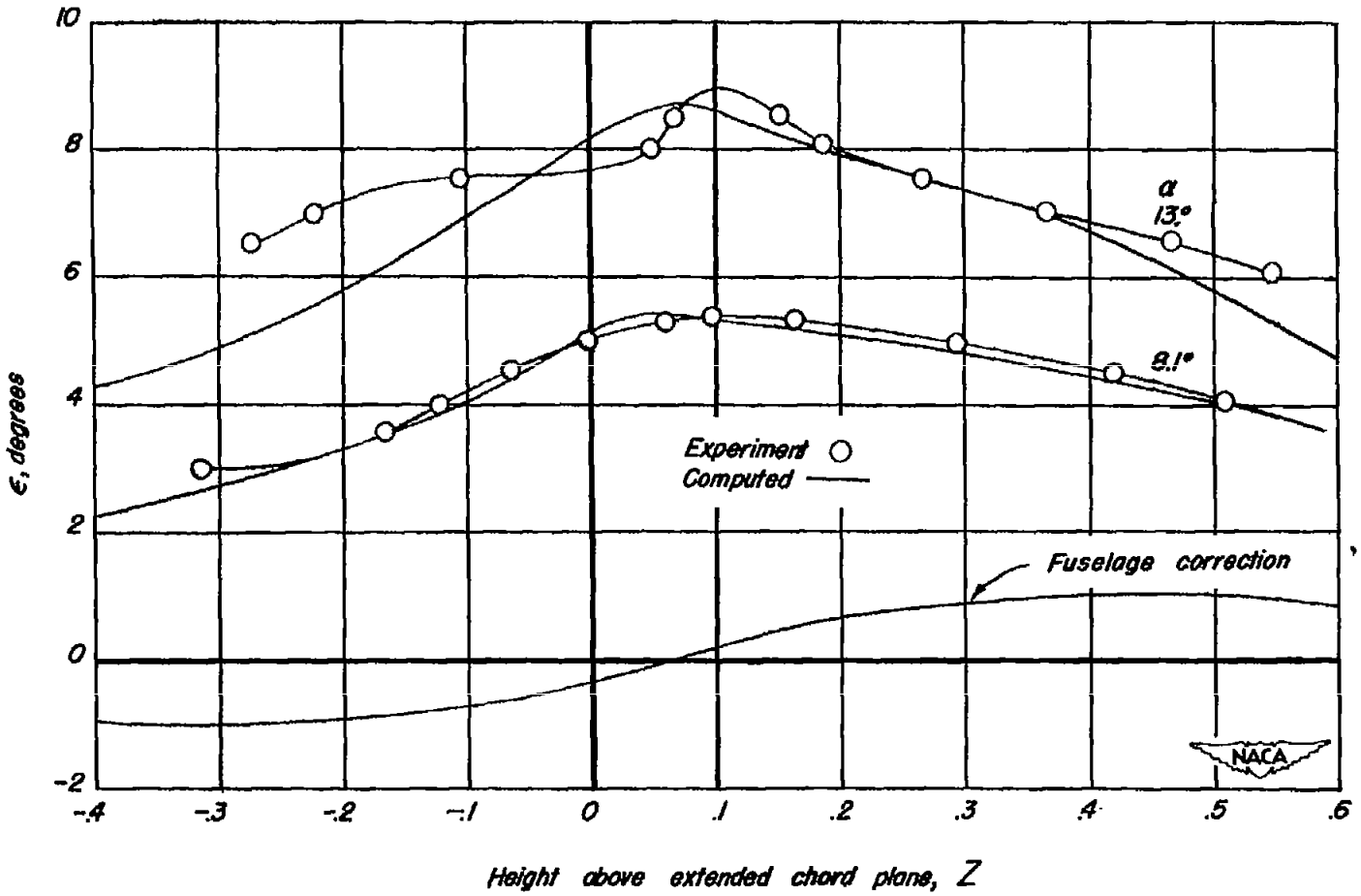

(b) $\eta = 0.383$

Figure 9.- Concluded.

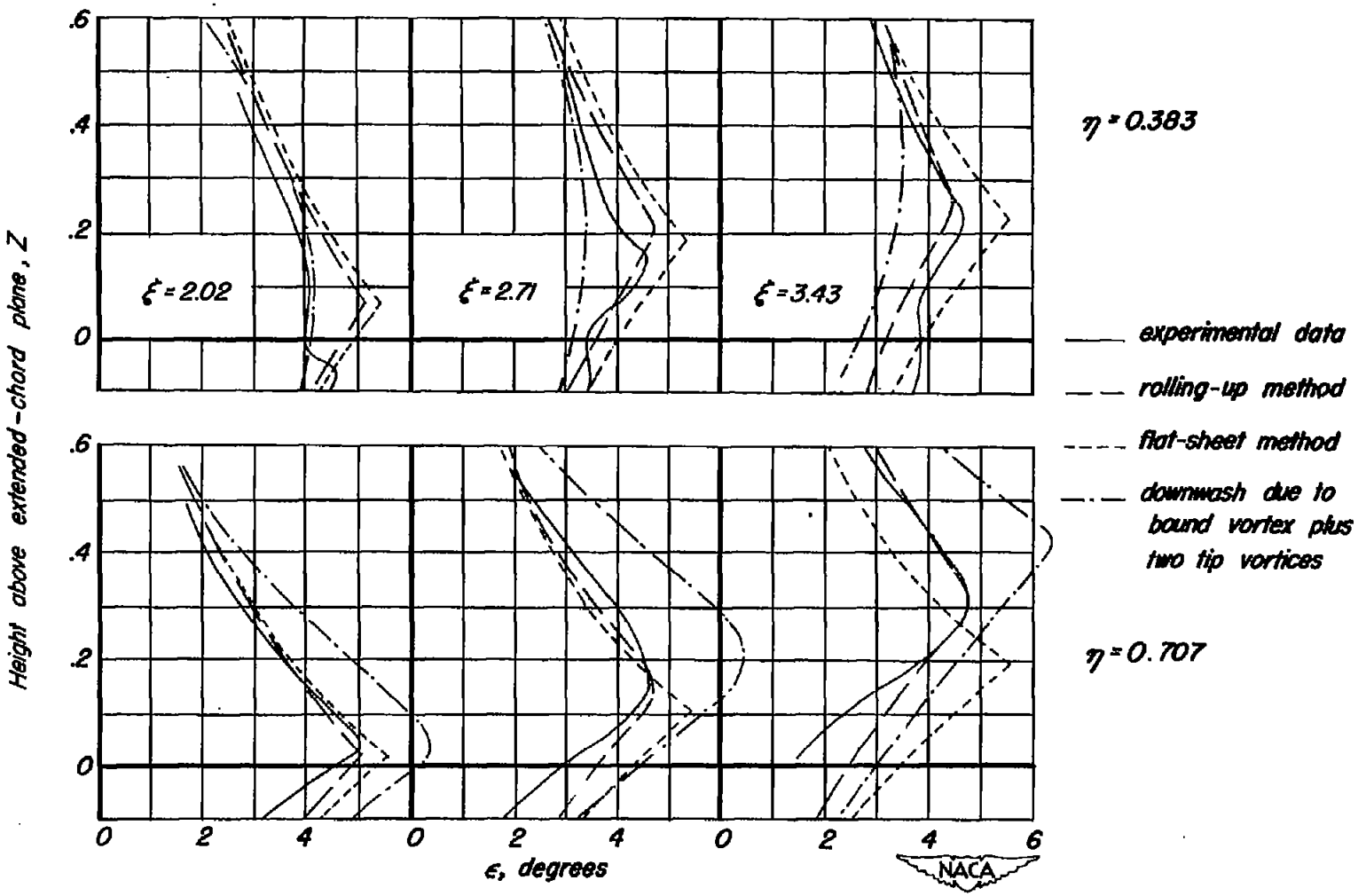

Figure 10.- Comparison of downwash angles obtained experimentally with those obtained by three theoretical methods; $\Lambda = 60^{\circ}$, $A = 3.5$, $\lambda = 0.25$, and $C_L \cong 0.5$.

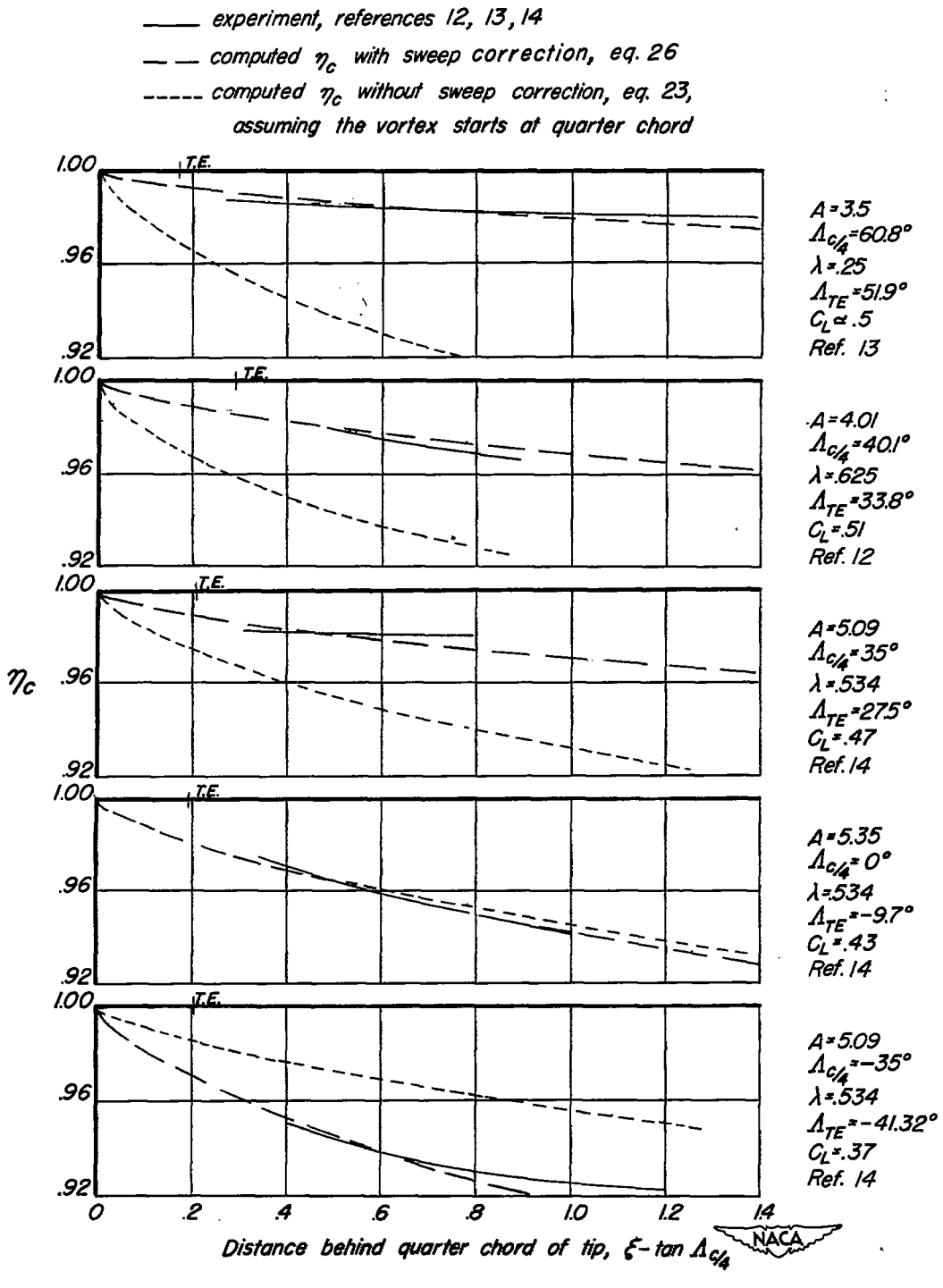

Figure 11.- Comparison of computed and experimental spanwise location, η_c, of the tip vortices behind several wings.

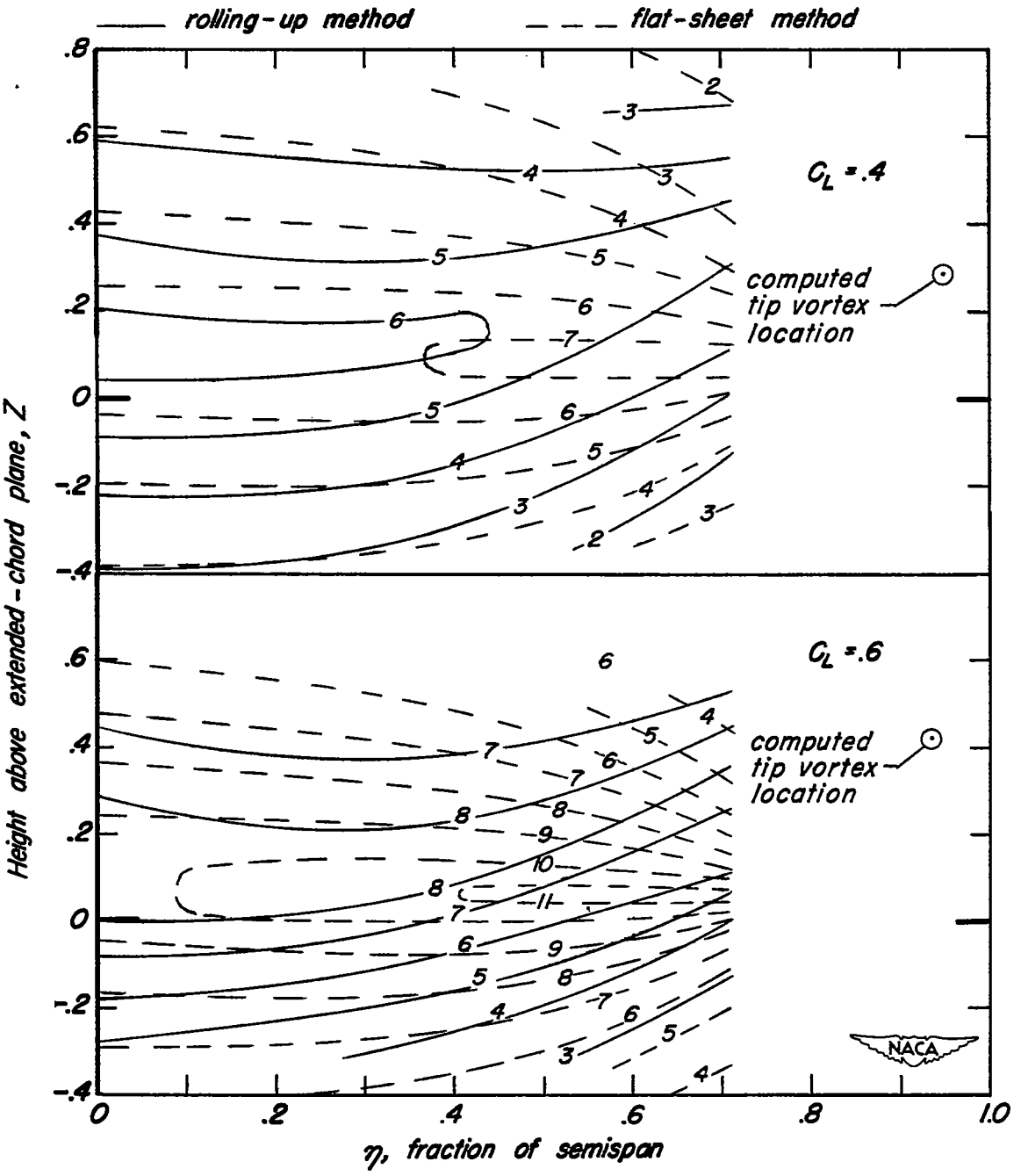

(a) A = 2

Figure 12.- Contours of constant downwash angle, degrees, at 2.0 M.A.C. aft of the quarter chord of the wing M.A.C. predicted by rolling-up method and by flat-sheet method; $\Lambda = 40^\circ$, $\lambda = 0.5$, A = 2 and 4, and $C_L = 0.4$, and 0.6.

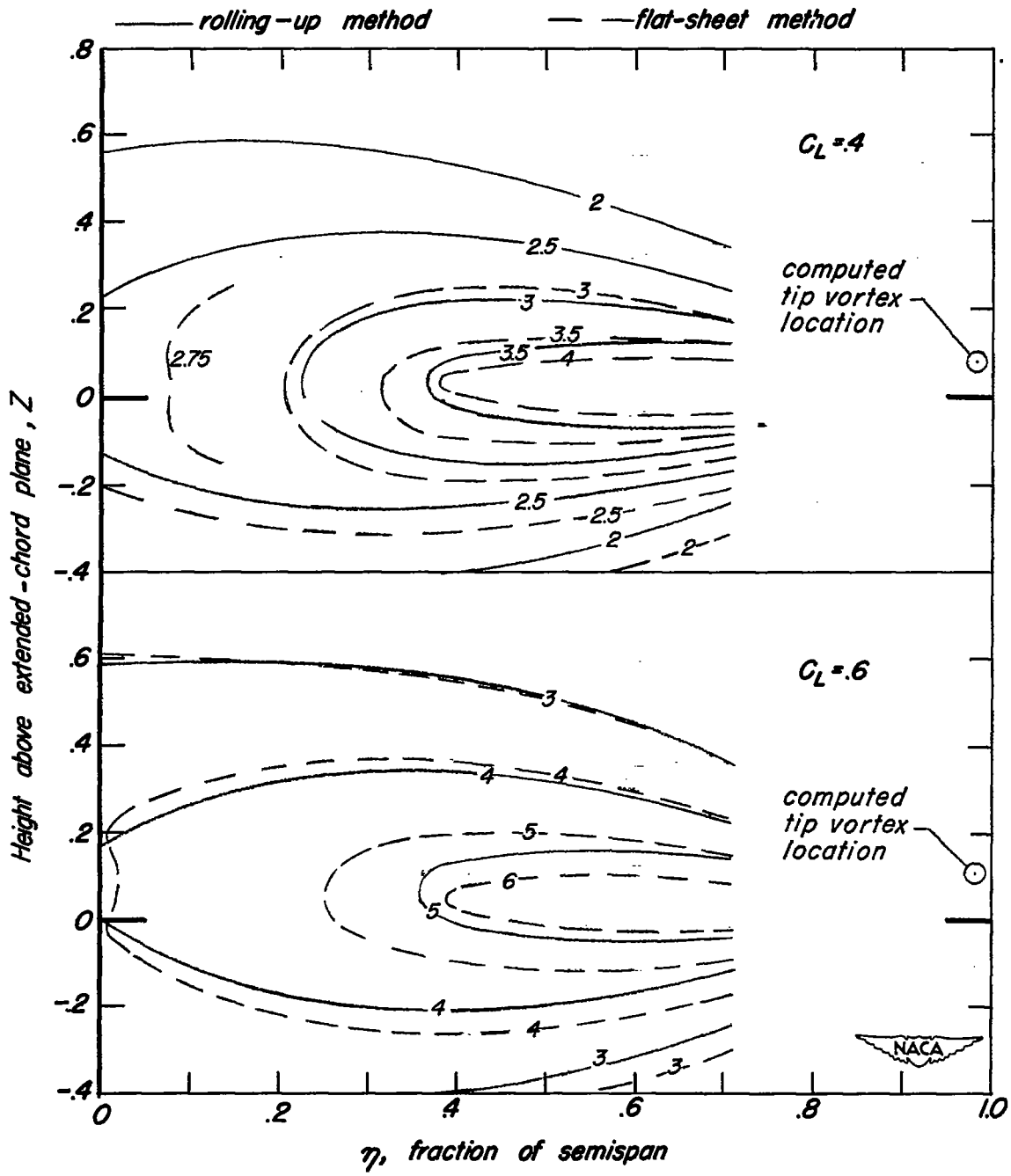

(b) A = 4

Figure 12.- Concluded.

NACA-Langley - 1-24-55 - 1000